BNL – 71044-2003
Formal Report

Proceeding of the Seeded X-Ray Free Electrron Laser Workshop

X.J. Wang, J.B. Murphy and L.H. Yu
National Synchrotron Light Source
Brookhaven National Laboratory
Upton, New York 11973

B. Faatz
DESY, Hamburg, Germany

Z. Huang
SLAC, CA, USA

S. Reiche
Department of Physics and Astronomy, UCLA, CA USA

M. Zolotorev
LBNL Berkeley, CA 94720, USA

December 2002

National Synchrotron Light Source

Brookhaven National Laboratory

Brookhaven National Laboratory
Operated by
Brookhaven Science Associates
Upton, NY 11973

Under Contract with the United States Department of Energy
Contract Number DE-ACO2-98ch10886

DISCLAIMER

Proceeding of the Seeded X-ray Free Electron Laser Workshop

X.J. Wang[1], B. Faatz[2], Z. Huang[3], J.B. Murphy[1], S. Reiche[4], L.H. Yu[1]
and M. Zolotorev[5]

[1]NSLS, BNL,, N.Y. 11973-5000, USA

[2] DESY, D-22607 Hamburg, Germany

[3]SLAC, CA 94025, USA

[4]Department of Physics and Astronomy, UCLA, CA 90095, USA

[5]LBNL, Berkeley, CA 94720, USA

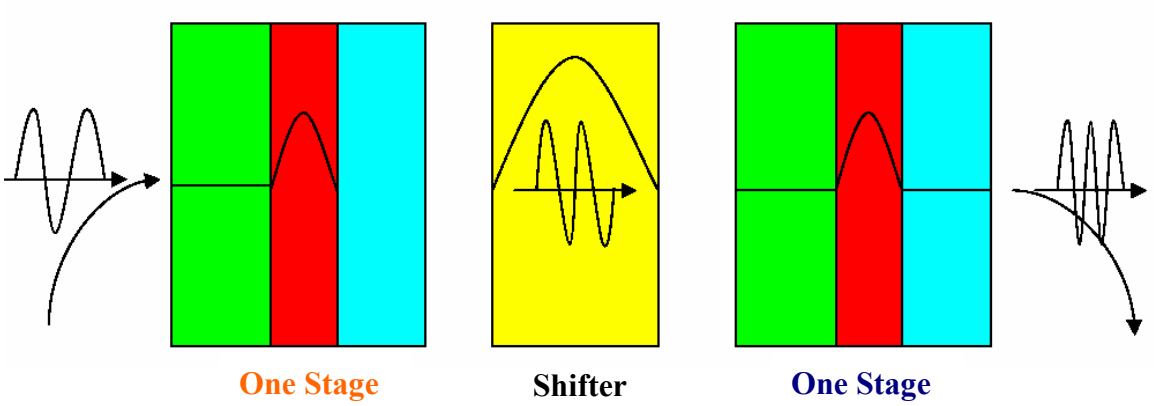

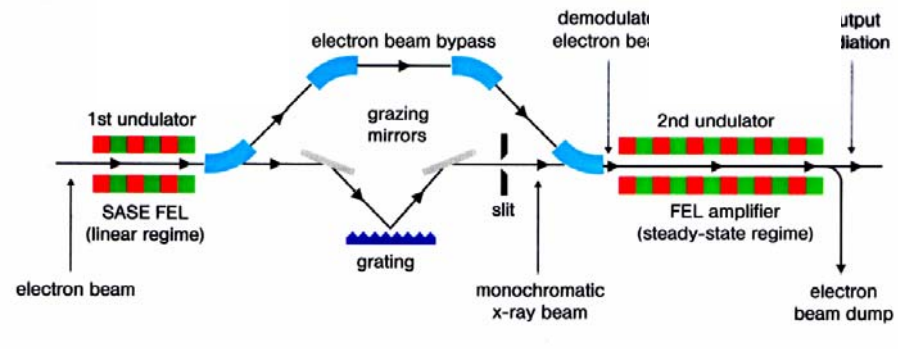

December 13-14, 2002
National Synchrotron Light Source
Brookhaven National Laboratory
Upton, NY 11973-5000, USA

Table of Contents

Introduction

The National Synchrotron Light Source (NSLS) of the Brookhaven National Laboratory (BNL) sponsored a **Seeded X-ray Free Electron Laser Workshop** on December 13-14, 2002 to explore the challenging issues for future light source based on free electron lasers. Representatives from BNL, DESY, LBNL, SLAC and UCLA made presentations on the novel schemes under consideration at their laboratories.

We would like to express our gratitude to all workshop participants, particular those from other labs. This proceeding reflects the wonderful work presented at the workshop.

It is almost unimaginable to have a workshop without the professional support from A. Bowden, K. Loverro and L. Miller. We would like to thank Dr. P. Paul and Dr. S. Dierker for their encouragement and support of FEL R&D and for making the workshop possible.

Workshop Co-Organizers
J. B. Murphy
X.J. Wang
National Synchrotron Light Source
Brookhaven National Laboratory
Upton, NY 11973, USA

Executive Summary

The underlying theory of a high gain free electron laser (FEL) has existed for two decades [1-2], but it is only in the last few years that these novel radiation sources have been realized experimentally. Several high gain FELs have successfully reached saturation in the infrared, visible and the VUV portion of the spectrum: the High Gain Harmonic Generation (HGHG) free electron lasers [3] at BNL and the Self Amplified Spontaneous Emission (SASE) FELs at LEUTL, VISA and TTF [4-6]. The outstanding challenges for future FELs are to extend high gain FELs to the X-ray regime, improve the longitudinal coherence of the radiation using seeded FEL schemes and generate ultrashort pulses (<100 fs). The National Synchrotron Light Source (NSLS) of the Brookhaven National Laboratory (BNL) sponsored a **Seeded X-ray Free Electron Laser Workshop** on December 13-14, 2002 to explore these challenging issues. Representatives from BNL, DESY, LBNL, SLAC and UCLA made presentations on the novel schemes under consideration at their laboratories.

To provide a ruler against which the seeded FEL schemes could be compared, Z. Huang of SLAC delivered an insightful overview of the properties of SASE FELs. A high-gain FEL operated in the SASE mode is the most straightforward approach to achieve an extremely high-brightness, next-generation X-ray source. The exponential growth and saturation, the transverse coherence, the longitudinal and statistical properties, as well as the nonlinear harmonic generation of SASE radiation originally predicted by theory have all been experimentally demonstrated in the IR-VUV region. The total intensity fluctuation of any future SASE X-ray FEL is expected to be small due to the presence of a large number of longitudinal modes, though the fluctuation for each mode will still be 100%. Seeded FELs would improve or eliminate the intensity fluctuations, provide better longitudinal coherence and much shorter pulses. The SASE radiation pulse length is determined by the electron pulse length, which at present is limited to about 100 fs (FWHM).

S. Reiche of UCLA presented several novel schemes under active study for shortening the SASE output pulse length at the LCLS. Short FEL pulses can be achieved by either manipulating the radiation pulse or the electron beam. Pulse compression and pulse slicing can be implemented by applying an energy chirp onto the electron beam and using X-ray optical elements to manipulate the FEL radiation. If the power handling of the optical elements is a problem, an extended two-stage setup solves this problem but requires about 30% more undulator length and an additional beam line component for the electron beam. FEL pulse manipulation is limited to around 10–20 fs due to the available energy chirp of the electron beam. To achieve shorter pulses, electron beam, pulseshortenings due to gain degradation are showing promising results in recent simulation. Pulse shortening using the wakefield effect of the long vacuum chamber in the undulator or using a transverse deflecting cavity to create a spatially-chirped bunch prior to the entrance of the undulator suggested that sub 10 fs pulses might be possible.

B. Faatz presented the DESY team's perspective on short pulse seeded FELs[7]. To improve the longitudinal coherence and reduce the fluctuation inherent in a SASE FEL,

the DESY team is implementing a two stage self-seeding FEL at the TTF II facility. This scheme consists of two undulators, a monochromator and an electron beam by-pass. The length of the first undulator ensures that FEL is still in the exponential gain, and the effective power after the monochromator is about two orders of magnitude above the shot noise when it "self seeds" the electron beam in the second undulator. The expected output radiation bandwidth is close to the Fourier transformation limit resulting in roughly two orders of magnitude increase of the spectral brilliance when compared to a SASE FEL. Shot-to-shot fluctuations of the pulse energy are reduced from 100% to less than 10% when the second undulator reaches saturation. A sideband seeded FEL capable of producing 30 fs pulses of soft X-rays is also proposed for the TTF II facility. Those schemes are compatible with a SASE FEL and can be added on later on with proper planning. DESY is exploring the possibility of producing attosecond X-rays for the TESLA XFEL project taking advantage of the spiky nature of the SASE FEL and HGHG [8].

L.H. Yu of BNL presented the only experimentally demonstrated laser seeded FEL – HGHG. An HGHG FEL consists of two undulators separated by a dispersive delay. The seed laser modulates the electron beam energy in the first undulator (modulator) by an inverse FEL interaction. The energy modulation is converted into a spatial modulation in the dispersive delay thereby generating abundant harmonics in the spatially modulated e-beam. The final undulator (radiator) is tuned to resonate with a harmonic of the seed laser. The radiation generated from HGHG is coherent in both the transverse and longitudinal dimensions. Recently the HGHG FEL at the BNL DUV-FEL facility reached saturation at 266 nm using an 800 nm seed laser. These results have also demonstrated the better stability and narrower spectrum made possible by the seeded HGHG FEL. Yu presented a conceptual design of a 20 fs XFEL based on cascading several stages of HGHG FELs. To control the signal to noise ratio degradation due to frequency multiplication, a higher power seed laser and a shorter modulator will be used along with the so-called fresh bunch technique. The possibility of taking advantage of the longitudinal coherence of the HGHG to produce attosecond XFEL was also discussed at the workshop.

Workshop participants had a lively discussion on the feasibility, performance and R&D issues associated with the seeded XFEL schemes. An improvement of the electron beam quality will certainly be necessary to drive the XFEL. Self-seeding SASE, cascaded HGHG, and SASE pulse compression FELs show the most promise for producing short pulse X-rays. Of these, only he self-seeded and HGHG schemes generate longitudinally coherent radiation. While the pulse length in the self-seeded scheme is determined by the electron bunch length (~100 fs), the pulse length in the HGHG scheme is determined by the short pulse seed laser, and so can be much shorter (~ 20 fs).

References

1. A.M. Kondratenko & E.L. Saldin, Part. Acc. **10**, 207 (1980).
2. R. Bonifacio, C. Pellegrini & L. Narducci, Opt. Com. **50**, 373 (1984).
3. L.-H. Yu, *et al*, Science, **289**, 932 (2000). T. Shaftan, et. al., Proc. FEL 2002 Conf. (2002).

4. S. Milton, *et al*., Science **292**, 2037 (2001).
5. A. Tremaine, *et al*., Phys. Rev. Lett**. 88,** 204801-1 (2002).
6. V. Ayvazyan, *et al*., Phys. Rev. Lett. **88**, 104802-1(2002); Eur. Phy. J. D **20**, 149 (2002).
7. W. Brefeld *e. al*., Schemes for Time Resolved Experiments at the TTF FEL, DESY report 02-038 (2002).
8. E.L. Saldin *et al*, Scheme for Attophysics Experiments at a X-ray SASE FEL, DESY report 02-070 (2002).

The Seeded X-ray Free Electron Laser Workshop Agenda

Conference Room A
Building 725
National Synchrotron Light Source
Brookhaven National Laboratory
Upton, NY 11973-5000, USA

Friday, Dec. 13, 2002 AM: Chair J.B. Murphy

- 9:00 – 9:10 AM: Welcome (P. Paul, BNL Director)
- 9:10 – 9:20 AM Charge to the group (S. Dierker, NSLS Chairman)
- 9:20 – 9:500 AM User Perspective (C.C. Kao, NSLS US)
- Oral Presentations of Seeded and SASE Schemes
- 9:50 – 10:30 AM Cascaded HGHG (L.H. Yu, NSLS)
- 10:30 – 10:40: Coffee Break
- 10:40 – 11:10: Transverse and longitudinal Properties of SASE (Z. Huang, SLAC)
- 11:10 – 11:50: DESY self seeding and laser seeding Schemes (B. Faatz)
- 11:50 – 12:30: Short Pulse at LCLS (S. Reiche, UCLA)
- 12:30 – 1:30 PM Box Lunch
- Friday PM: Max Zolotorev Chair , Conference Room A, Building 725
- 1:30 – 2:00 PM: TTF2 and Its User Program (B. Faatz)
- 2:00 – 3:30 Discussion on critical issues in seeded FEL
- 3:30 – 3:40 PM: Coffee Break
- 3:40 – 4:30 PM: Discussion: Critical experiments for Seeded FEL
- 4:30 – 5:30 PM: Tour SDL (T. Shaftan)
- 6:30 PM Dinner

Saturday, Dec.14, 2002, AM & PM Chair Z. Huang

- 9:30 AM – 3:30 PM Discussions and Report writing

High Gain Harmonic Generation FEL

L.H. Yu

NSLS, BNL, Upton, NY 11973-5000, USA

1. High Gain Harmonic Generation (HGHG)

In the HGHG scheme, there are three components, i.e., one undulator used as the modulator, one dispersion section, and a second undulator used as the radiator. A seed laser, together with an electron-beam, is introduced into the modulator. So, in the modulator, the seed laser interacts with the e-beam, and energy modulation is formed in the e-beam. Then the energy-modulated e-beam passes through the dispersion section (a three-dipole chicane), where the energy modulation in the e-beam is converted into spatial modulation.

Abundant harmonics exist in such spatially modulated e-beam. Then such spatially modulated e-beam enters the radiator. The radiator is designed to be resonant to one of the harmonics of the seed laser. So, once the spatially modulated e-beam enters the radiator, rapid coherent emission at this resonant harmonic is produced, and then, this harmonic is further amplified exponentially until saturation.

2. Cascading stages of HGHG to produce soft x-ray

Cascading two stages of HGHG for soft x-ray FEL to 6 nm has been proposed before. To reach 2.1 nm, we need more than two stages and there are new issues to be addressed here.

There exist commercially available lasers with wavelength about thousands Angstrom. On the other hand, we hope to produce x-ray with a wavelength around several Angstroms. To achieve 2.1 nm by one step of HGHG would require very high harmonic of the order of several hundreds. Previous analysis showed that to generate high harmonic, one needs very high input seed laser power. Beyond 60'th harmonic, this becomes difficult. Also, as we will discuss in the section 3 of this paper, when harmonic is too high, stability of the output is not good. So, we need some modification

1. We need multiple stages. During each stage the n'th harmonic of the seed laser will be produced at the end of the radiator, and then this harmonic will be used as the seed for the next stage. In reality, n should not be too large. In our design we use n = 5 to achieve stable performance. So, if we start from available commercial laser of hundreds nm as the seed, we would need three stages to reach soft x-ray with a wavelength of several nm.

2. Conceptually, the device is composed of two parts. A converter, and an amplifier. The converter consisting of several stages, converts the seed laser to the designed wavelength step by step. Then at the end, an amplifier exponentially amplifies the radiation obtained from the last stage to saturation.

3.Except for the second stage and the last amplifier, each stage only converts the light to its n'th harmonics, and there is almost no exponential growth.

4.Since we need cascade several stages of HGHG, we need some extra components. Each stage will be the same as shown in Fig. 1, i.e., each stage will consist of one modulator, a dispersion section, and one radiator. The physics process in each stage will be the same as in the recent experiment [1,2]. During the process, the output radiation has disturbed a part of e-beam, which coincides with it. So in order to achieve best efficiency to carry out the next stage of HGHG, we need use a fresh e-beam. For this purpose, after one stage of HGHG, we shift the laser (i.e., the output radiation from the previous HGHG stage) to the front part of the same e-beam, so that the laser will interact with a "fresh" part of the same e-beam. This is the "fresh bunch technique" [3, 4]. This is schematically plotted in Fig. 1. We use a chicane (a "shifter") to shift the laser to the "fresh" part of the same e-beam.

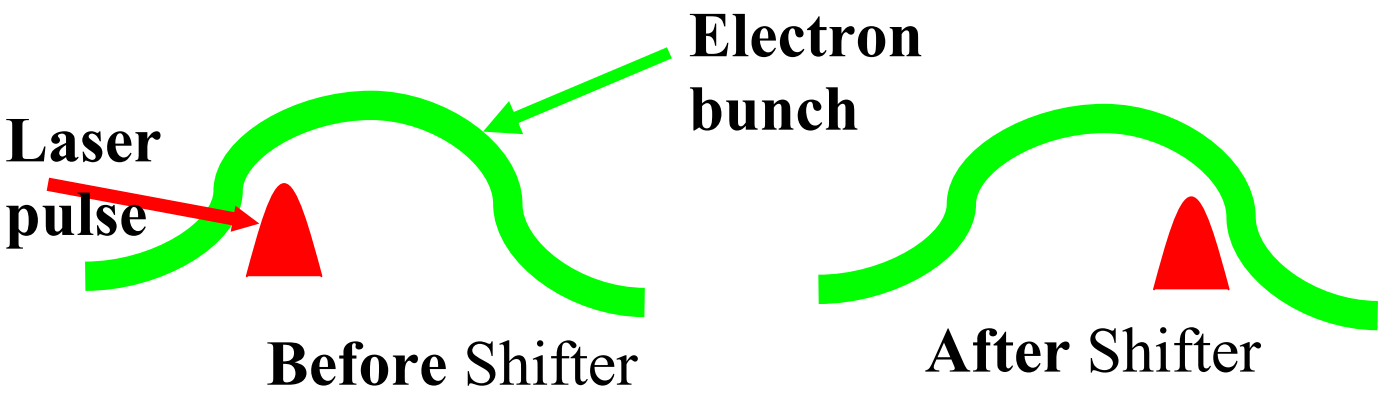

Figure 1. Fresh bunch technique

3. Description of the system

As shown in Fig. 2, we consider an available laser with a wavelength of 266 nm, and a peak power of P_{in}=500MW, and pulse length of 20 fs. The corresponding start-up shot-noise power [11] is only about P_{noise}=30W. So, the input seed laser power dominates the shot-noise power. This is true for all seed lasers into the three stages and the last amplifier. This dominance is necessary, because even though there is only negligible noise power in the initial stage, the "signal-to-noise" ratio of the final radiation at 2.1 nm might be degraded [8]. Calculation (as will be explained in section 3) shows that a 500MW seed laser could ensure that the signal-to-noise ratio at the final 2.1 nm radiation to be around 1000. After 3 stages, we have 2.1 nm radiation, and then this 2.1 nm radiation is amplified to the saturation region with a peak power around 1.7GW by traversing the last undulator, the amplifier.

The parameters for the electron beam, the undulators, and the dispersion section are given in the Figure 3 and the Table 1. Let us first explain the meaning of each parameter in Fig. 3. The number on the first row stands for the output power of each stage. The output power of one stage is the input power of the next stage, though diffraction effect should be taken into consideration as we will discuss shortly. The second row stands for the corresponding wavelength of the radiation. The e-beam parameters are printed just below the schematic device. The system has a betatron function of 6.8 m.

The e-beam has a peak current of 750 Amp , an energy of 2.6 GeV , normalized emittance $\epsilon_n = 1$ mm-mrad , and initial relative local energy spread $\sigma_\gamma/\gamma = 2 \times 10^{-4}$. Due to spontaneous radiation, this is increased. We further upgrade [5] our code to simulate the growing of the relative local energy spread along the undulator, and we found that the results obtained using the same relative local energy spread ($\sigma_\gamma/\gamma = 2 \times 10^{-4}$) agree well with the results given by the upgraded code, so the effect is negligible.

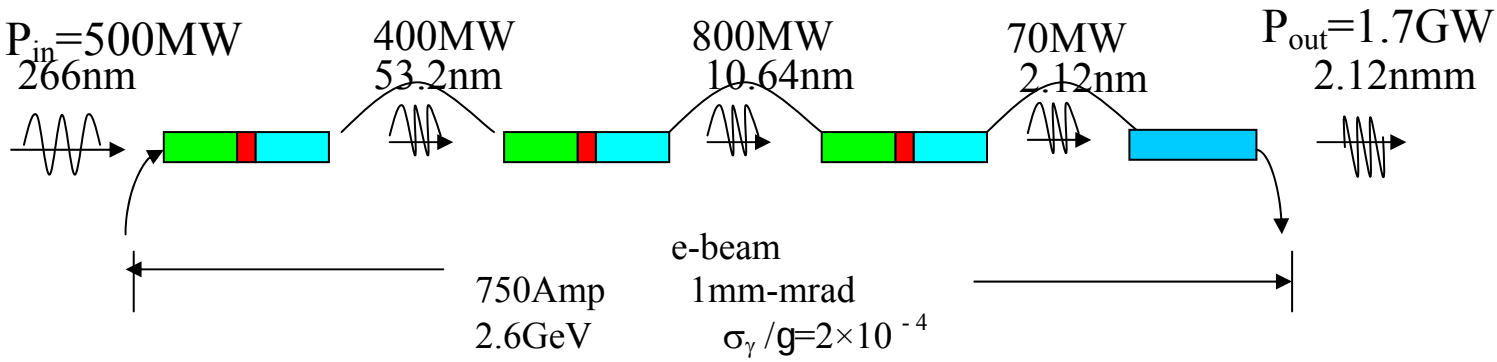

Figure 3.

	1st Stage		2nd Stage		3rd Stage		Amplifier
λ (nm)	266	53.2	53.2	10.64	10.64	2.128	2.128
λ_w(cm)	11	6.4	6.4	4.16	4.16	2.7	2.7
$d\psi/d\gamma$	1.0		1.0		0.5		
L_w(m)	2	6	2	8	2	4	12
L_G(m)	1.6	1.3	1.3	1.4	1.4	1.75	1.75

L_{total}=36 m to reach 1.7 GW

Table 1

For the table, the fist row gives the radiation wavelength. The second row is the undulator period. The third row is the dispersion strength. The fourth row is the length of the undulators (modulators, radiators, and the amplifier). For an example, the last amplifier has a length of 12 m . The fifth row stands for the power e-folding length in each undulator without energy modulation. The table has 4 boxes, the first three stand for the three harmonic generation stages, while the last one stands for the amplifier. In each of these boxes, which stands for each stage, the left column gives the parameters for the modulator, while the right column gives those for the radiator. The numbers in the middle, stand for the dispersion strength $d\eta/d\gamma$ (η is the phase in the radiator).

For an example, the second box stands for the second stage. The left column in this second box stands for the modulator of the second stage. The table shows that in the modulator the resonant radiation has a wavelength of 53.2 nm, the modulator has a period of 6.4 cm , the length of the modulator is 2 m , and the corresponding power e-folding length without energy modulation is 1.3 m . The right column shows that the radiation in the radiator has a wavelength of 10.64 nm , the radiator has a period of 4.16 cm , the length of the radiator is 8 m long, while the corresponding power e-folding length is 1.4 m . The numbers in the middle, i.e. 1.0, stands for the dispersion strength $d\eta/d\gamma$, and energy spread 2×10^{-4} . Similarly for the other boxes, except for the fourth box. The fourth box stands for the amplifier, so there is no dispersion strength $d\eta/d\gamma$. The effect of the global energy spread (or correlated energy spread, in the terminology of certain other workers in this field) is addressed in the following discussion of the sensitivity to the parameter variation, for its effect is essentially an issue of detuning.

Now, let us explore the physics process in such device. As shown in Fig. 3, the 266 nm laser, with a peak power of 500 MW, together with the 2.6 GeV e-beam, are introduced into the modulator of the first stage. So an energy modulation is formed in the e-beam. Then by passing through the following dispersion section, the energy modulation is converted into a spatial modulation. Such a spatially-modulated e-beam will then be introduced into the following radiator. The radiator is resonant to the fifth harmonic of the seed laser, so we will have 53 nm coherent emission to reach 400 MW. The length of the radiator is only four gain lengths so there is almost no exponential growth. In order to go to next stage, we need a shifter, in which the e-beam is magnetically delayed by a small chicane. Therefore effectively, the 53 nm radiation is shifted by 40 fs to the front part of the same e-beam, where the e-beam is still ``fresh''. To have the electron path longer than the straight line by 40 fs, the chicane is 0.35 meter long, with maximum field of 1.5 Tesla.

For the 2.6 GeV e-beam and the parameters we choose for the undulators, we calculated the energy spread increase induced by spontaneous radiation in the undulator, or the quantum diffusion effect [6], and found the effect is negligible, as we mentioned before. So we continue to use the same energy spread of $s_g/g = 2 \mu 10^{-4}$.

Now, the 53 nm radiation serves as the seed laser in the second stage, where the 53 nm radiation input generates a 10.6 nm output with 800MW. Next, after passing through another shifter to interact with the fresh part of the electron bunch, the 10.6 nm radiation is the seed laser for the next stage to be converted to 2.1 nm . Here, we would like to emphasize that, for the first and third stage, the radiators work at the coherent emission region, i.e. after the coherent emission is finished, the radiation is introduced to the next stage almost without exponential growth. This is the key point to make the total length of the device short. Finally, the 2.1 nm is again shifted to a fresh part of the electron bunch to be amplified exponentially to deep saturation at 1.7GW in the last undulator, i.e. the amplifier, of the device.

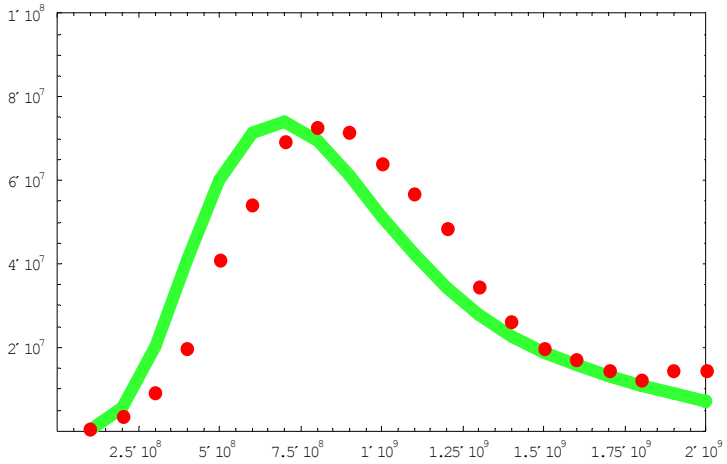

Fig. 4 Output power as function of input power for the third stage. Red dots are simulation using TDA code. Green curve is the analytical estimate of coherent radiation without exponential growth.

We emphasize, in the radiator for the first and third stages, there is almost no exponential growth of the harmonic, but rather, after the coherent emission is finished, the harmonic is introduced to the next stage directly. For an example, the length of the 3rd radiator is only 4 m long, while the corresponding power e-folding length without energy modulation is about 1.4 m. With energy modulation in the harmonic generation process, the gain length is further increased, so no exponential growth is expected.

When the radiation traverses the shifter, there is diffraction loss in the radiation, and has been taken into account. The coherent synchrotron radiation effect (CSR) in the shifter and dispersion magnets has been estimated to be negligible. The path length changes in these chicanes are much smaller than the electron bunch compressor.

We have compared our simulation with an analytical calculation [7]. As an example we plot the output power as a function of the input power in Figure 4. The agreement is similarly good for all other stages.

3. Stability and Signal Noise Ratio

Stability

We need to check the stability of the performance of this system. For each stage, the fluctuation in any parameter of the e-beam, or the seed laser will lead to the fluctuation of the output power of the harmonic at the end of the radiator. But, this output harmonic is the input seed laser for the next stage. Therefore, the fluctuation in the output power of the harmonic in one stage is just the fluctuation in the input power of the seed laser for the next stage. So, the stability consideration could be simplified, i.e. we need only check whether each stage of HGHG could reduce the fluctuation. To make it more explicit, we need to check whether the fluctuation of the output power of the harmonic in each stage is less than the fluctuation in the input power of the seed laser of the same stage.

In Fig. 4, we plot the relation between the output power and the input power for the third stage. The variation in the output power is about 30 % when the input power changes from 60 MW to 120 MW . Thus the fluctuation is reduced. This is an attractive feature of the HGHG scheme. This result is a trade off between better stability and total wiggler length, i.e., if we use lower harmonic number and increase one more stage, the stability will be further improved. Analytical study shows that such attractive feature holds as long as the harmonic number is not too high. In our scheme, we use harmonic number 5. Now that each stage reduces the fluctuation, we could expect that, the radiation fluctuation caused by the fluctuation in the parameters of the previous stage will be stabilized in the following stage. Therefore, not much fluctuation is expected after the whole three stages. So the stability of the whole system is determined mostly by the last amplifier. Since it is only 12m long, compared with the 35 m long undulator in the SASE scheme (about 20 gain lengths to reach saturation for SASE), the stability of the HGHG scheme is expected to be better than the SASE scheme. The results of the calculation confirmed this.

Issues on noise degradation in HGHG process

Saldin et. al. [8] pointed out the shot noise in the undulator may cause a significant degradation of the coherent properties of the HGHG output at very high harmonics. The noise to signal ratio at the input and output satisfies

$$\left(\frac{P_n}{P_s}\right)_{out} = N^2 \left(\frac{P_n}{P_s}\right)_{in} \tag{3.1}$$

where N is the harmonic number. In their case, in order to generate very small energy modulation, the input laser power is of order of several tens of megawatts. The start-up noise (shot noise) is about 100 watt, and the harmonic number is about 30 to achieve 8 nm, then Eq.(4.7) gives an output noise to signal ratio of about 1%. Let us consider applying Eq.(4.7) to the scheme proposed here. The scheme employs a fresh bunch technique [3] where after each HGHG stage the (short) laser pulse is shifted to a new (fresh) part of the electron bunch. In this approach, we can generate very large energy modulation at each HGHG stage and generate harmonic radiation at several hundreds megawatts level. The input laser power of the modulator of the first stage is 500MW, while the shot noise is only 30 watt. Therefore, the noise given by Eq.(4.7) using the harmonic number N=125 is 0.1% of the output signal at the 2.1 nm. The radiator is 6 m long with SASE output about 600 W, while the output is 400 MW for this stage. Hence the noise given by Eq.(4.7) is also 0.1% of the output signal at the 2.1 nm. For the second stage, power input is 400MW, but now the harmonic number is lower by a factor of 5. For other stages, since the harmonic number is further reduced, the contribution to the noise degradation is negligible in our case. Therefore the shot noise in the undulator, even though an important issue, coverts to a noise level at the final output of order of about 0.1% of the signal.

4. Challenges

There are many challenging issues with the development of the soft-x-ray FEL using HGHG scheme. Clearly, the requirement on the electron beam quality is very challenging, in particular the high current and the low emittance. In this section, we emphasize the following issues associated with FEL itself:

1. The synchronization between the electron bunch and the laser seed. The fresh bunch technique overcomes the issue created by the FEL interaction of one HGHG stage by shifting the light pulse to a new and fresh part of the electron bunch, thus allowing strong energy modulation and thus significantly improve the efficiency of the harmonic generation process, and reduces the degradation effect of the shot noise. However, this requires that the jitter between the laser and the electron bunch to be much smaller than the bunch length. For a bunch length of 500 fs, and input laser pulse length of 20fs, we assume the shifters shift the light pulse 40 fs between stages. Thus the total used part of the electron bunch after the electron bunch passes through the whole system is about 200 fs. Hence the jitter between the laser and the electron bunch should be less than 100fs. The current system used for our UVFEL has a time jitter about 0.5 ps. Therefore we need to develop a feedback system to reduce the jitter to bellow 0.1ps. The DUVFEL program provides an opportunity to carry out such a research and development project.
2. Recent SASE experiment at DUVFEL project showed that the start-up noise in SASE at 400 nm is larger than SASE theory's shot noise prediction by about a factor 30. The source of this increase is still under investigation. One possible reason is that in the compression process, the structures in the longitudinal phase space of the electron bunch is amplified and creates enhanced micro-bunching with components in the wavelength

range of 400 nm. This micro-bunching produces coherent radiation in the beginning section of the undulator which is then amplified exponentially, and evidenced itself as an enhanced start-up noise. If we use this enhanced start-up noise in eq.(3.1) to estimate the output noise degradation, we find that the noise signal ratio is increased from 0.1% to 3%. This level is an acceptable level. However, we need to understand the mechanism of this enhanced start-up noise, study its frequency dependence to see its effect in the soft-x-ray region, and find methods to reduce this noise. Again, the current DUVFEL provides an opportunity for this investigation.

One possible method is to remove energy chirping, and then send the electron bunch through a chicane to wash out the micro-structure in the electron bunch. This may also help to reduce the damaging effect of the coherent synchrotron radiation in the compression process

3. Undulator trajectory error tolerance. The most stringent requirement for trajectory in the undulator is determined by the 12 meter 2.1 nm amplifier (L_w =12 m, λ_s=2.1 nm). We assume that, as described before, the undulator system consists 2 meter long modular sections separated by 0.5 meter spaces, and there are position monitors in the middle of modular sections so that the trajectory can be corrected every L_s =1.25 meter. The gain length is L_G =1.75 m. When the spacing between the correction station L_s is smaller than the gain length L_G, as is our case, the trajectory tolerance is derived from a fomula given in the reference [9]:

$$x_{tol} = \left(\frac{L_s}{L_G}\right)^{\frac{3}{4}} \times 0.266\sqrt{\lambda_s L_G}\left(\frac{L_G}{L_w}\right)^{\frac{1}{4}} \qquad (4.1)$$

This formula has been compared with simulation for many different occasions, the agreement is within about 40%. When we substitute the parameters into this equation, we find the tolerance is 8 μm. If the trajectory is deviating from the axis by more than this, the output power is dropped by half. For a single pass FEL with exponential growth, this is acceptable loss which can be compensated by appropriate increase of the length of the undulator. But this tolerance still give an rough estimate of the allowable tolerance on the trajectory. The present diagnostic system based on HeNe laser alignment in the DUVFEL has achieved reproducibility and resolution of 20 μm. We need to further improve the quality of the HeNe profile images in the undulator to obtain a better resolution. Because the present resolution is determined mostly by the defects of the YAG crystal of the beam position monitors, and the mechanical reproducibility of the position of the BPM, this improvement can be achieved. Another important direction for trajectory correction is the beam based alignment procedure being developed now for the DUVFEL[10]. Because e-beam size is much smaller than the HeNe beam size, the resolution will clearly be better. The analysis also provides information about the trajectory between monitors. Therefore the DUVFEL program provides

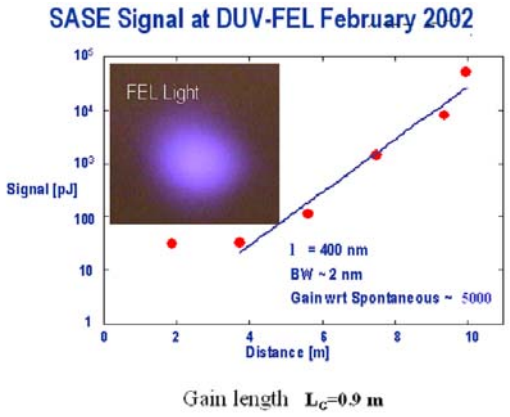

Fig. 5 The output radiation profile and the measured power as function of distance in NISUS in the 400 nm SASE experiment of Feb. 2002

another opportunity for us to meet the challenges.

5. Resent DUVFEL Experiment

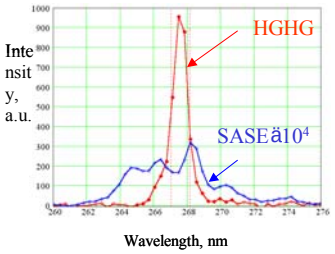

Fig. 6 The single shot spectrum of HGHG and SASE for the same electron beam condition in the 266 nm HGHG and SASE experiment on October 28, 2002

The DUVFEL experiment is carried out in the Source Development Lab (SDL) of the National Synchrotron Light Source (NSLS). In February of 2002, we achieved SASE at 400 nm in the radiator undulator named NISUS. In figure 5, the radiation power measured along the NISUS undulator is plotted versus the distance in the NISUS, showing the exponential growth of radiation. This plot gives the gain length of 0.9 m. When compared with the gain length of 1.1 m based on the design parameters, this shows that the system already satisfied the required conditions for the HGHG experiment. In May we began to install the seed laser injection line, and in September we installed the 0.8 m modulator named the MINI undulator. In late October, we achieved successful output of HGHG, generating 266 nm from an 800 nm titanium sapphire laser seed. In figure 6, we show the HGHG and the SASE single shot spectrum for the same electron beam condition. In order to show them on the same scale we need to multiply the SASE spectrum by 10^4. The fluctuation of the HGHG is 15%, as compared with the 39% of SASE for the same electron beam condition (Figure 7). The fluctuation of HGHG is due to the large electron beam fluctuation on the day of the measurement, while that of the SASE came from both the intrinsic fluctuation and the beam fluctuation. This shows the significant improvement in the stability of the HGHG process.

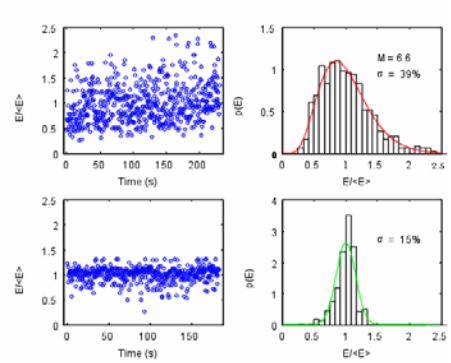

Fig.7 Output intensity vs. time and its distribution histogram for SASE (top row) and HGHG (bottom row) under the same electron beam condition

The output reached 130 mJ with a sub-pico-second pulse length. The measure power vs. undulator distance shows clearly the saturation (Figure 8). The theory predicts a 3rd harmonic output at 88 nm that would be 1% of the fundamental at 266 nm when saturation is achieved. This has been confirmed recently. The 88 nm radiation will become useful for many new types of experiments in chemistry. In January the first user application experiment of the DUVFEL has started. In the experiment, ethane molecules were ionized by the intense 88 nm radiation, the velocity distribution of the fragments was measured, providing information about the molecular structure and dynamics. If we upgrade our electron beam energy from the present maximum of 200 MeV to 300 MeV, we can generate coherent radiation below 100 nm with more than 100 mJ per pulse. This will produce an unprecedented high brightness radiation in this

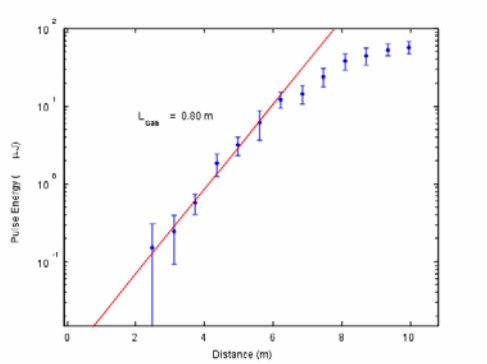

Fig.8 Output intensity vs. the undulator distance in logarithmic scale showing exponential growth, and saturation at about 8 m.

wavelength region, which will allow for many new applications in different branches of chemistry.

5. Conclusion

In conclusion, the cascading HGHG scheme is an attractive scheme to generate coherent soft-x-ray. Among advangates, the most attractive feature is that, the HGHG FEL will provides an intense output as short as 20fs, another advantage is its stability and its longitudinal coherent output. There are many challenging issues associated with this scheme, the DUVFEL program provides an excellent opportunity to study these issues.

References

1. L.-H. Yu, M. Babzien, I. Ben-Zvi, L.F. DiMauro, A. Doyuran, W. Graves, E. Johnson, S. Krinsky, R. Malone, I. Pogorelsky, J. Skaritka, G. Rakowsky, L. Solomon, X.J. Wang, M. Woodle, V.Yakimenko, S.G. Biedron, J.N. Galayda, E. Gluskin, J. Jagger, V. Sajaev, I. Vasserman, Science, 289 (5481), 932(2000).
2. A. Doyuran[1, †], M. Babzien[1], T. Shaftan[1], S.G. Biedron[2] ,L. H. Yu[1], I. Ben-Zvi[1], L.F. DiMauro[1], W. Graves[1] , E. Johnson[1], S. Krinsky[1], R. Malone[1], I. Pogorelsky[1], J. Skaritka[1], G. Rakowsky[1], X.J. Wang[1], M. Woodle[1], V. Yakimenko[1], J. Jagger[2], V. Sajaev[2], I. Vasserman[2] , "CHARACTERIZATION OF A HIGH-GAIN HARMONIC GENERATION FREE-ELECTRON LASER AT SATURATION", Phys. Rev. Lett. 86, 5902 (2001)
3. L.H. Yu, and Ilan Ben-Zvi, Nucl. Instrum. Methods Phys. Res. A393, 96(1997).
4. I. Ben-Zvi, K.M. Yang, and L.H. Yu, Nucl. Instrum. Methods Phys. Res. A318, 726(1992).
5. Juhao Wu, private communication
6. E.L. Saldin, E.A. Schneidmiller, and M.V. Yurkov, Nucl. Instrum. Methods Phys. Res. A 381, 545(1996)
7. Li Hua Yu and Juhao Wu, Nucl. Instru. Meth. A483 (2002) 493-498
8. E.L. Saldin, E.A. Schneidmiller, and M.V. Yurkov, Opt. Commun. 202, 169 (2002)
9. L.H. Yu, S. Krinsky, R.L. Gluckstern, and J.B.J. van Zeijts, Phys. Rev. A45, 1163(1992).
10. L. H. Yu[1], L.F. DiMauro[1], A. Doyuran[1, †], W. Graves[1], E. Johnson[1], S. Krinsky[1], S. Mikhailov, G. Rakowsky , J. Skaritka[1], T. Shaftan[1], B.Sheehy, J.H.Wu,"The DUV-FEL Development Program, Proceedings of PAC2001, Chicago (2001)
11. Li Hua Yu, Phys. Rev. E 58, 4991(1998).
12. Doyuran, W. Graves, R. Heese, E. D. Johnson, S. Krinsky, H. Loos, J.B. Murphy, G. Rakowsky, J. Rose, T. Shaftan*, B. Sheehy, J. Skaritka, X.J. Wang, L.H. Yu, "First SASE and Seeded FEL Lasing of the NSLS DUV FEL at 266 & 400 nm ", Proceedings of FEL 2002, Chicago (2002

SASE FELs

Z. Huang
SLAC, CA 94025, USA

The third-generation synchrotron radiation facilities make use of the bright spontaneous radiation from undulators in the straight sections of optimized electron storage rings. Single-pass, high-gain free-electron lasers (FELs) based on self-amplified spontaneous emission (SASE) are proposed for the next generation of high-brightness x-ray sources [1,2]. For the spontaneous emission, the radiation intensity is an incoherent sum of contributions from individual electrons. For SASE [3], the initial spontaneous radiation interacts back with the electron beam in a long undulator and creates energy and density modulations on the scale of the radiation wavelength λ (referred as "microbunching"). Hence, the SASE radiation is amplified exponentially due to the microbunching process, until the radiation intensity is saturated at a level that is roughly one million times higher than the spontaneous radiation. Together with its excellent transverse coherence and a much shorter pulse duration (typically on the order of a hundred femtosecond instead of tens to hundreds picosecond from the third-generation facilities), SASE radiation offers a potential peak brightness enhancement of about ten orders of magnitude. Due to the unprecedented peak brightness, the average brightness of SASE sources driven by even a low repetition-rate electron linac can still exceed the performance of the third-generation light sources.

A remarkable feature of the SASE radiation is its transverse coherence. For the spontaneous undulator radiation, the transverse phase space is the incoherent sum of the electron phase space, which is typically larger than the diffraction-limited phase space area $\lambda/4\pi$ at x-ray wavelengths. In a SASE FEL, the initial transverse phase space of the spontaneous emission consists of many spatial modes. Higher-order spatial modes have stronger diffraction than the fundamental mode, while the beam-radiation interaction is localized within the electron beam. Thus, the fundamental mode has the highest gain and eventually becomes the preferred spatial distribution for the SASE radiation, which appears to be guided throughout the undulator (referred as "optical guiding" or "gain guilding"). This implies that the SASE radiation is almost fully transversely coherent after a sufficient undulator distance. The e-folding length of the radiation power in the fundamental mode is the gain length and is an important design parameter that depends on both electron and undulator parameters.

Although SASE FELs have excellent transverse coherence, its temporal properties are far from ideal. The FEL gain bandwidth is typically much larger than the Fourier transform limited bandwidth at x-ray wavelengths, implying the coherence length much smaller than the pulse length. Due to the noisy start-up, SASE is a chaotic light temporally with M coherent modes, where M is the ratio of the x-ray pulse length and the coherence length. In other words, the longitudinal phase space of SASE is M times larger than the Fourier transform limit. The total radiation energy exhibits statisical fluctuate, with an rms deviation given by $M^{-1/2}$. Note that M is not a constant in the SASE process. In the

exponential growth regime, M decreases as the coherence length builds up. However, after saturation, M starts to increase due to the reduced coherence. For recent SASE experiments at longer wavelengths, M is typically just a few, and the intensity fluctuation may be dominated by the statistical fluctuation. For an x-ray SASE FEL, M is typically on the order of 100, and the statistical fluctuation of the radiation energy could be much smaller than fluctuations from machine jitters. In the frequency domain, there is also about M modes that are separated by the Fourier-transform limited bandwidth. Using a monochromator, a single frequency mode may be selected with a hundred percent intensity fluctuation.

In addition to the intense radiation at the fundamental resonant wavelength λ, SASE FELs employing a planar undulator are capable of generating significant harmonic radiation, especially at the third harmonic wavelength $\lambda/3$. This is because the density modulation created by the FEL interaction becomes very spiky near saturation, consisting of rich harmonic content. Since the FEL microbunching is driven by the radiation at the fundamental wavelength, the gain length, the transverse coherence, and the temporal structure of these induced harmonics are governed by those at the fundamental. For example, driven by the third power of the fundamental field, the third nonlinear harmonic grows three times faster, is also transversely coherent, and has a more spiky temporal profile with a larger shot-to-shot fluctuation when compared with the fundamental. Near the FEL saturation, the intensity of the third nonlinear harmonic radiation is on the order of one percent of the fundamental and can be used to extend the wavelength reach of SASE sources.

Driven by the intense R&D efforts towards x-ray FELs, a large number of SASE experiments push the lasing wavelengths from infrared to visible and on to ultraviolet. Several recent experiments have reached intensity saturation and have confirmed most of the theoretical predictions about SASE FELs. For example, the LEUTL team at Argonne National Laboratory demonstrated exponential growth and saturation of radiation energy at 530 nm and 380 nm [4]. Frequency-resolved optical gating (FROG) techniques were used to characterize both the intensity and the phase of the LEUTL FEL [5]. The VISA group at Brookhaven National laboratory characterized the properties of the second and the third nonlinear harmonic radiation near and at saturation [6]. The TTF collaboration at DESY measured the SASE fluctuation that is predicted by the statistical fluctuation and demonstrated the excellent transverse coherence of the source [7]. Successful user operations were conducted at the TTF FEL near 100 nm, the shortest wavelength FEL up to date.

Nevertheless, an x-ray SASE FEL is still two or three orders of magnitude shorter in wavelength than the present FELs. In addition to higher electron beam energy and longer undulator distance, the brightness of the electron beam must also be sufficient to drive an x-ray FEL. Therefore, many technical challenges are still ahead, such as generation and preservation of high-brightness electron beams, machine stability and error tolerances [8].

In summary, a high-gain FEL operated in the SASE mode is the most straightforward approach to achieve extremely high-brightness, next-generation x-ray sources. However,

the temporal properties of SASE FELs may be further improved upon if necessary. For example, in order to reduce the SASE bandwidth and the intensity fluctuation, a temporally coherent source may be achieved by using an external seed laser at longer wavelengths (such as in HGHG) or by self-seeding (such as in a two-stage approach). In addition, SASE pulse lengths are determined by electron bunch lengths and are typically on the order of a hundred femtosecond. Many advanced applications require x-ray pulse lengths on the order of tens of femtosecond or less. Thus, SASE FELs can be tailored to produce x-ray pulses that are much shorter than the electron bunch length. The unique properties of SASE x-ray sources together with developments of many improvement schemes will have the opportunity to revolutionize the field of synchrotron radiation science.

[1] TESLA Techinical Design Report, DESY TESLA Report 2001-23, DESY TESLA-FEL 2001-05 (2001).

[2] Linac Coherent Light Source Design Study Report, SLAC-R-593, UC-414 (2002).

[3] For a review on SASE physics and a partial list of references, see K.-J. Kim and Z. Huang, *Present Status of X-ray FELs*, in Proceedings of the ICFA Beam Dynamics Workshop on the Physics of and Science with the X-ray Free-Electron Laser (AIP Conference Proceedings **581**, New York, 2001), and also see Refs. [1,2] and references therein.

[4] S. Milton *et al*., Science **292**, 2037 (2001).

[5] Y. Li *et al*., Phys. Rev. Lett. **89**, 234801 (2002).

[6] A. Tremaine *et al*., Phys. Rev. Lett. **88**, 204801 (2002).

[7] V. Ayvazyan *et al*., Phys. Rev. Lett. **88**, 104802 (2002); Eur. Phy. J. D **20**, 149 (2002).

[8] For a review on accelerator physics issues, see P. Emma, *Accelerator Physics Challenges of X-ray FEL SASE Sources*, in Proceedings of the Eighth European Particle Accelerator Conference (Paris, France, 2002).

Short Pulse Program of LCLS

S. Reiche

Department of Physics and Astronomy
UCLA
LA, CA 90095, USA

1 The LCLS Short Pulse Program

1.1 Introduction

The Linac Coherent Light Sources (LCLS) is an X-ray Free-Electron Laser project, currently under construction at SLAC, Stanford. A driving beam of 15 GeV and a 120 m long undulator with a period length $\lambda_u = 3$ cm and an rms undulator parameter of $a_u = 2.27$ yield a resonant radiation wavelength of 1.5 Å. The wavelength range is extendable to 15 Å with lower beam energies.

To reach saturation within the 120 m of the LCLS undulator, beam parameters of 3.4 kA current, 1.2 mm·mrad transverse emittances, and $5 \cdot 10^{-5}$ energy spread or better are required. The total charge is 1 nC with a step profile for the longitudinal charge distribution and a FWHM bunch length of 230 fs. Detailed simulation, starting from the rf photo-gun through the beam line and undulator have shown that all effects, which can degrade the FEL performance, reduces the output energy of the LCLS FEL only by 20-30 % compared to the design parameters. The reduction is acceptable with respect to an overall gain of over 6 orders of magnitudes.

After the initial stage of experiments at LCLS are finished experiments are planned to reduced the FEL pulse length down to 40 fs or less. The motivation comes from experiments such as single shot imaging of molecules/proteins or spectral analysis of ultra-fast chemical processes. (femto-chemistry). Longer pulses would degrade the resolution of these experiments beyond an acceptable level. Before the proposal will be written in summer 2003, different methods to shorten the FEL pulse are studied for performance and realization within the frame of the existing LCLS beamline. This article is a review of all schemes considered. Those, which show the most promising performances, will be used in the proposal.

1.2 Radiation Beam Manipulation

All schemes, which are manipulating the radiation beam, require a chirp, a correlation between radiation wavelength and longitudinal position. It is achieved by running the electron bunch with less charge than 1 nQ. The wakefields in the main part of the SLAC linac are reduced and do not compensate the electron beam chirp, used for bunch compression. With the control on the bunch charge, the degree of energy chirp can be controlled up to an limit of roughly 1% over the entire length of the bunch (230 fs FWHM). Due to the square dependence of the radiation wavelength on the beam energy, the frequency chirp is twice as large as the energy chirp of the electron beam. The cooperation length for LCLS is less than 1 fs, about 200 slices of the electrons bunch amplifies the radiation field independently, resulting in a smooth frequency chirp along the pulse.

1.2.1 Pulse Compression

For pulse compression the output radiation of the FEL is injected into an optical beamline with gratings and mirrors, optimized for the X-ray wavelength of the FEL. The gratings reflects the incident radiation under different angle for different frequencies. In a set-up, similar to the magnetic chicane of a bunch compressor, higher frequency components are deflected less and, thus, have a shorter path length than those for lower frequencies.

The compression is estimated to be a factor of around 10, resulting in pulse lengths between 10 – 40 fs. The longitudinal coherence of the FEL is not further improved and in average a spike per femtosecond is present.

This scheme conserves the energy of the FEL pulse and the number of photons. The radiation power and the photon flux is increased by about one order of magnitude due to the compression. All other schemes, discussed in the following, only preserves the photon flux. Thus pulse compression is most promising for experiments, requiring a large peak power level. The disadvantage is that the radiation pulse exhibit a wide spectrum, twice as large as the energy chirp of the electron bunch. In addition the transverse overlap is not perfect because the individual spikes before compression have a slight variation in transverse size, diffraction angle and wavelength. The transverse coherence of the compressed pulse is degraded.

1.2.2 Pulse Slicing

Pulse slicing is similar to pulse compression, where the dispersive pair of gratings is replaced by a narrow bandwidth monochromator. Due to the energy chirp a correlation between the frequency and the longitudinal position of the spikes is introduced. The frequency bandwidth of each individual spike is about 2ρ, roughly corresponding to the Fourier limit of the spike length of about 1 fs.

A suitable monchromator is Ge(111) with a relative bandwidth of $1.3 \cdot 10^{-4}$, which is about a tenth of the FEL bandwidth. As a consequence each spike, passing the monochromator, is stretched by a factor of 10. Due to the frequency chirp only a few spikes in the frequency domain fall within the bandwidth of the monochromater.

The required wavelength chirp can be estimated by $\Delta\omega/\omega_0 = 2\rho\Delta T/\Delta t$, where ΔT is the full pulse length of the FEL pulse at the exit of the undulator and $\Delta\omega$ is the corresponding frequency width. The desired length of the slice is Δt. With $\rho \approx 5 \cdot 10^{-4}$ and $\Delta t = 10$ fs, the required chirp is 2%. It selects about 10 slices. Due to the stretching of each spike the resulting pulse length is about 20% – 40 % larger than the estimate, given above.

The bandwidth of the monochromator is close to its optimum value. A narrower bandwidth would stretch the spikes too much, while a wider bandwidth would require a stronger chirp than 1% in the beam energy, which is the limit of the LCLS beamline without reoptimization of rf phases and bunch compressor settings.

1.2.3 Two Stage Pulse Slicing

The two stage pulse slicing tries to avoid the power load problem of optical elements in the pulse slicing scheme, described above. Most of the saturated FEL pulse with an average power of about 5 GW is absorbed, causing damage to the monochromator and thus reducing its life time.

In the two stage set-up the first undulator is shorter than the saturation length. Because the power level is lower the heat load of the monochromator is reduced and the life time is enhanced. A magnetic chicane for the electron beam bypasses the optical elements and recombines the electrons with the monochromized FEL pulse at the beginning of a second undulator. This stage acts as an FEL amplifier, where the seeding 10 fs signal is amplified up to saturation. To conserve the bunch length the second stage has to fulfill two conditions. The first condition is that the power level of the seeding pulse is much larger than the shot noise power level of the electron bunch. Second, the undulator should be short enough, that only the seeding pulse reach saturation but not the SASE amplification of the remaining part of the bunch, which cannot be suppressed. If the average seeding signal is higher in power, the length of the second stage FEL can be reduced.

The estimated loss in the transmission line between the exit of the first stage to the entrance of the second stage is estimated with 90 %. Compared to an amplification of about 4 order of magnitudes in the first stage, the seeding signal is in average three orders of magnitude above shot noise power. The overall length of the two stage FEL is 30 – 40 % longer than the standard undulator for LCLS.

1.3 Electron Beam Manipulation

In contrast of manipulating the radiation beam, electron beam parameters can be alter during or before the FEL amplification to reduce the pulse length. The straight forward solution to reduce the overall bunch length is not beneficial because a stronger compressed bunch causes stronger wakefields and degrades the electron beam quality. The other method of running the LCLS linac with a much lower charge and a shorter pulse is limited by the resolution of the beam diagnostic along the beam line. In addition the entire linac has to be reoptimized to achieve optimum bunch compression.

In the electron beam based schemes most of the bunch is inhibited to amplify the spontaneous radiation to achieve short FEL pulses. The required beam conditioning can yield a strong distortion in the orbit within the undulator, up to a point, where beam losses occurs. The resulting radiation background reduces the lifetime of the undulator modules. Therefore it is desirable to scrape those part of the bunch, which are not conditioned to lase. The most promising method is to scrape the tail of the electron bunch in the dispersive section of the second bunch compressor of the LCLS beam line. The wakefields are unaltered over the remaining part of the bunch while accelerating and transporting the bunch to the undulator. Because the bunch is not reduced down to 10 - 40 fs, it

has not the low charge limitation as discussed in the previous paragraph. The aim is to shorten the bunch length to around 100 fs, removing all those part, which can cause beam losses in the undulator due to the beam manipulation, described in the next sections.

1.3.1 Undulator Wakefields

Undulator wakefields act on the electron bunch as a local change of the beam energy. It is always synchronized to the electron beam. If the total energy change at any position of the electron bunch is larger than the FEL bandwidth, the FEL amplification stops for the central resonant wavelength and the SASE process selects a different wavelength to be amplified. Because the undulator wakefield is still the same, neither this new frequency nor any of the following adjustments in the resonant wavelength will reach saturation.

The undulator wakefields have three different sources. The dominant is the resistive wall wakefields of the vacuum chamber. Geometric wakefields (change in the vacuum pipe aperture) and surface roughness wakefields are on a percent level compared to the resistive wall wakefields. The parameters of the resistive wall wakefield are the beam pipe diameter, which is fixed in the LCLS undulator design and the vacuum chamber material. Copper plated vacuum chambers for the first stage of LCLS yield the overall smallest wakefields and least modulation in the beam energy.

With a linear taper of the undulator field a fixed energy loss by wakefields can be compensated. Due to the energy bandwidth of the FEL of about 2ρ FWHM only those parts of the bunch amplifies the spontaneous radiation, where the energy loss differs only slightly from the compensated energy loss. For the LCLS ρ-parameter of $5 \cdot 10^{-4}$ the acceptance bandwidth is 100 ke/m around the compensated energy loss.

The wake potential for the copper-plated vacuum chamber and the design LCLS profile (step profile) lies within this energy acceptance for most parts of the bunch. Only the transient of the wakefields at the head of the bunch has larger gradient. Adjusting the taper for the maximum in the wake potential reduces the bunch length to 40 μm.

The choice of other vacuum chamber materials alters the wake potential. In particular materials with higher resistivity increases the wakefield amplitude and, thus, reduces the part of the bunch, which falls within the energy loss acceptance of the undulator taper. Promising is graphite, which increases the wake potential, so that it almost grows linearly along the bunch. The compensated energy loss occurs only once within the wake potential and allows to chose the taper gradient freely. In comparison the wake potential for copper is not monotonic over the bunch length and enforces that only the maximum of the wake potential can be compensated by the taper to avoid multiple FEL pulses per electron bunch. Simulation for graphite shows that FEL pulse lengths of around 5 fs can be achieved, while the remaining part of the bunch emits close to the power level of the spontaneous radiation.

The use of the wake potential can be combined with methods of beam con-

ditioning prior to injecting into the undulator. Start-end simulation for the standard LCLS case indicate a trailing spike in the current of about 15 kA, while the part of the bunch after that spike is spoiled for the FEL amplification due to high energy spread and emittance. Selecting this spike, where the wake potential for copper is similar in amplitude to the amplitude for the graphite case of a flat profile, roughly the same FEL pulse length of about 5 fs can be achieved.

Further investigation of this method includes the high frequency limit of the wake potential, where the explicit wake potential might differ from the model, used for the initial simulations.

1.3.2 Beam Conditioning

Unlike the undulator wakefields, which acts during the FEL amplification, beam conditioning is applied within the LCLS beam line before the undulator. There are various methods to condition the bunch. The simplest one is a correlation between longitudinal and transverse position. Within the LCLS an offset of more than 10 microns would strongly reduced the FEL amplification for a given electron slice, because the centroid of the slice performs the betatron oscillation within the FODO lattice of the undulator and reduces the overlap with the radiation field. To select a subsection of the bunch of about 20 fs, the overall offset between head and tail of the full LCLS bunch (about 200 fs) is no more than 200 microns. This tilting of the bunch is done in the second bunch compressor, when the dispersion is not compensated at the end of the bunch compressor, or be an rf deflecting cavity.

Another method is to inject the electron through a higher order mode cavity, combined with a solenoid. The time-dependent effects of the rf-field introduces a longitudinal variation in the orientation of the transverse phase space distribution. Instead of a centroid offset, described in the previous paragraph, the beam will be strongly mismatched to the undulator FODO lattice, except for the short part of the bunch, which is not affect by the higher order mode field. The minimum FEL pulse length, obtained by this scheme, has still to be estimated.

1.4 Conclusion

Short FEL pulses can be achieved by either manipulating the radiation pulse or the electron beam. Pulse compression and pulse slicing are easy to implement and allows also a control over the pulse length with the applied energy chirp of the electron beam. If power handling of the optical elements (grating, monochromator) is a problem an extended two-stage set-up solves this problem but requires about 30 % more undulator length and additional beam line component for the electron beam.

FEL pulse manipulation are limited to around 10 – 20 fs. To achieve shorter pulses electron beam manipulations are showing promising simulation results. The use of undulator wakefields requires a change in the undulator vacuum chamber material. This would automatically exclude the long pulse operation

of LCLS. A solution would be a combination between wakefield effects for the standard copper plated chamber and an asymmetry in the current profile and slice emittance and energy spread. The latter can be controlled to a certain degree by changing the bunch compressor settings and the rf phase. A similar method is to alter electron slice parameter prior to injecting into the undulator, such as tilting the beam along one of the transverse axises, or a longitudinal change in the orientation of the transverse phase space distribution by using higher mode cavities.

The schemes, presented here, are part of a proposal for a short pulse experiment at LCLS. All schemes have to be analyzed in detail in the near future. The most promising methods will be used for the proposal, to be written in summer 2003.

Seeded FEL R&D at DESY

B. Faatz for DESY TEAM
DESY, D-22607 Hamburg, Germany

1. Self-Seeding (two-stage) Scheme

A single-pass X-ray SASE FEL can be modified to reduce significantly the bandwidth and the fluctuations of the output radiation [1]. The modified scheme consists of two undulators and a monochromator between them. The first undulator operates in the linear regime starting from noise and the output radiation has the usual SASE properties, i.e. following Gaussian statistics. Behind the first undulator the electron beam is guided through a bypass and the photon beam enters the monochromator which selects a narrow band of radiation. At the entrance of the second undulator the monochromatic beam and the electron beam are superimposed. Along this undulator, the radiation is amplified until saturation is reached. The scheme is illustrated in Fig 1.

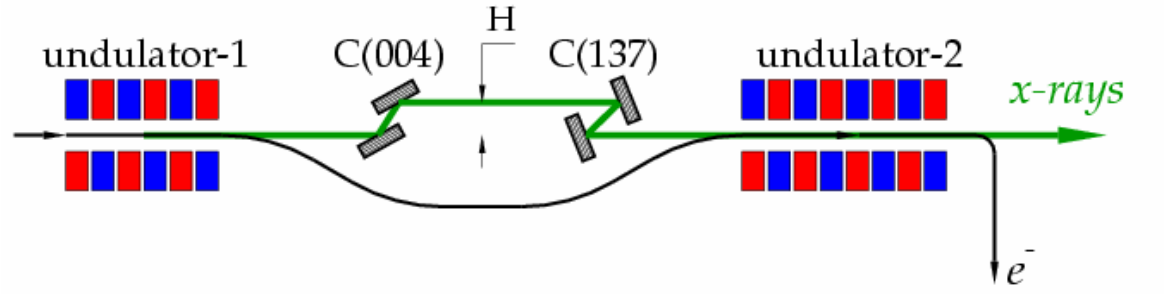

Figure 1: Schematic layout of the two-stage FEL with the SASE FEL (left), a monochromator and electron debuncher (middle) and an amplifier (right). In this example, optical elements in the X-ray wavelength range are shown.

The electron micro-bunching induced in the first undulator must be destroyed before the electrons arrive at the second undulator. This is achieved by path length differences due to the natural energy spread of the electron beam when guided through the bypass. At the entrance of the second undulator, the monichromatized radiation dominates significantly over the shot noise and the residual electron bunching, and the input signal bandwidth is small with respect to the FEL amplifier bandwidth. The monochromatization is performed at a relatively low level of radiation power, which allows the use of conventional X-ray optical elements for the monochromator design. X-ray grating techniques can be used successfully down to wavelengths of several nanometers, but at shorter wavelengths crystal monochromators are required. The remainder of this section deals with parameters for the X-ray FEL. A more detailed design in the VUV wavelength range will be briefly discussed at the end.

The SASE FEL bandwidth at the exit of the first stage is about 7×10^{-4} and weakly depends on the gain. The monochromator bandwidth needed is about 1.4×10^{-6}. Its overall efficiency is expected to be in the range of 0.3 - 0.5. Requiring the input radiation power at the entrance to the second undulator to exceed the effective shot noise power by two orders of magnitude (see [2]) a gain of 1.5×10^{5} has to be achieved in the first

undulator. The SASE FEL gain at saturation would be about 4×10^6, so that the first undulator is indeed still in the linear regime as required.

For a 1.3° bending angle of the chicane magnets, the total length of the chicane is about 40 m. The electron beam microbunching is completely destroyed at the end of the bypass due to the uncorrelated energy spread and reasonable longitudinal dispersion of the chicane [1]. Due to the small angular divergence of the radiation coming out of the first undulator, focusing of this radiation is not necessary. Indeed, calculations show that if the radiation is optimally focussed, the input coupling factor to the eigenmode in the second undulator is larger by about 30% [3]. The main requirements for the X-ray monochromator of the two stage XFEL are:

1. degree of monochromatization: $\lambda/\delta\lambda = E/\delta E = 0.7 \times 10^6$.
2. tunability range: a few keV.
3. resistance to high heat load.

A value of monochromatization of 10^7 and more is possible using Bragg reflections. For our applications, the relative spectral width for a given Bragg reflection is independent of the energy or glancing angle of X-rays and defined merely by properties of the crystal and the reflecting atomic planes. In particular, the dynamic diffraction theory implies that the choice of a crystal, the reflecting atomic planes and the crystal temperature determine the spectral resolution. The range of tunability is limited only by the lowest X-ray energy allowed by the Bragg's law and is sufficient when one uses either Silicon or Diamond crystals (see Ref. [4]). The bigvantage of diamond is its ability to withstand the high heat load due to the extremely high thermal conductivity, low thermal expansion, small X-ray absorption, and high reflectivity [5].

The proposed two-stage scheme possesses two significant advantages. First, it opens a perspective to achieve monochromaticity of the output radiation close to the limit given by the finite duration of the electron pulse and to increase the spectral brilliance 500 times compared to a usual SASE FEL. Second, shot-to-shot fluctuations of the pulse energy are reduced from 100% to less than 10% when the second undulator section reaches saturation [2]. Since it is a single bunch scheme, it does not require any special time diagram of the accelerator operation. A more detailed study, including details on the monochromator, can be found in Ref. [4].

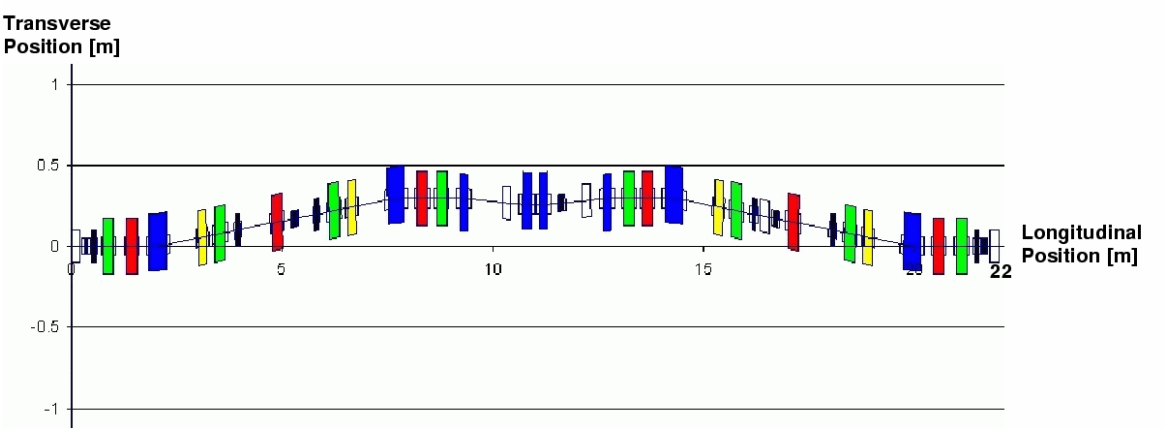

Figure 2: Electron bypass design for the TESLA Test Facility self-seeding option. Indicated are steerers (black), dipoles(blue), horizontally focusing (red) and defocusing (green) quadrupoles and sextupoles (yellow). The small chicane in the middle is to match to the wavelength dependent pathlength difference of the photon beam.

The design of a self-seeding scheme in the VUV wavelength range has been finished recently at DESY. As compared to the schematic layout presented for the X-ray, the complete design in the VUV looks more complicated. In Fig. 2, the detailed design of the electron bypass (de-buncher) is shown. It is optimized to minimize CSR effects and (slice) emittance growth. In Fig. 3, the optical elements are show needed to monochromatize and collimate the photon beam. More details can be found in Ref. [6].

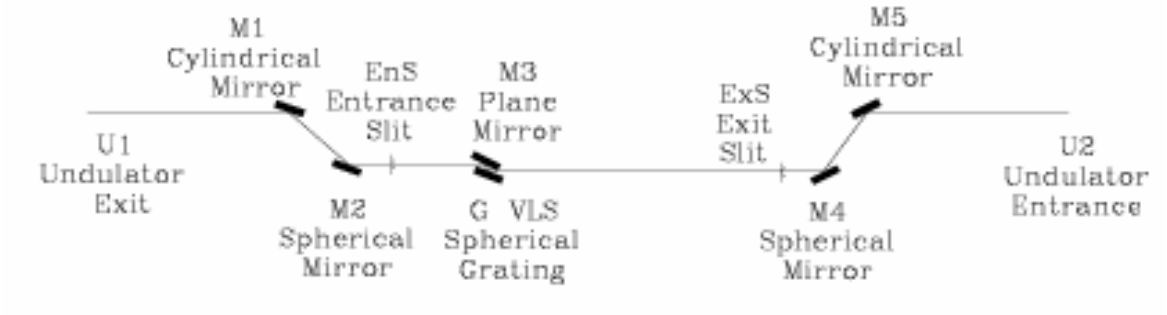

Figure 3: Monochromator design for the TESLA Test Facility VUV FEL at DESY. The present design works in the wavelength range from 6 to 60 nm.

2. Scheme for single spike Photon Pulses

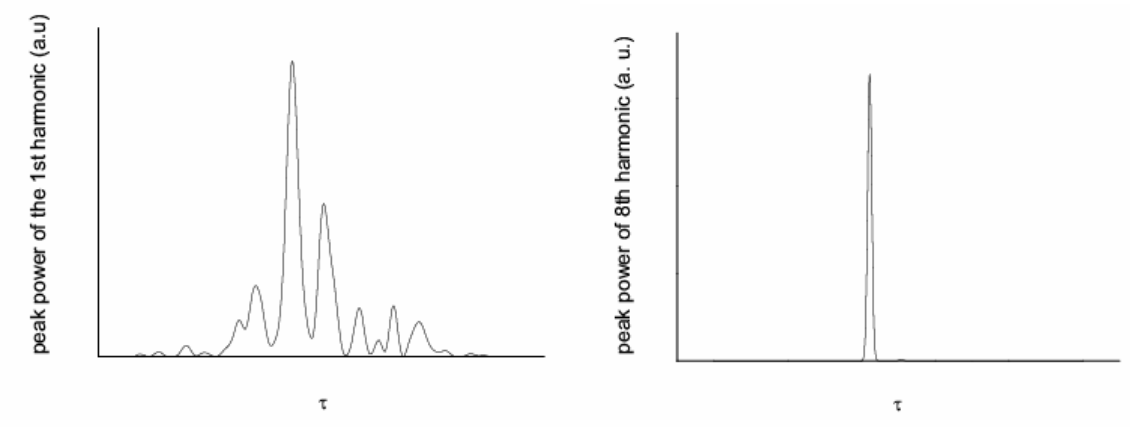

Figure 4: Illustration of the results of nonlinear transformation. Sample function of the instantaneous power for SASE FEL pulse (left) and the nonlinear transform representing the 8th harmonic (right).

As already mentioned, a SASE FEL produces radiation pulses consisting of independent wavepackets (spikes). The typical duration of a spike can be as short as 300 attoseconds for an X-ray FEL. Single-spike pulses can be produced, for example, when the electron bunch length is comparable with the cooperation length. This is technically possible in the VUV range [7], but is not realistic for an X-ray FEL, since the electron bunch length would need to be below a micrometer. However, one can make use of the statistical properties of the FEL radiation [8]. Radiation from a SASE FEL operating in the linear regime is described by Gaussian statistics (in other words, it is simply completely chaotic polarized light) [3]. An important characteristic of a radiation pulse is the number of modes M (i.e., average number of spikes), which is typically above a hundred for a hard X-ray FEL. Therefore, the probability to obtain a single-spike pulse is very low. However, the situation changes dramatically when we apply a nonlinear transformation to the Gaussian statistics. The possibility of single-spike pulse production is demonstrated in an example.

With reference to the left-hand plot in Fig. 4, consider an intensity function I in the SASE FEL radiation pulse at the fundamental frequency versus time τ (Gaussian statistics). Subjecting it, for example, to an 8th harmonic transformation, we obtain the "image" shown in the right-hand plot in Fig. 4. The instantaneous intensity function $I(t)$ and the transformed function $[I(t)]^8$ differ considerably. Due to the nonlinear generation mechanism, the temporal structure of the 8th-harmonic radiation is similar to the fundamental, but with more fluctuations from spike to spike. The fact that the 8^{th} harmonic intensity is a single spike implies that the fluctuation of the fundamental intensity about the mean is rather pronounced.

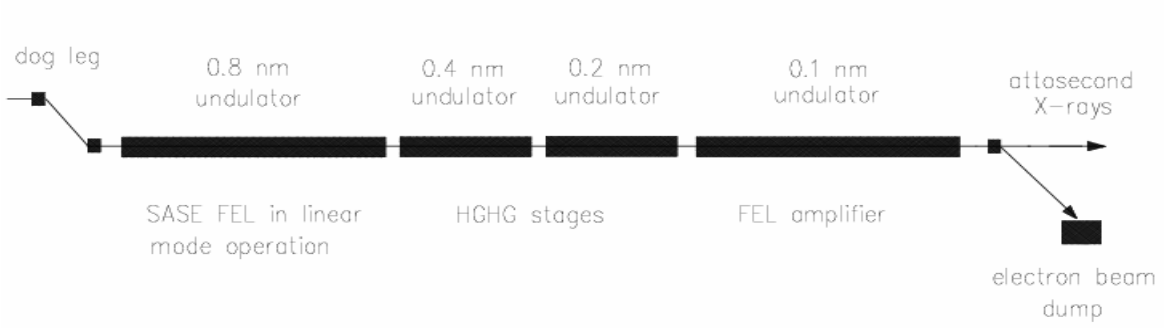

Figure 5: Concept of the attosecond X-ray facility. It produces ultrafast X-ray pulses during a single pass of an electron beam through a sequence of undulators which are resonant at different wavelengths. The amplification process develops from shot noise. Single-spike pulses can be selected by using a special trigger.

The nonlinear transformation described above can be realized with a single-bunch, multistage High Gain Harmonic Generation (HGHG) FEL scheme (see Fig. 5)[9]. In this scheme the second harmonic in the *n*-th stage becomes the fundamental in the *(n+1)*-th stage. Each stage (except the first one) consists of a radiator undulator, a dispersive section (demodulator), an FEL amplifier and an end-stage dispersive section (modulator). The main difference to previous HGHG schemes [10-14] is that frequency multiplication is performed with a single electron bunch consecutively passing all HGHG stages. Previous studies [8] have shown that parameters for each stage can be tuned in such a way that the amplitude of the second harmonic of the density modulation dominates significantly over the amplitude of shot noise harmonics, and the modulation of the beam density can be used as input signal for the next HGHG stage. Thus, the shot noise in the electron beam (having features of gaussian statistics[3]) serves as a seed signal for the multistage FEL, where gaussian statistics are naturally subjected to the required nonlinear transformation. As a result, the output radiation has much more pronounced spikes. The average number of spikes is reduced so much that it becomes probable to generate pulses consisting of a single spike.

Since the amplification process starts from shot noise, the properties of single-spike selection should be described in statistical terms. The statistics are defined over an ensemble of radiation pulses. If we define the contrast C as the ratio of the number of photons in the main spike to the total number of photons in the pulse, we find that $\langle C \rangle$ asymptotically approaches unity as the ratio $E_{th}/\langle E_{(8)} \rangle$ increases, where E_{th} is the threshold level of the 8th harmonic energy pulse discriminator and $\langle E_{(8)} \rangle$ is the mean energy of the 8th harmonic (averaged over the ensemble of pulses). Clearly, the larger the threshold level of discriminator $E_{th}/\langle E_{(8)} \rangle$, the larger the number of shots per trigger pulse N_{sh}. Note that the number of degrees of freedom M of the fundamental radiation pulse is a parameter of the functions $\langle C \rangle = F(M, E_{th}/\langle E_{(8)} \rangle)$, and $\langle N_{sh} \rangle = f(M, E_{th}/\langle E_{(8)} \rangle)$.

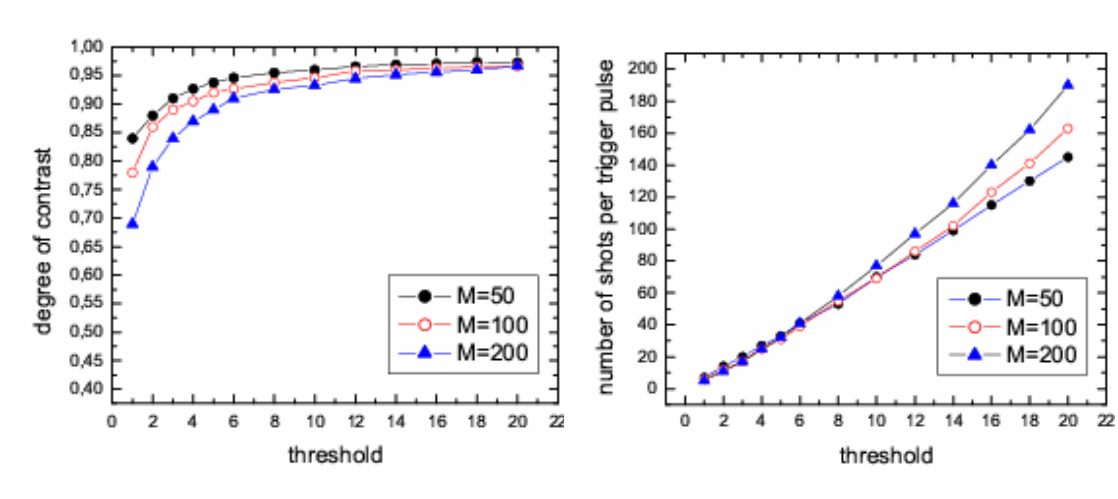

Figure 6: Left: Degree of contrast <C> versus energy threshold $E_{th}/<E_{(8)}>$. Right: Number of shots per trigger pulse N_{sh} versus energy threshold $E_{th}/<E_{(8)}>$.

Figure 6 shows the basic characteristics of the single-spike pulse selection process. The dependence of the degree of contrast $<C>$ on the value of the energy threshold $E_{th}/<E_{(8)}>$ is presented in the left-hand plot in Fig. 6. It is seen that the contrast increases with increasing energy threshold, and that it asymptotically approaches unity. Simulations at different values of M show that the degree of contrast does not differ significantly when the number of modes is within the limits $50 < M < 200$. The right-hand plot in Fig. 6 shows the number of shots per trigger pulse $<N_{sh}>$ versus $E_{th}/<E_{(8)}>$ for several values of the parameter M. From Fig. 6 it is quite clear that the dependence of $<N_{sh}>$ on the number of modes M is not strong within the interval M = 50-200 and can be ignored.

The final steps involved in obtaining single-spike pulses of the 8th-harmonic radiation are as follows. The energy in the high-harmonic radiation pulse must be measured with a transparent detector that lets the main part of the radiation pulse continue to the sample. After each shot, the signal from the energy detector is sent to a discriminator having a threshold $E_{th} = 2<E_{(8)}>$. After discrimination, the signal is used to initiate a trigger. A register is used to store information concerning the trigger and sample detector events. In the case of TESLA XFEL, the number of modes in the fundamental radiation pulse at a wavelength of 0.1 nm is about $M \approx 50$-100. If the required contrast is 90%, i.e. 90% of all photons are in one spike, the corresponding discriminator threshold is about $<E_{th}/E_{(8)}> \approx 2$ (see Fig. 6). If the number of modes is close to M ≈ 100, the right-hand side of the figure shows that the number of shots per trigger pulse is about 10. Hence, the single-spike pulse repetition rate is a few kHz. On the other hand, if a contrast of 97% is of interest, the number of shots is about $<N_{sh}> \approx 100$, and the number of the single-spike pulse decreases to a few hundred per second. Thus, we can state that the superconducting linear accelerator is an ideal accelerator to drive an attosecond XFEL. The high repetition rate of the TESLA accelerator (40000 pulses per second) should be sufficient to obtain an average kHz-level pulse repetition rate of single spikes. The development and test of the attosecond XFEL at TESLA is greatly facilitated by the fact that undulators with the required parameters are being developed for the SASE option. Also, the

length foreseen for installation of SASE undulators is sufficient to accommodate the attosecond option.

3. Sideband seeded FEL

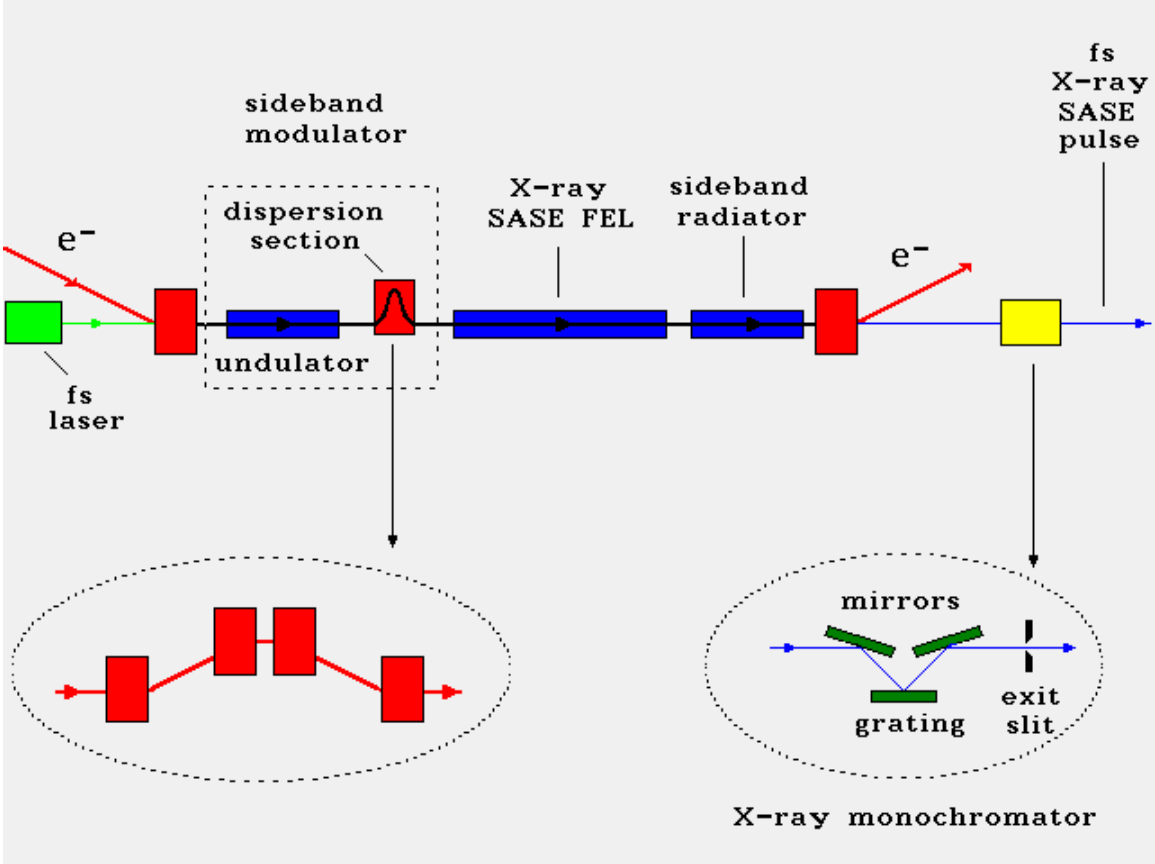

Figure 7: Basic scheme of a sideband seeded SASE FEL

Another proposal capable of producing femtosecond pulses is the sideband seeded FEL (see Figs. 7, 8). An ultrashort laser pulse is used to modulate the density of electrons within a femtosecond slice of the electron bunch at a frequency ω_{opt}. We begin the FEL operation by positioning the interaction region on the electron bunch. The seed laser pulse will be timed to overlap with central area of the electron bunch. This ultrashort laser pulse serves as a seed for a modulator which consists of an undulator and a dispersive section. The interaction of seed pulse with the electron beam produces an energy modulation at ω_{opt} inside the undulator. This energy modulation is converted into spatial bunching in the dispersive section. The density modulation at the modulator exit is about 10%. The energy modulation, introduced by the modulator, is smaller than the initial energy spread. Following the modulator, the beam and seed radiation enter SASE undulator which is resonant with X-ray radiation at frequency ω_0. The process of amplification of the radiation in the X-ray undulator develops in the same way as in the conventional SASE FEL: fluctuations of the electron

beam current density serve as the input signal. The seeding optical radiation does not interact with the electron beam in the X-ray undulator and is diffracted out of the electron beam. By the time the beam is bunched in the SASE FEL undulator at frequency ω_0, the X-ray radiation power has reached saturation. This leads to amplitude modulation of the density at the sidebands $(\omega_0 \pm \omega_{opt})$. The sideband density modulation takes place only within that part of the electron bunch defined by the length of the seed laser pulse that is much shorter than the electron bunch. Following the SASE FEL undulator the beam and X-ray radiation enter an undulator section (radiator) which is resonant with the $\omega_0 - \omega_{opt}$ radiation. Because the beam has a relatively large component of bunching at the longer wavelength sideband, coherent emission at $\omega_0 - \omega_{opt}$ is copiously produced within a femtosecond slice of electron bunch. After leaving the radiator the electron beam is deflected onto a beam dump, while the photon beam enters the monochromator, which selects the femtosecond soft X-ray pulse. Because the central and sideband frequency have to be separated, i.e. have to be much larger than the SASE bandwidth, the minimum wavelength for which this scheme works is in the VUV or soft X-ray regime. For shorter wavelengths, the method in the previous section can be used.

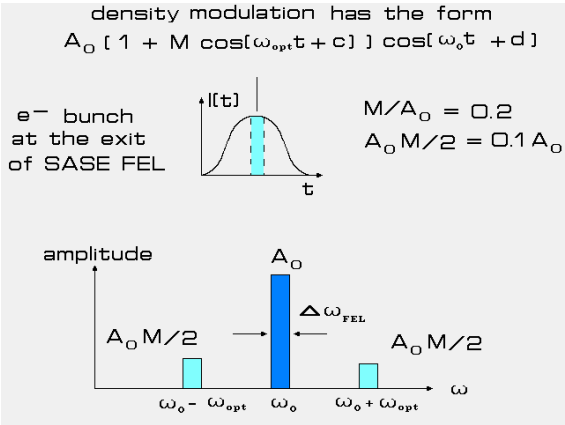

Figure 8: Description of the sideband generation for the case of a density modulation as initial condition.

On the basis of the parameters of TTF SASE FEL [15] and laser pulses of 25 fs duration and 6μJ energy at a repetition rate of 10 kHz (from a Ti:sapphire laser system), it should be possible to achieve an average brilliance of 10^{22} photons s^{-1} $mrad^{-2}$ mm^{-2} per 0.1% BW in the photon energy range 25-100 eV. The femtosecond SASE FEL will provide soft X-ray pulses with 30 fs (FWHM) duration. The number of photons at the monochromator exit (at monochromator efficiency 10%) can exceed 10^{11} per pulse which is by three orders of magnitude above the background. This creates perfect conditions for experiments. Note that the proposed femtosecond option of an FEL is an addition to a fully functioning SASE FEL improving the output radiation beam properties considerably and thus extending the range of possible applications. Parameters of modulator and sideband undulator, the seed laser and characteristics of the monochromatized radiation are listed in Table 1. In addition to these components and a standard SASE FEL, a chicane and a monochromator are needed.

Table 1: parameters of the seed laser, modulator undulator, sideband radiator and output radiation after monochromatization.

Seed laser	
Wavelength, nm	400

Min. pulse duration, fs [FWHM]	25
Energy per pulse, μJ	6
Spectral width	Transform limited
Rep. Rate, kHz	10
Modulator Undulator	
Type	Planar
Number of periods	5
Period, cm	7.5
Peak field, T	0.7
External beta-function, m	1.7
Radiator undulator	
Type	Planar
Number of periods	150
Period, cm	2.73
Peak field, T	0.51
External beta-function, m	1.7
Output radiation after monochromator	
Wavelength, nm	10-40
Min. pulse duration, fs [FWHM]	30
Photons per pulse	10^{11}
Spectral width, % [FWHM]	0.5

The entire process has been simulated using the simulation code FAST [16]. Modifications to the code for the sideband seeding option are discussed in Ref. [17]. In Fig. 9, the radiation pulse at the radiator exit is shown before and after spectral filtering.

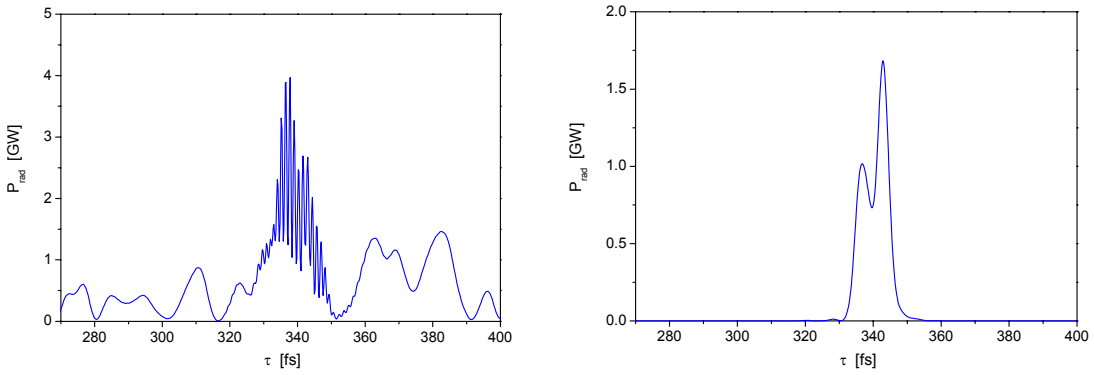

Figure 9: Pulse at the exit of the radiator undulator before (left) and after (right) spectral filtering at the sideband.

References

[1] J. Feldhaus, E.L. Saldin, J.R. Schneider, E.A. Schneidmiller, and M.V. Yurkov, Opt. Commun. 140 (1997)341.

[2] E.L. Saldin, E.A. Schneidmiller, and M.V. Yurkov, Nucl. Instrum. and Methods A445 (2000)178.

[3] E.L. Saldin, E.A. Schneidmiller, and M.V. Yurkov, *The Physics of Free Electron Lasers*, Springer, Berlin, 1999.

[4] E.L. Saldin, E.A. Schneidmiller, Yu.V. Shvyd'ko, M.V. Yurkov, Nucl. Instrum. and Methods A475 (2001) 357.

[5] A.K. Freund, Optical Engineering 34 (1995) 432.

[6] R. Reiniger, Optics parameters of the beamline for the seeded FEL, DESY bestellung 609/430150132, October 3, 2001.
[7] V. Ayvazyan, Phys. Rev. Lett. 88, 104802 (2002)
[8] E. L. Saldin, E. A. Schneidmiller and M. V. Yurkov, Opt. Commun., in press
[9] E. L. Saldin, E. A. Schneidmiller and M. V. Yurkov, Opt. Commun. 202(2002)169
[10] I. Schnitzer, A. Gover, Nucl. Instr. Meth. A 237(1985)124
[11] R. Bonifacio, L. De Salvo, P. Pierini, Nucl. Instr. Meth. A 293(1990)627
[12] L. H. Yu, Phys. Rev. A 44(1991)5178
[13] I. Ben-Zvi et al., Nucl. Instr. Meth. A 304(1991)151
[14] J. Wu, L. H. Yu Nucl. Instr. Meth. A 475(2001)104
[15] J. Rossbach et. Al.,Nucl. Instr. Meth. A 375(1996)269
[16] E. L. Saldin, E. A. Schneidmiller and M. V. Yurkov, Nucl. Instr. Meth. A 429(1999)233
[17] W. Brefeld et. Al., DESY-print 01-63 (2001)
[18] W. Brefeld et. Al., ,Nucl. Instr. Meth. A 483(2002)62

Cascading stages of High-Gain Harmonic-Generation

Li Hua Yu

National Synchrotron Light Source

Brookhaven National Laboratory

Outline

- Basic Principle
- DUV FEL Experimental Results
- Calculations for a Cascaded HGHG FEL

Basic Principle of HGHG

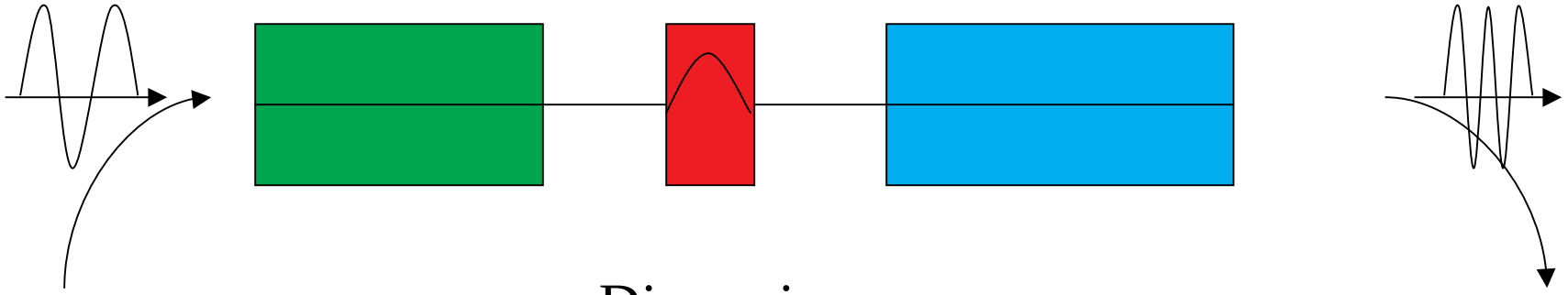

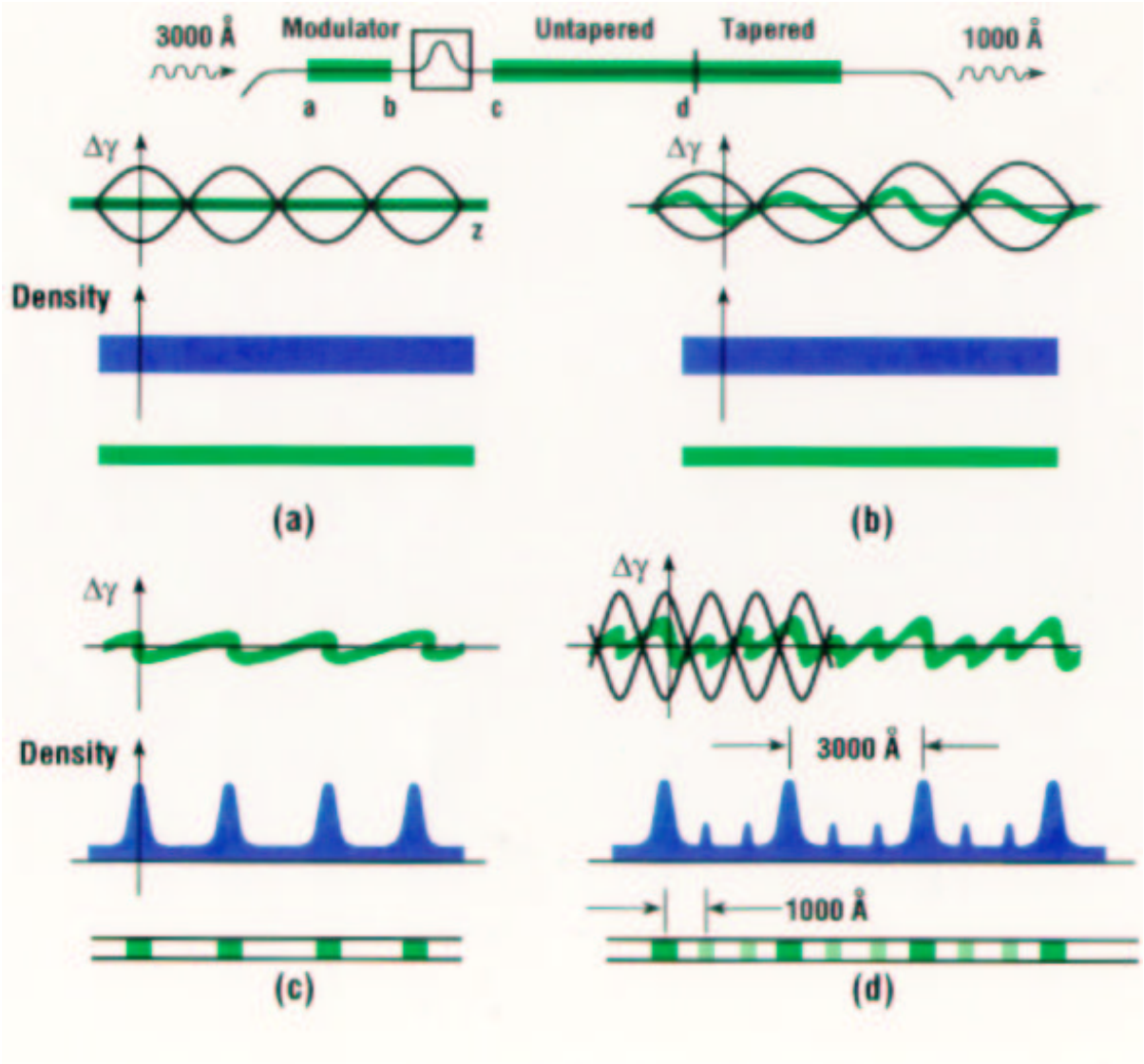
3000 Å
Modulator
Untapered
Tapered
1000 Å
a
b
c
d
Δγ
z
Density
(a)
(b)
(c)
(d)
3000 Å
1000 Å

Advantages of HGHG

•Narrow bandwidth

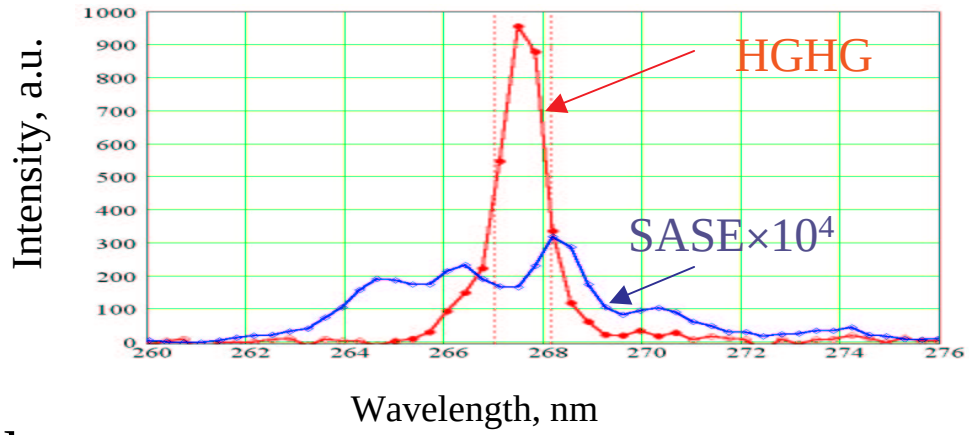

•Stable central wavelength

•Fourier transform limited

•Larger ratio of output/spontaneous radiation

•Short pulse (20fs)

•Stable Intensity from shot to shot

•Can be cascaded to short wavelength

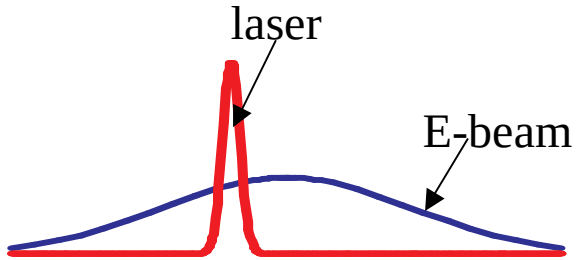

HGHG Experimental Results

Deep UV Free Electron Laser at the Source Development Laboratory

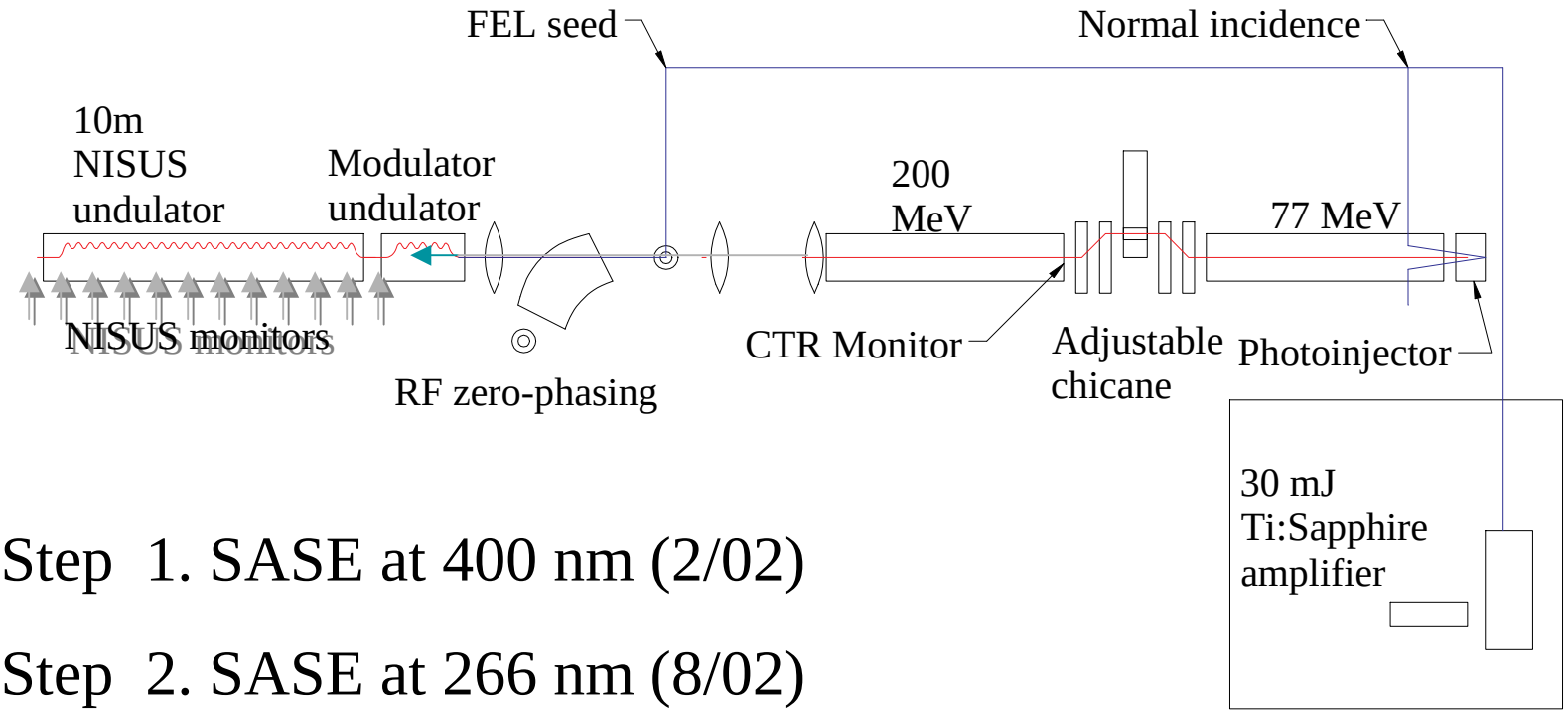

Step 1. SASE at 400 nm (2/02)

Step 2. SASE at 266 nm (8/02)

Step 3. Direct seeding at 266nm(9/02)

Step 4. HGHG 800 nm → 266 nm (10/02)

Undulator & Electron Beam Parameters

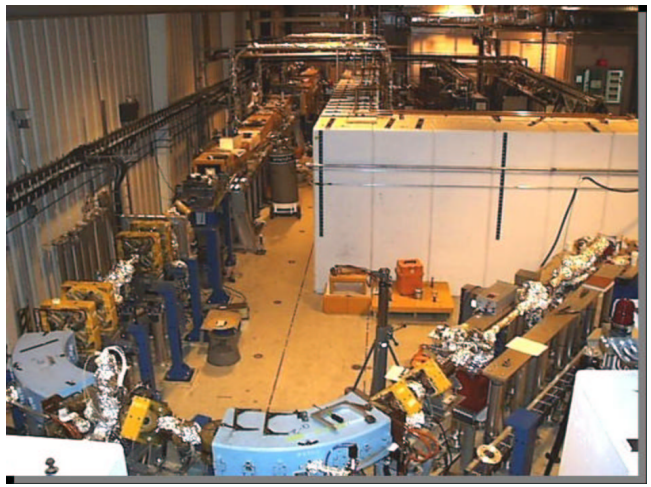

Measured electron beam parameters

Energy	Up to 200 MeV
Charge	300 pC
Normalized emittance	4 mm*mrad
Compressed bunch length, RMS	0.3-0.6 ps
Energy spread, RMS	0.3 %

Undulator NISUS parameters

Period	3.89 cm
Number of periods (length)	256 (10 m)
Peak field	0.31 T
Betatron wavelength (at 140 MeV)	20 m
Electron beam size, RMS (4 mm mrad)	250 um

Measurements of Electron Beam Properties

Charge, peak current, bunch length, energy, energy spread, emittances, envelopes

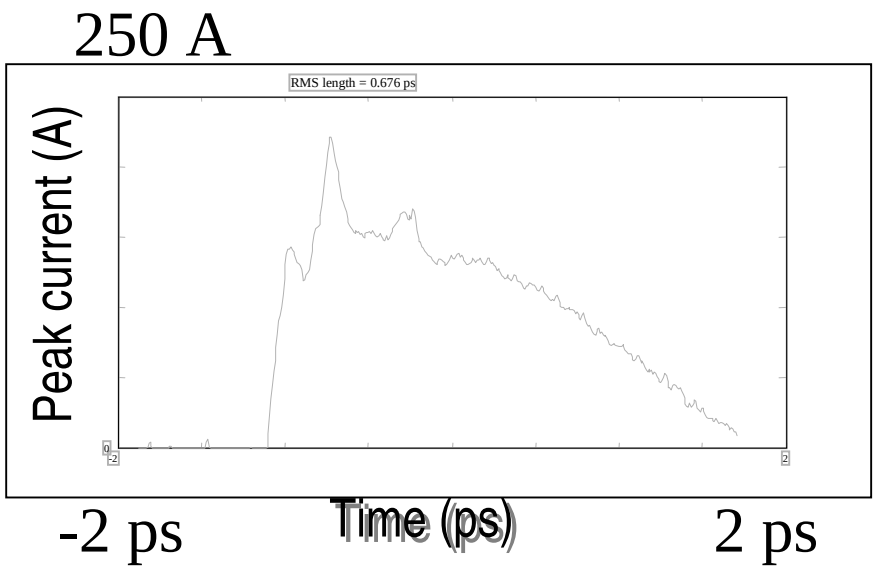

Longitudinal beam parameters

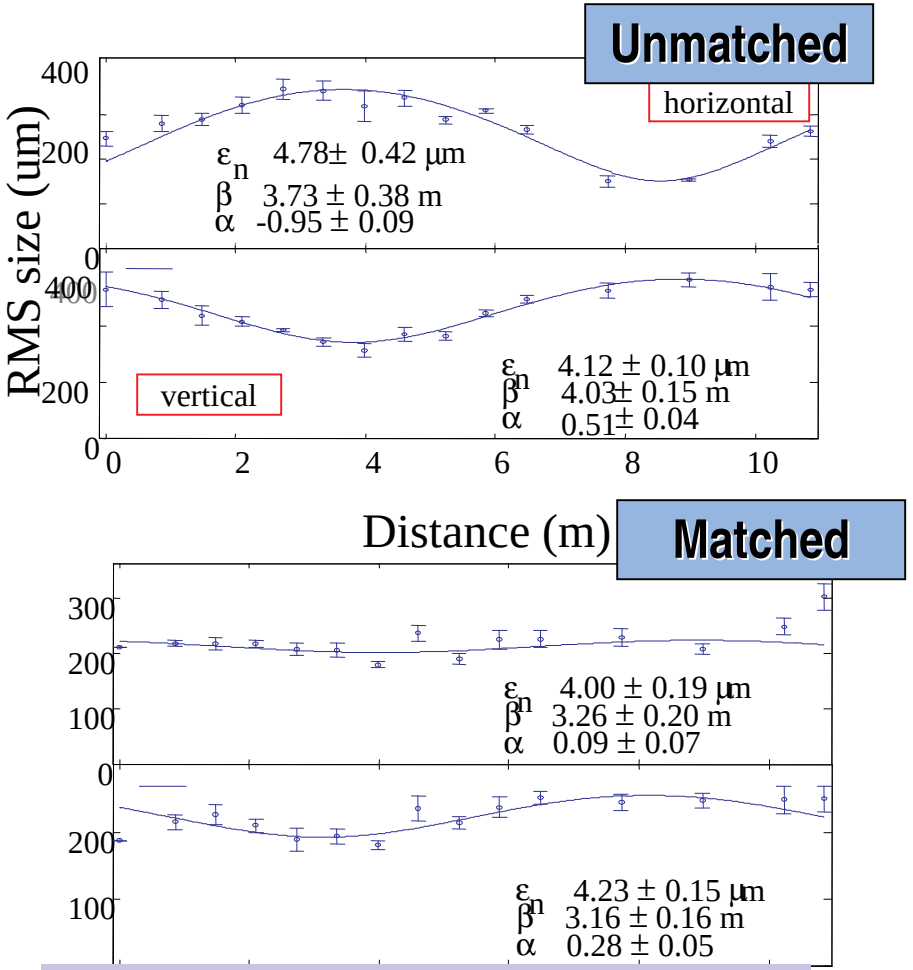

Transverse beam parameters

SASE Signal at DUV-FEL February 2002

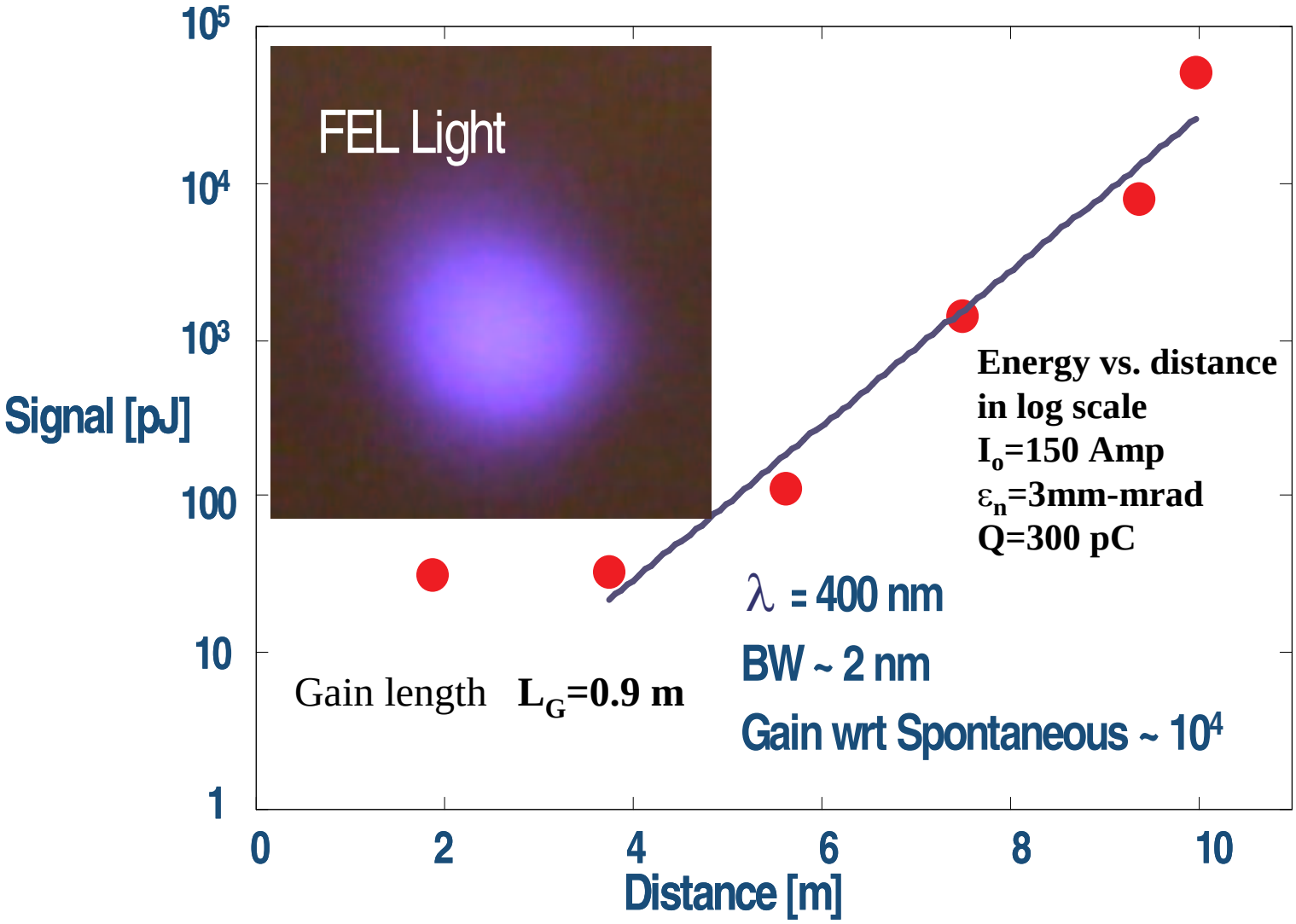

266 nm SASE Signal along NISUS Wiggler

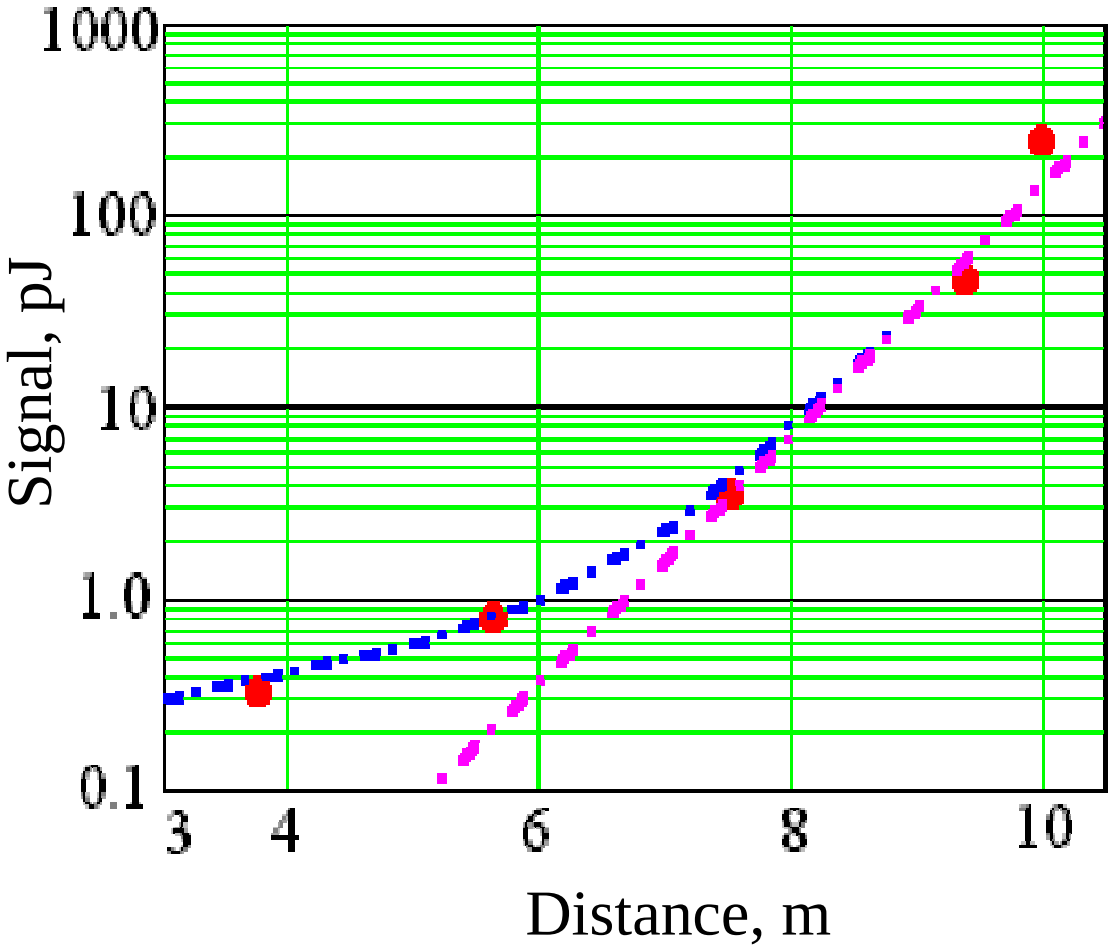

L_G= 0.66 m
I_o=550 Amp
ε_n=3 mm-mrad
Q=300 pC

Deep Ultraviolet Free Electron Laser Reaches New Milestone Using BNL's Unique HGHG Process

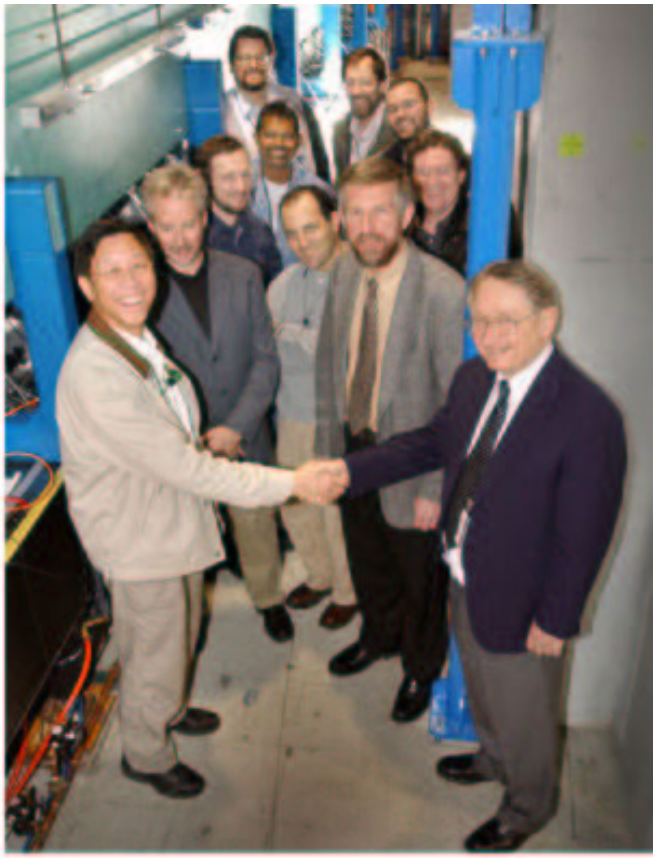

Interim Lab Director Peter Paul (right) celebrates the latest milestone at BNL's deep ultraviolet free electron laser with NSLS department members (foreground, from left) Li Hua Yu, James Murphy, Adnan Doyuran, NSLS Chair Steve Dierker; (back, from left) Timur Shaftan, John Skaritka, Pooran Singh, Erik Johnson, Henrik Loos, and Brian Sheehy.

HGHG and SASE Spectrum for the Same Beam Condition (10/28/02)

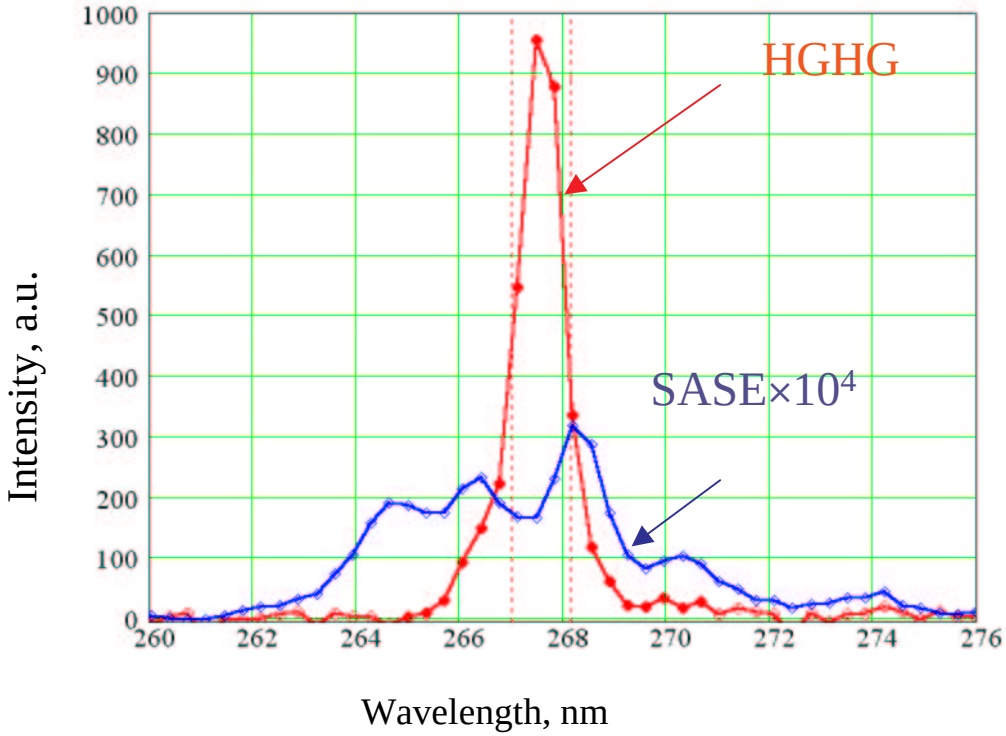

Power vs. Distance in NISUS (12/11/02)

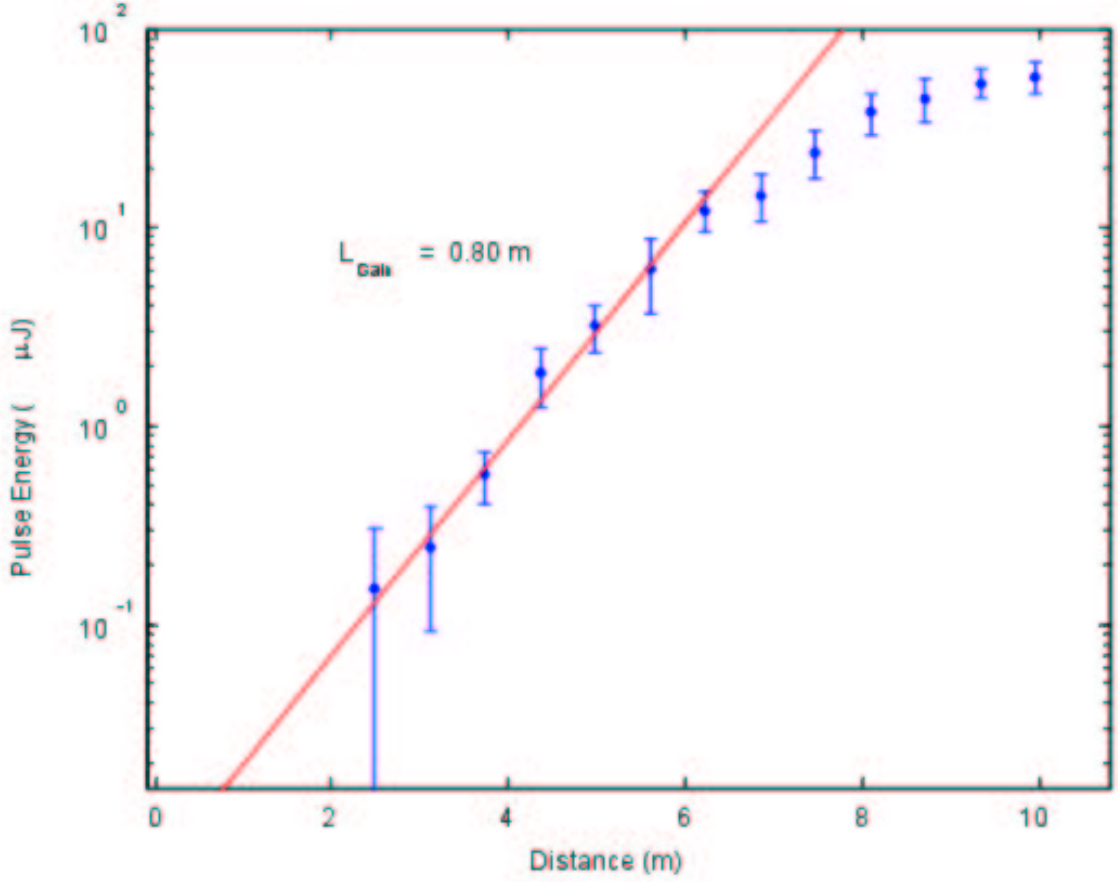

300 pC 4.3 μm (rms) 1 ps (FWHM)

Average output: 60μJ

Intesity Fluctuation of SASE and HGHG

Normalized to the same average intensity and the same area (12/11/02)

SASE

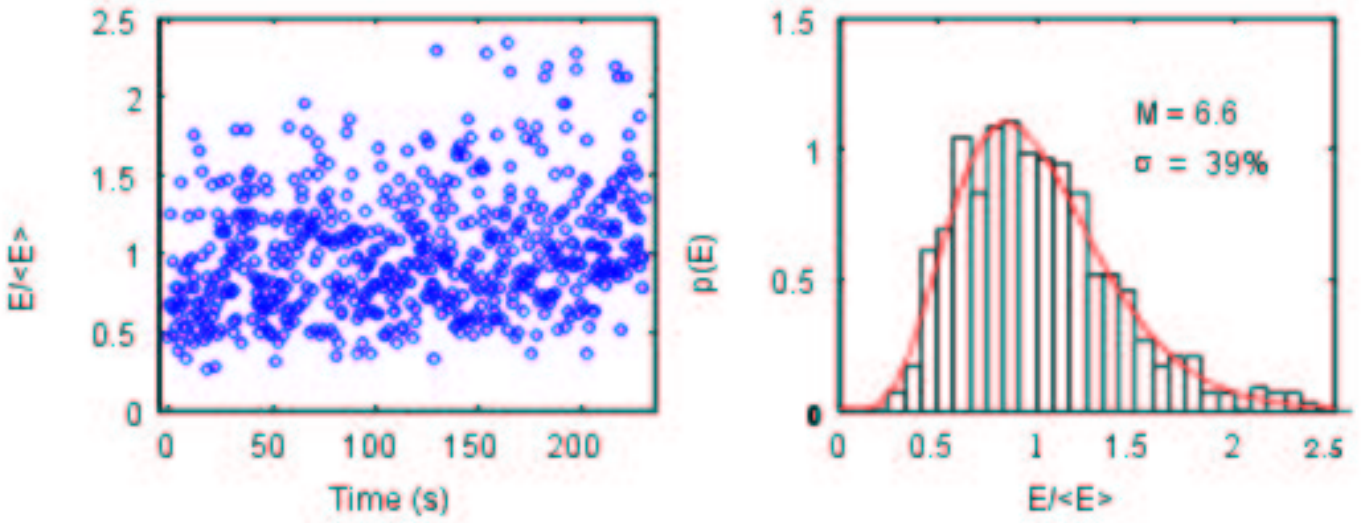

HGHG

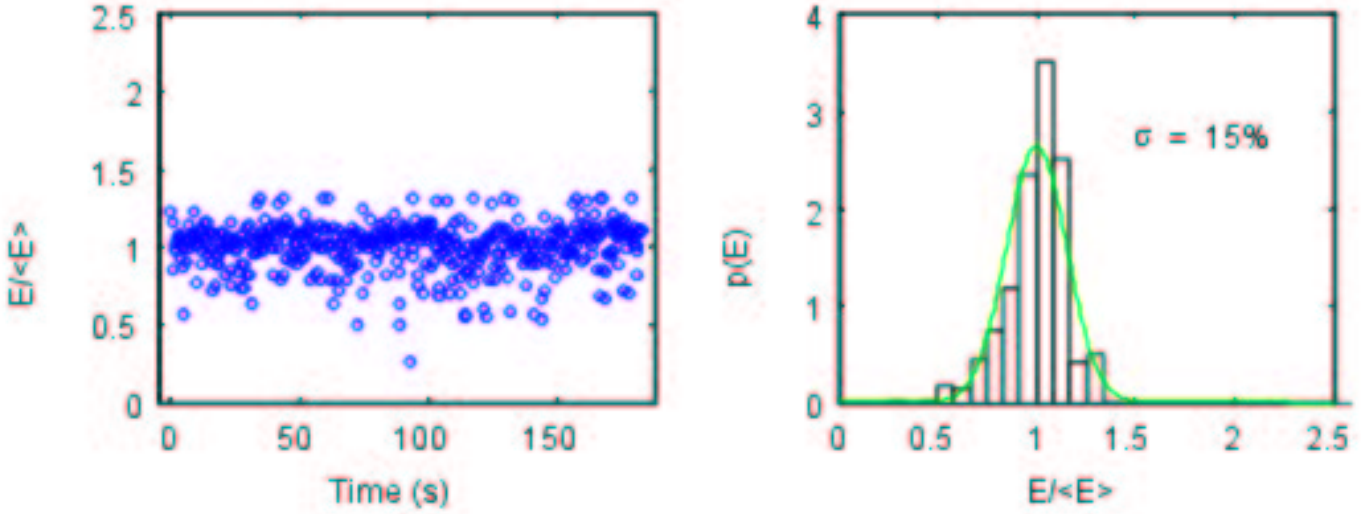

Local Energy Spread

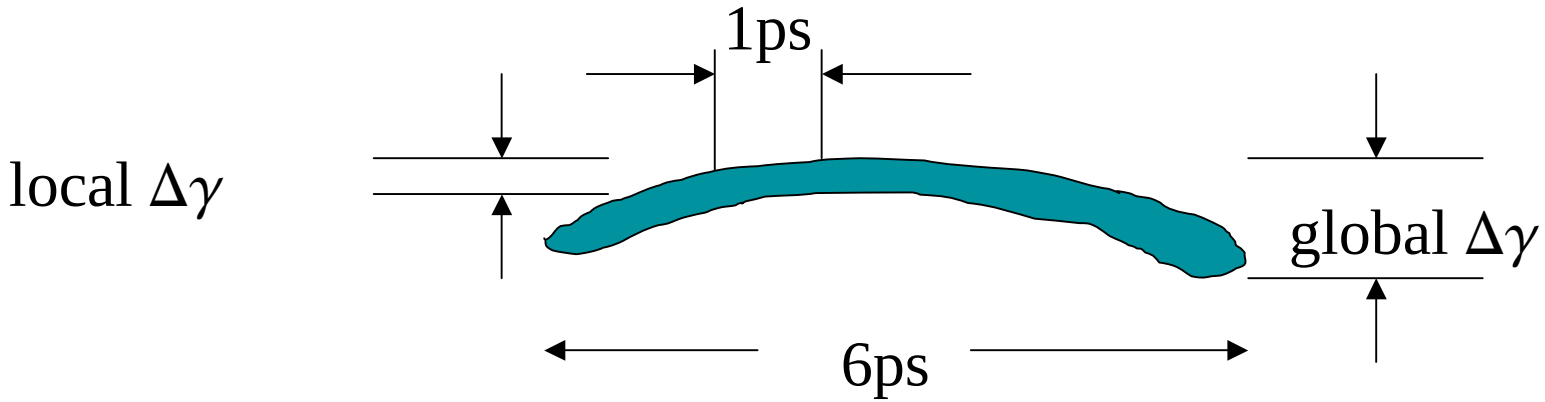

Example, ATF HGHG at 5.3 μ:

N_w=60, λ_s=5.3 μ

$N_w \lambda_s$=300 μ → 1 ps

bunch length: 6 ps

SASE/HGHG bandwidth ratio is also 6:

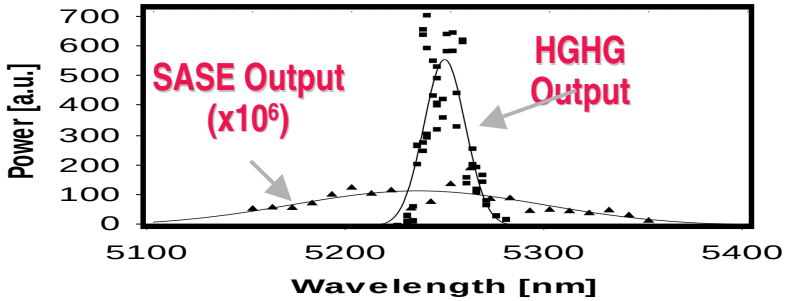

Local energy spread can be very small

Recent measurement at SDL: 250pc bunch 75MeV

Global rms energy spread = **0.014%**

Local energy spread is smaller

Global energy spread

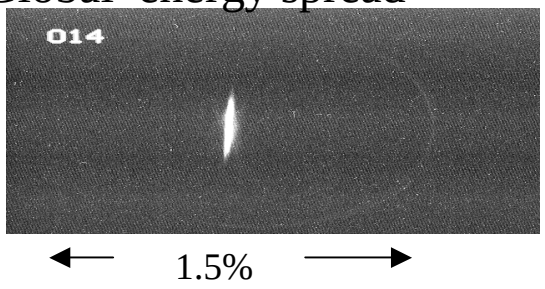

Output vs. input power gives information about local energy spread

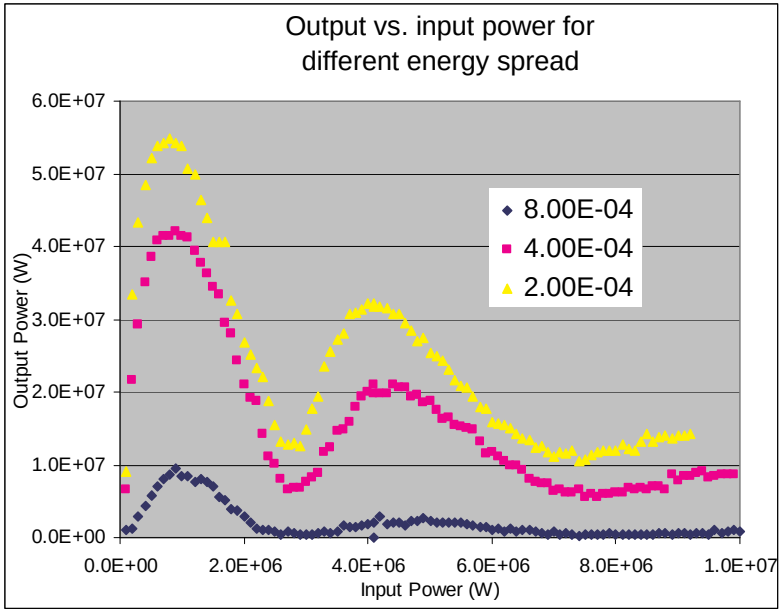

Measurement

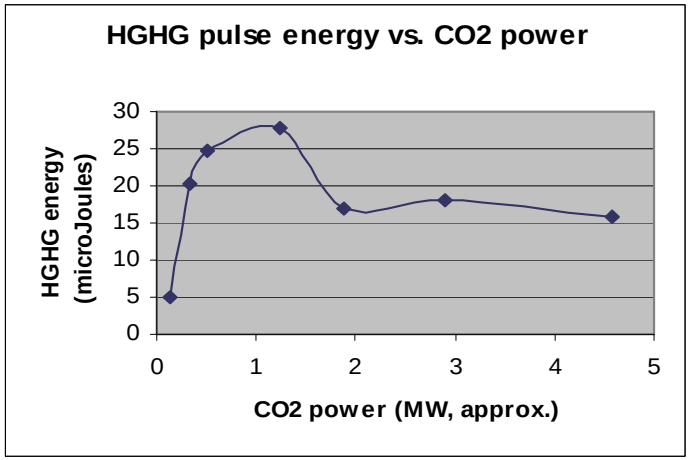

$$\frac{\text{second peak}}{\text{first peak}} \geq 0.6$$

Local Energy Spread of UVFEL

Recent DUVFEL HGHG:130μJ maximum. Dispersion was 4 times larger than designed value for an energy spread of 2×10^{-4}, indicating very small energy local spread.

Summary of DUV FEL Exps

- Narrower bandwidth
- Less intensity fluctuation
- Relaxed e-beam quality condition
- Indication of very small local energy spread
- Maximum pulse energy 130 μ ≈ designed saturation value → whole electron pulse contributes to the output
- Further characterization of HGHG in progress

Calculations for a Cascaded HGHG FEL

Two Stages with a Shifter

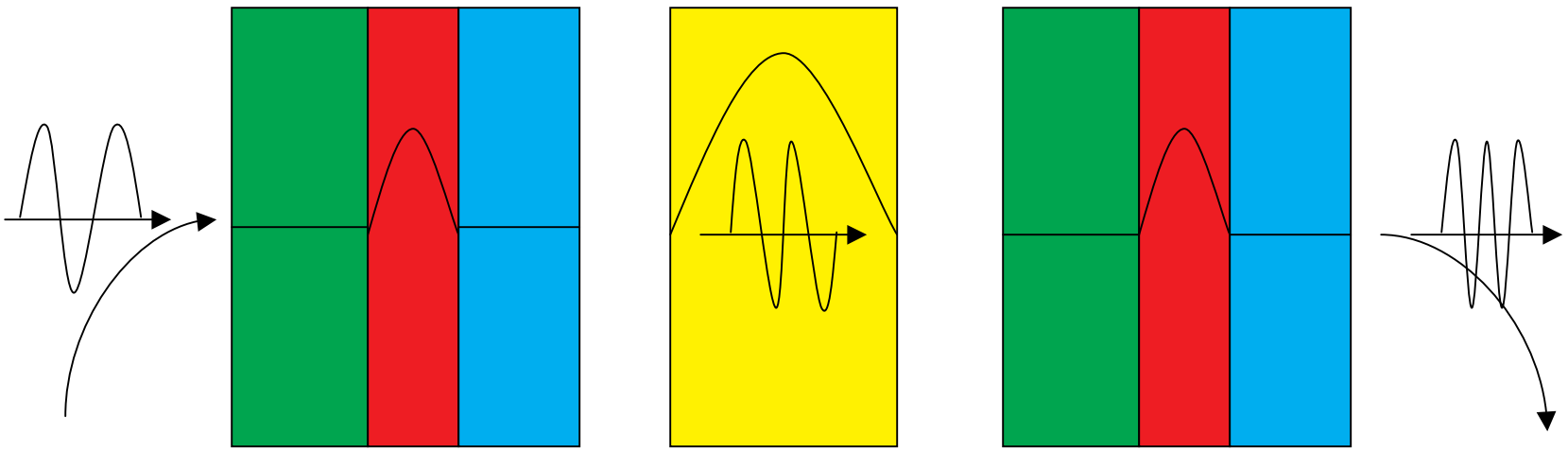

One Stage **Shifter** One Stage

Fresh Bunch Technique

Shift laser pulse from one part of an electron bunch to a fresh part of the electron bunch

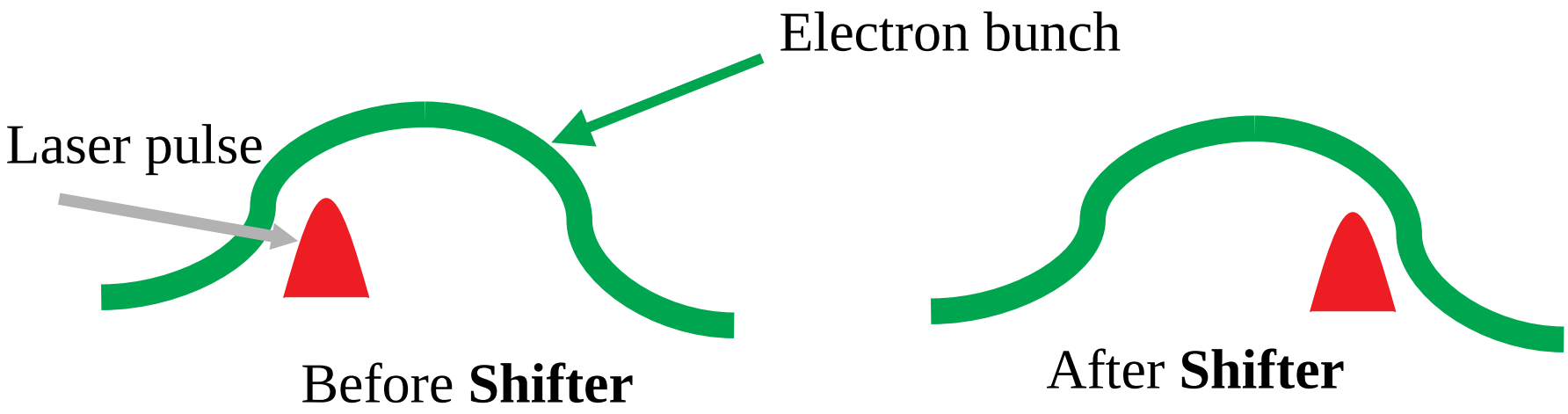

This makes it possible to use large energy modulation:

Bunching parameter → order of 1

Soft X-Ray Free-Electron Laser

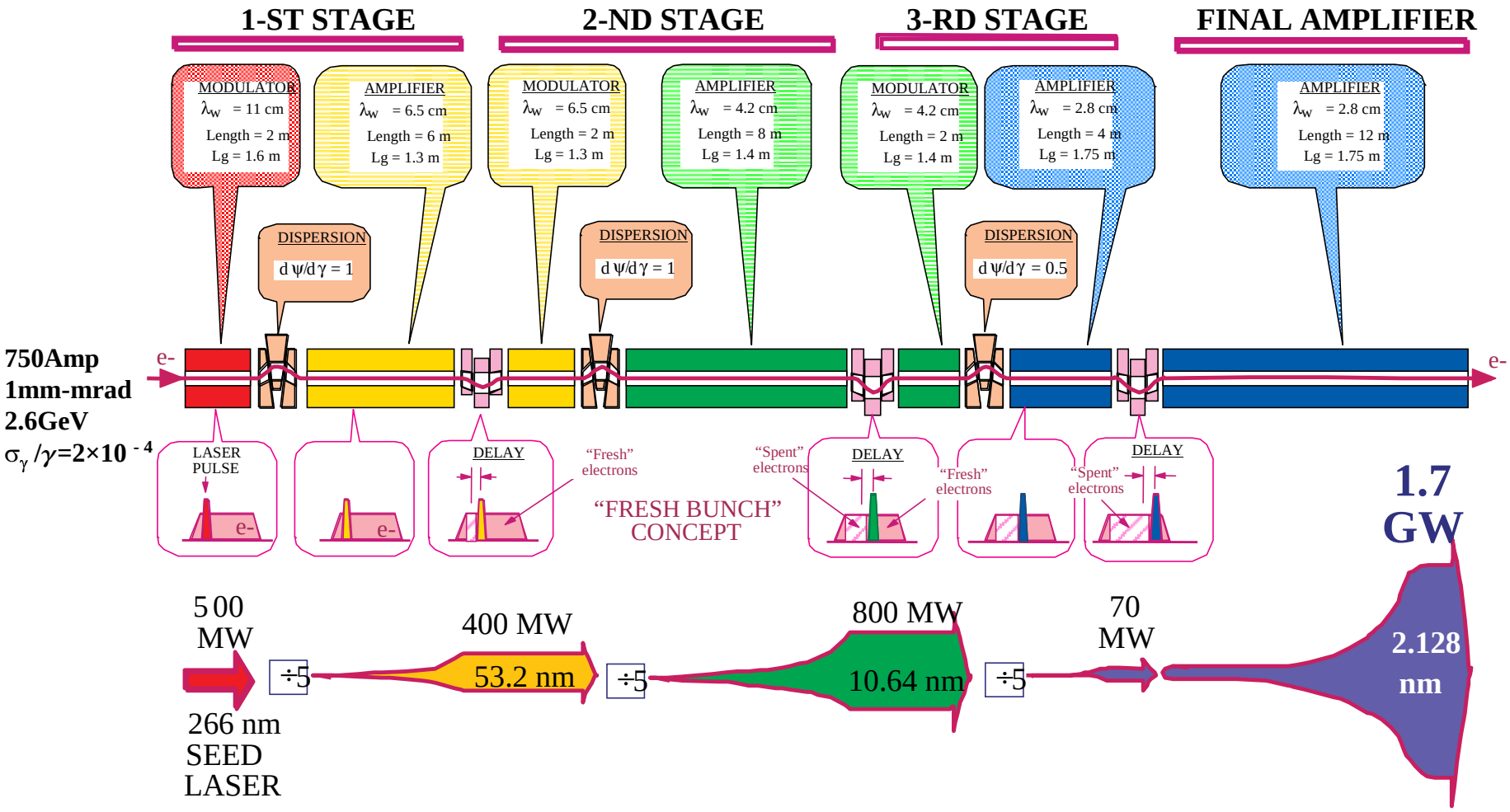

HGHG Theory

$\Delta\gamma$

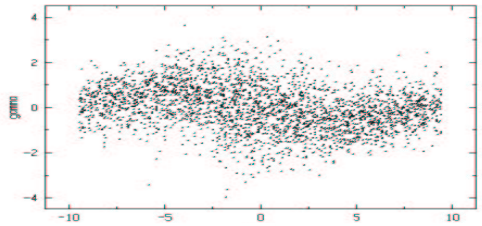

ψ

$$b_n = \langle e^{i\psi} \rangle = e^{-\frac{1}{2}\left(\frac{\partial\psi}{\partial\gamma}\sigma_\gamma\right)^2} J_n\left[\frac{\partial\psi}{\partial\gamma}\Delta\gamma\right]$$

$J_5(x)$

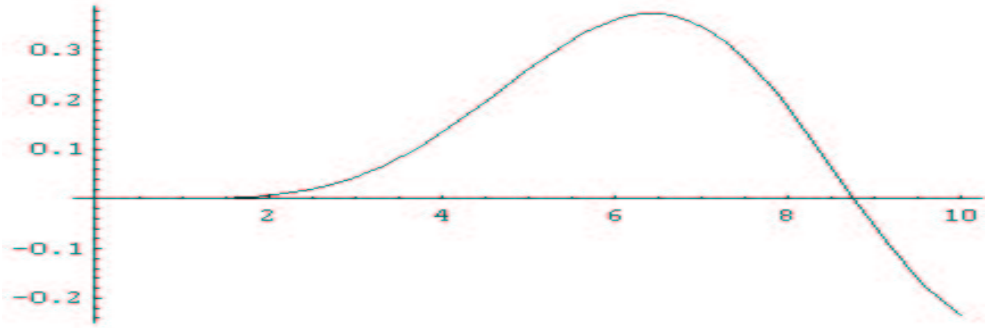

ψ

The factor $e^{-\frac{1}{2}\left(\frac{\partial\psi}{\partial\gamma}\sigma_\gamma\right)^2}$ requires

So $\frac{\Delta\gamma}{\gamma} > n\frac{\sigma_\gamma}{\gamma}$ keeps bunching

Intensity Stability

$$P_{out} \sim b_n^2 \sim \left(J_n\left[\frac{\partial \psi}{\partial \gamma} \Delta\gamma \right] \right)^2$$

$$\Delta\gamma \sim \sqrt{P_{in}}$$

When n=3, if P_{in} changes by a factor 3, P_{out} changes by less than 2

This makes cascading HGHG possible

$$\left(J_3 \left(\sqrt{X} \right) \right)^2$$

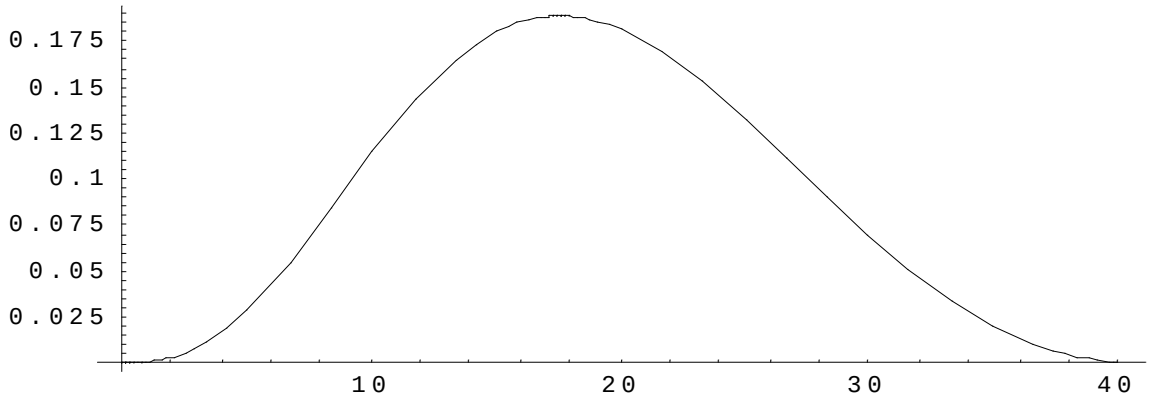

X

For a flat top model with same σ_x

$$P = C P_{2 L_G} e^{\frac{z}{L_G}}$$

$$P_{2 L_G} = \frac{(I_0)^2 Z_0}{8} \left(\frac{K F_{B2}}{\gamma}\right)^2 \frac{1}{4 \pi \sigma_x^2} \left| \int_0^{2 L_G} \overline{b_n} \, dl z \right|^2$$

$$C \simeq \frac{3.71}{12} \simeq \frac{1}{3}$$

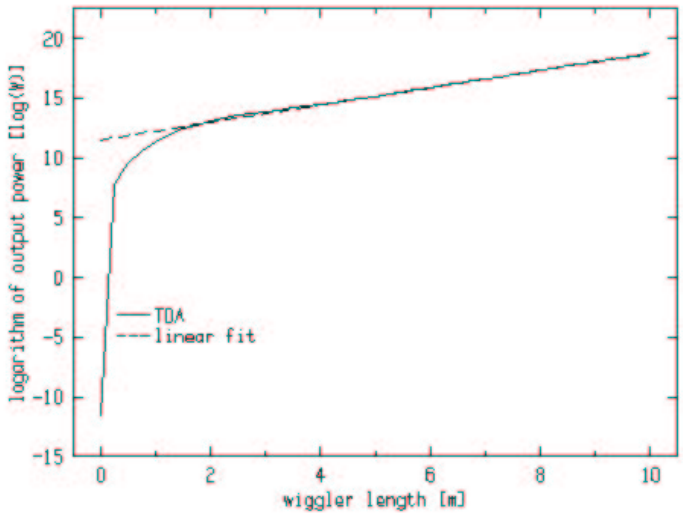

L_G is calculated using effective energy spread:

$$\sigma_{\gamma 2} = \sqrt{\sigma_\gamma^2 + \left(\frac{\Delta\gamma}{\sqrt{2}}\right)^2}$$

If $\frac{\Delta\gamma}{\gamma} > \rho$, growth rate is reduced,

Preferred condition:

$$\rho > \frac{\Delta\gamma}{\gamma} > n\,\frac{\sigma_\gamma}{\gamma}$$

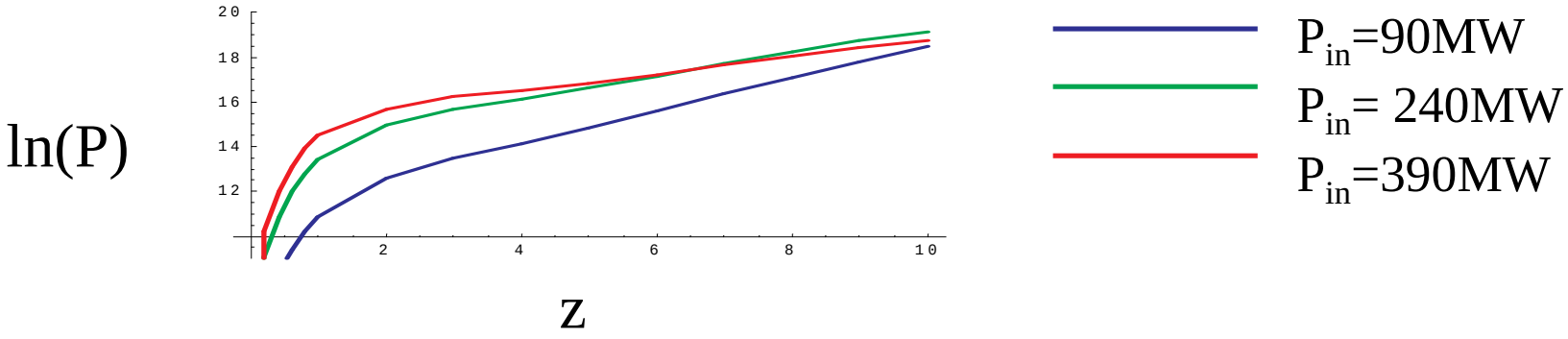

Output vs. Input for the 3rd HGHG Stage

When input varies 100%, the output varies 30%, so the fluctuation is reduced

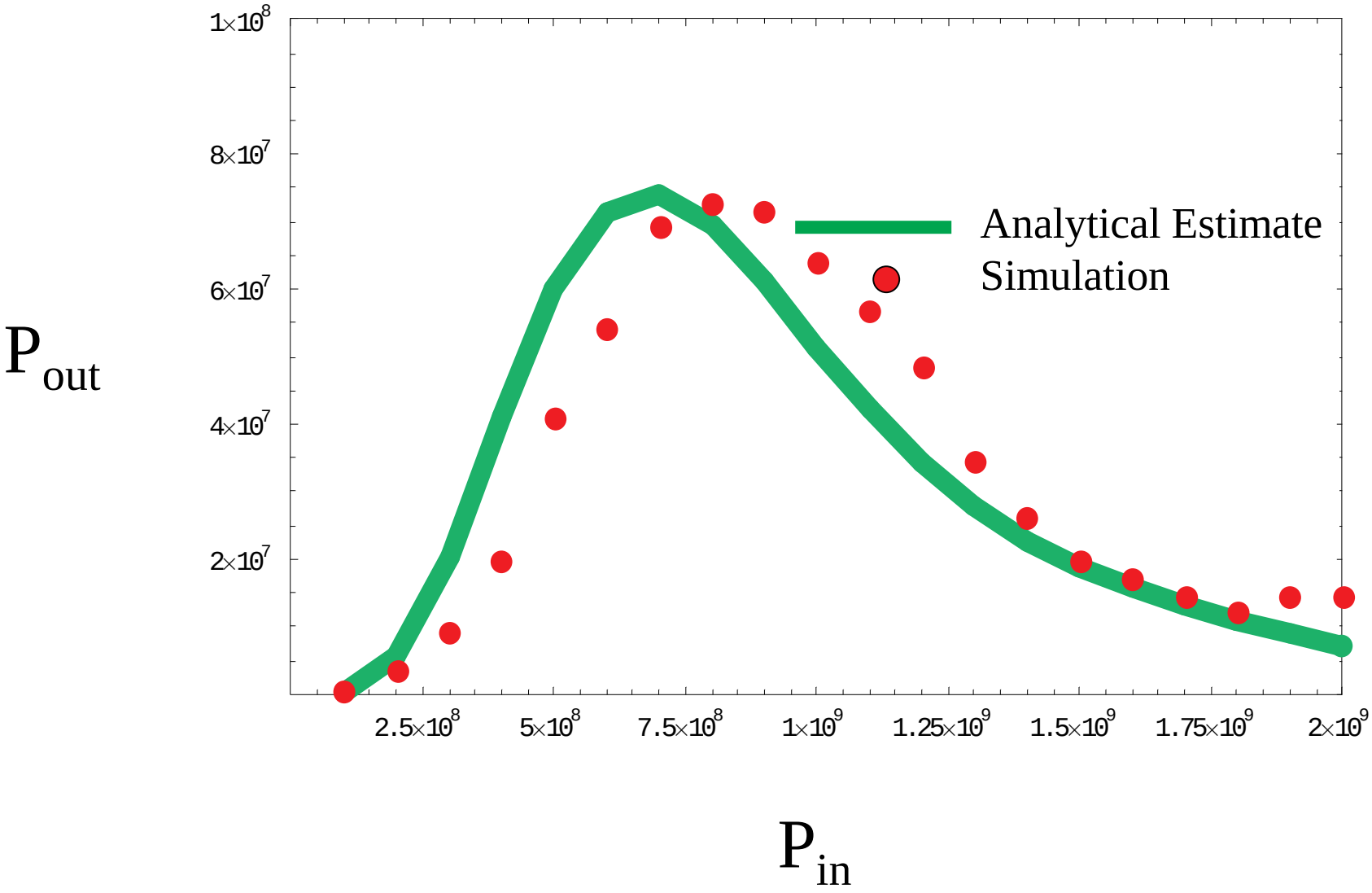

Pulse shape after the first stage

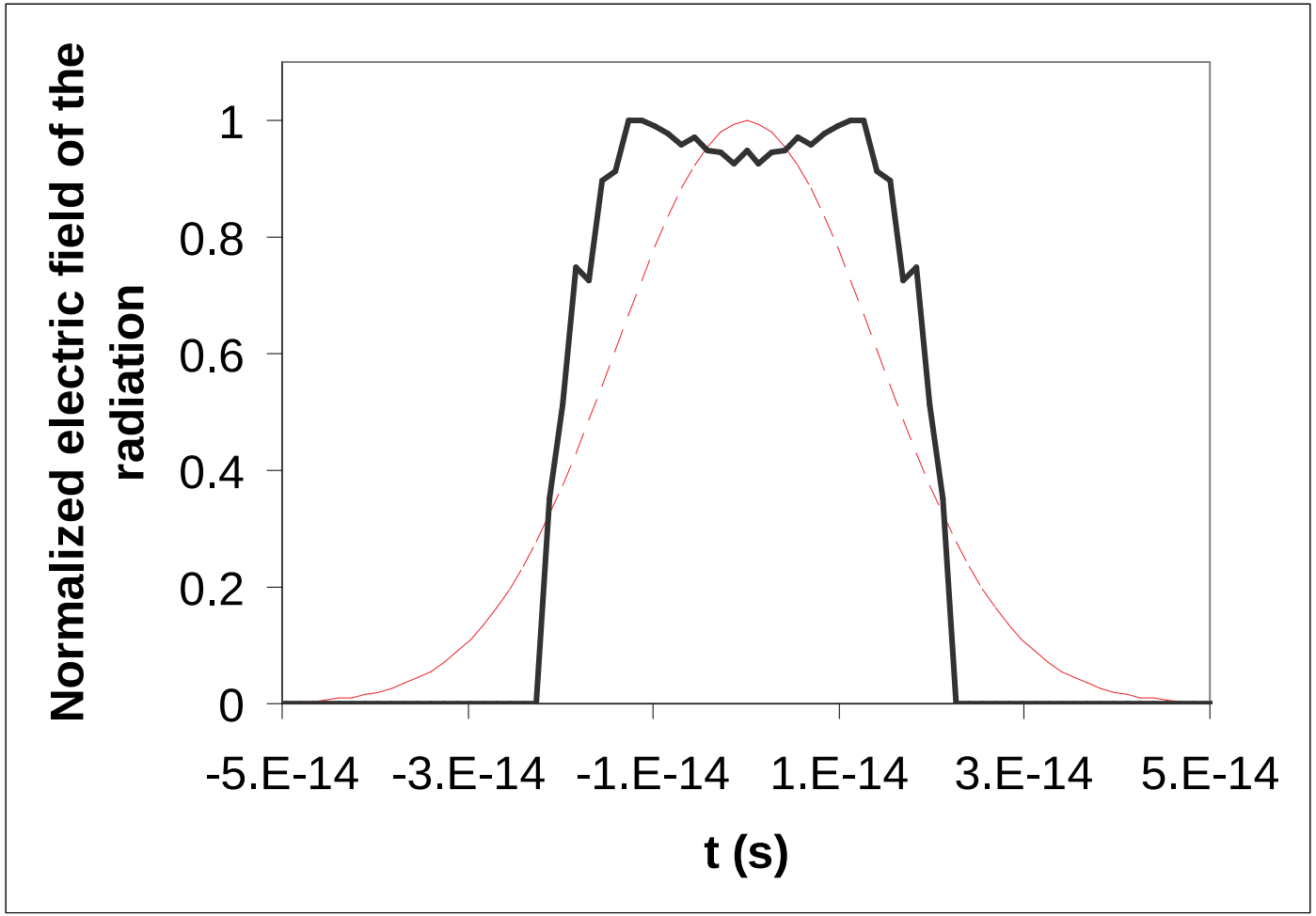

Solid line:

Output pulse at 450 (Å);

Dashed line:

Input pulse at 2,250 (Å).

After the second stage

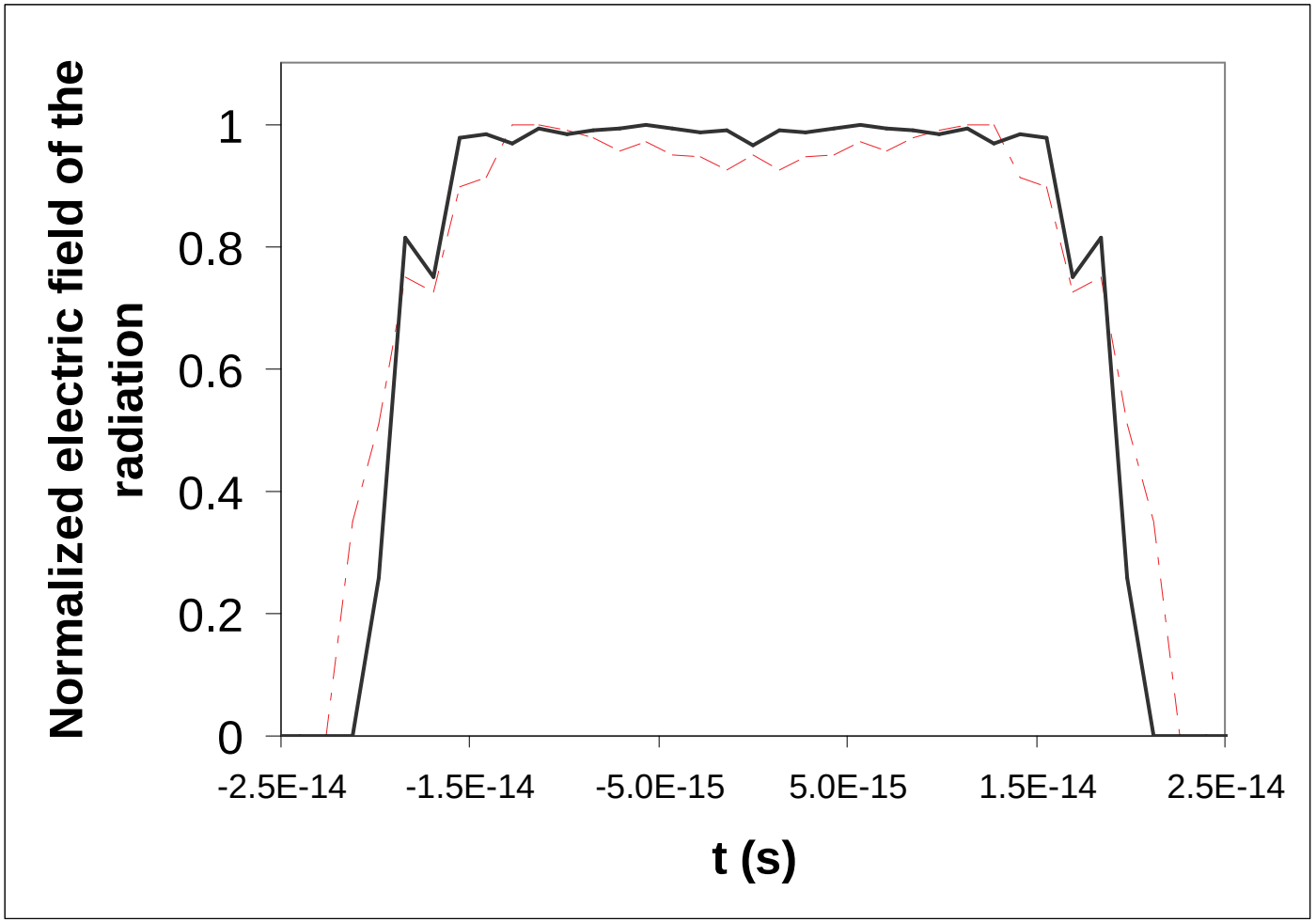

Solid line:

Output pulse at 90 (Å);

Dashed line:

Input pulse at 450 (Å).

Effective Energy Spread of Finite Emittance in Dispersion Section

Path difference due to angular spread is found same as a drift space s

$$\Delta S = T_{511} x'^2 = \frac{1}{2} S x'^2$$

Example: UVFEL $\lambda_s = 100\ nm$

$$\frac{\sigma_{\gamma\ eff}}{\gamma} < 10^{-5}$$

Effect of emittance in dispersion section is weak (Boscolo, Stagno,82), the system is sensitive to local energy spread. Present design may not have taken full advantage of this.

- **Shot noise in undulator**

(W. Brefeld et al. (2001))

Shot noise corresponds to phase error $\phi(t)$

$$E_{in} = a(t)\,Sin[\omega t + \phi(t)]$$

Frequency multiplication N

$$\omega t + \phi(t) \rightarrow N(\omega t + \phi(t))$$

Noise to signal ratio:

$$\left(\frac{P_n}{P_s}\right)_{out} = N^2 \left(\frac{P_n}{P_s}\right)_{in}$$

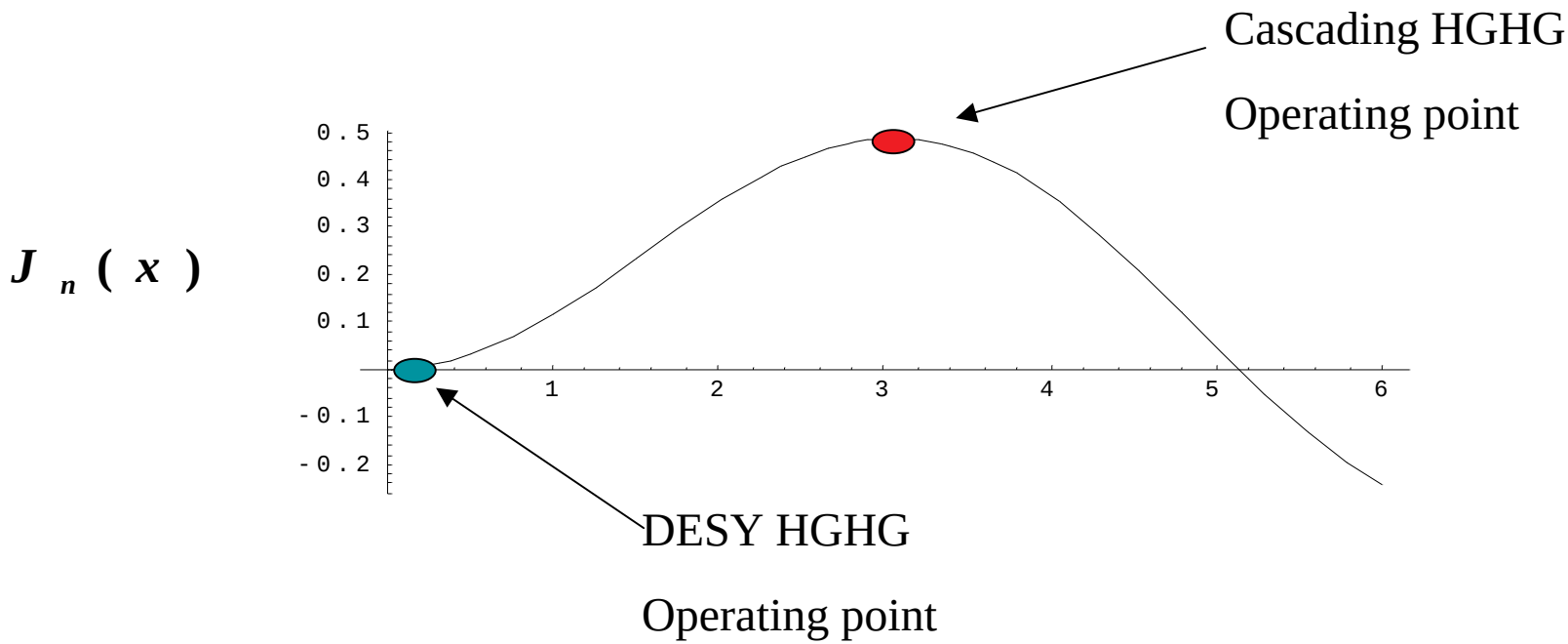

DESY HGHG Example at 8 nm

$$\left(\frac{P_n}{P_s}\right)_{out} = N^2\left(\frac{P_n}{P_s}\right)_{in} = \left(\frac{256nm}{8nm}\right)^2 \frac{100W}{10MW} = 1\%$$

Soft-X-ray Cascading HGHG example at 2.1 nm

$$\left(\frac{P_n}{P_s}\right)_{out} = N^2\left(\frac{P_n}{P_s}\right)_{in} = \left(\frac{266nm}{2.1nm}\right)^2 \frac{30W}{500MW} = 0.1\%$$

Key Technical Challenge

Develop a feedback system to reduce time jitter between the laser pulse and the electron pulse from 0.5 ps to below 0.1 ps

1 Å HGHG FEL

- Noise/Signal ~ 10% instead of 0.1% for 20Å
- Uncertainty in noise generated by CSR?
- We may lose temporal coherence, but still have the good stability, and short pulse length
- Total undulator length similar to SASE or shorter; depends on local energy spread

Conclusion

- Cascading HGHG is an attractive scheme to generate coherent x-ray.
  - Longitudinally fully coherent radiation;
  - Short pulse length (20fs)
  - Total length about same as SASE
  - The device will provide excellent stability.
- Technical challenge: reduce the time jitter from 0.5 ps to 0.1ps.

Transverse and Temporal Properties of SASE FELs

Zhirong Huang

SLAC
Stanford University

SASE FELs

- Undulator radiation starts up from noise to interact with the e-beam

- Energy modulation ➔ density modulation at λ (microbunching) ➔ coherent radiation at λ ➔ exponential growth (L_G)

- At sufficiently high power, electrons fully microbunched with large energy spread ➔ reach saturation (P_{sat})

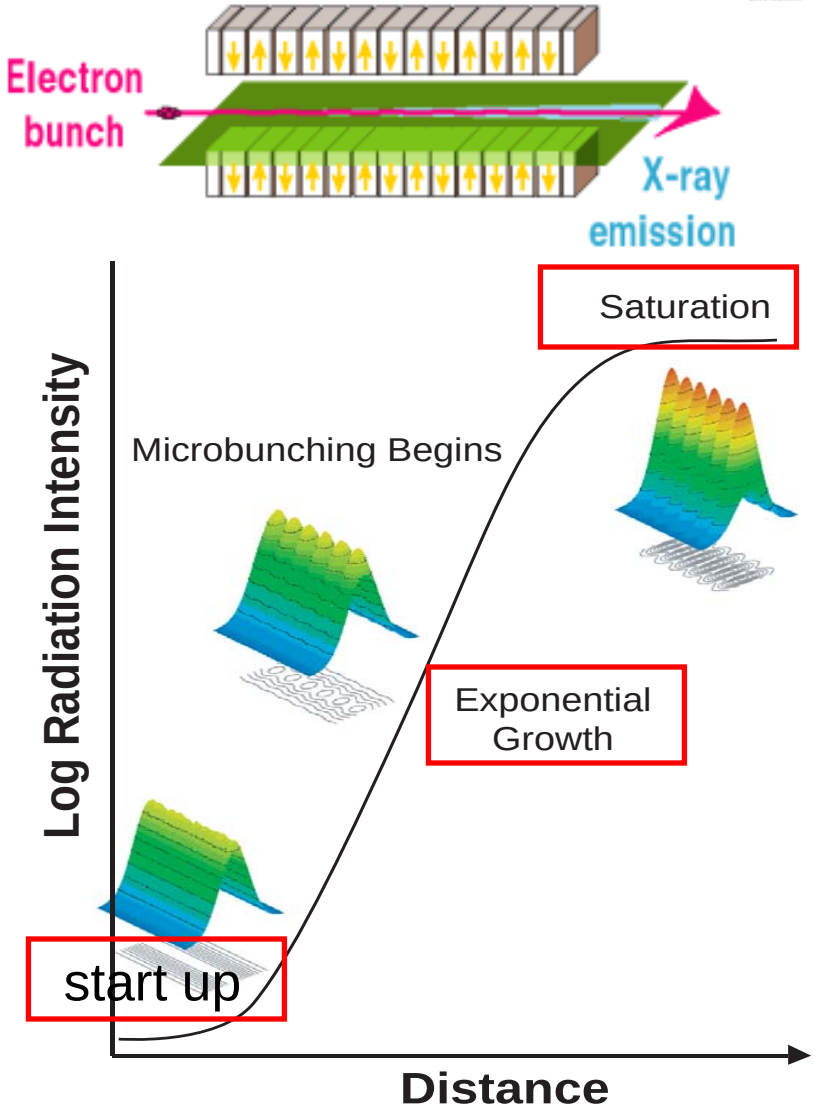

Peak Brightness Enhancement From Undulator Radiation To SASE

$$B = \frac{\#\text{of photons}}{\Omega_x\,\Omega_y\,\Omega_z} \qquad (\Omega_i\text{- phase space area})$$

	Undulator	SASE	Enhancement Factor
# of photons	αN_e	$\alpha N_e N_{l_c}$	$N_{l_c} \sim 10^6$
$\Omega_x\Omega_y$	$(2\pi\varepsilon_x)\,(2\pi\varepsilon_y)$	$(\lambda/2)^2$	10^2
Ω_z	$\frac{\Delta\omega}{\omega}\cdot\left(\frac{\sigma_z}{c}\right) = 10^{-3}\times 10\,ps$	$\frac{\Delta\omega}{\omega}\cdot\left(\frac{\sigma_z}{c}\right)_{\text{compressed}} = 10^{-3}\times 100\,fs$	10^2
B	10^{23}	10^{33}	**10^{10}**

N_{lc}: number of electrons within a coherence length l_c

Transverse Coherence

• Spontaneous undulator radiation phase space is the incoherent sum of the electron phase space, consists of many spatial modes

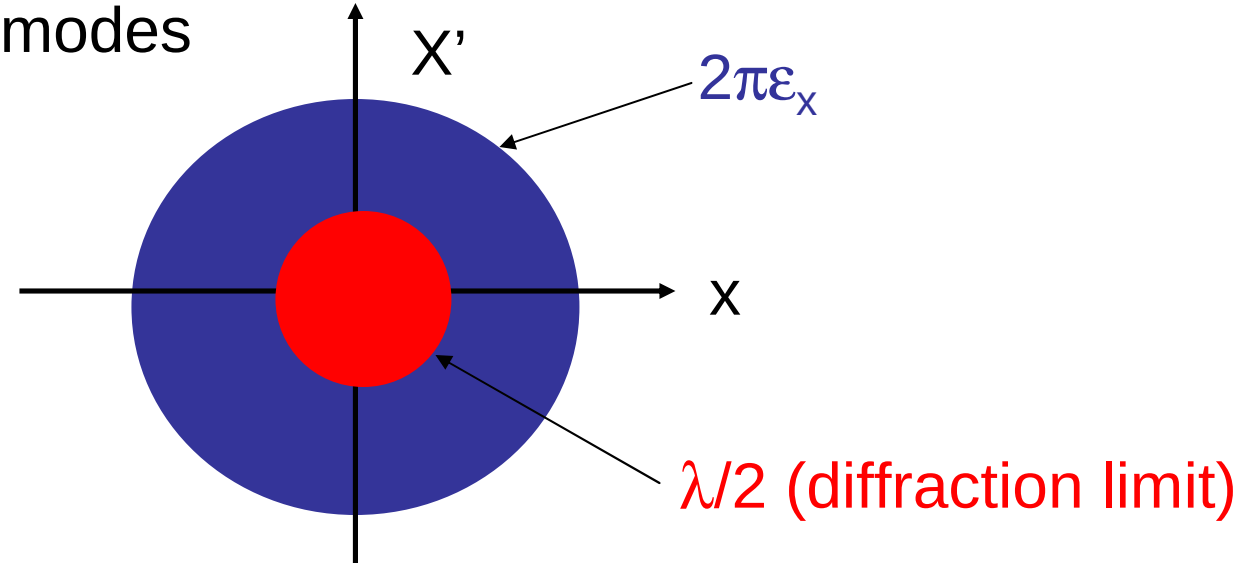

• SASE: higher-order modes have stronger diffraction + FEL gain is localized within the electrons

➔ selection of the fundamental mode (gain guiding)

➔ Fully transversely coherent even $\varepsilon_x > \lambda/4\ \pi$

Gain Guiding (LCLS)

Z=25 m

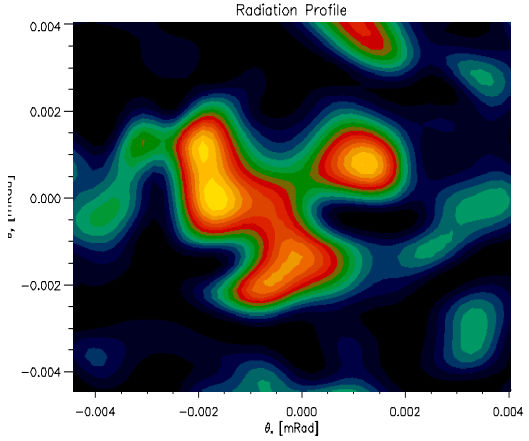

Z=37.5 m

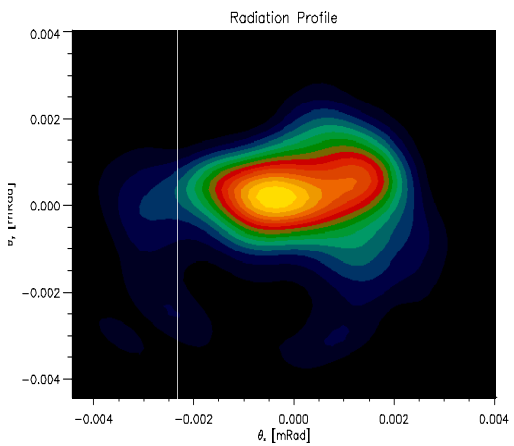

Z=50 m

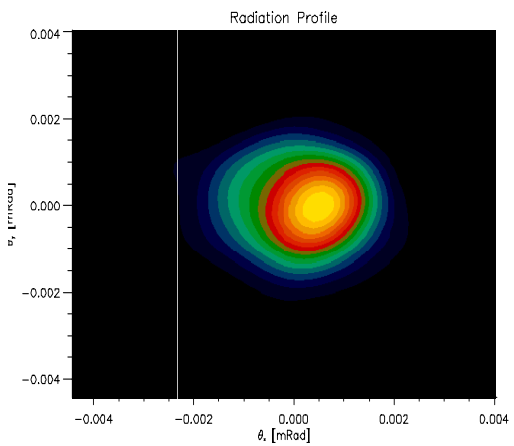

Z=62.5 m

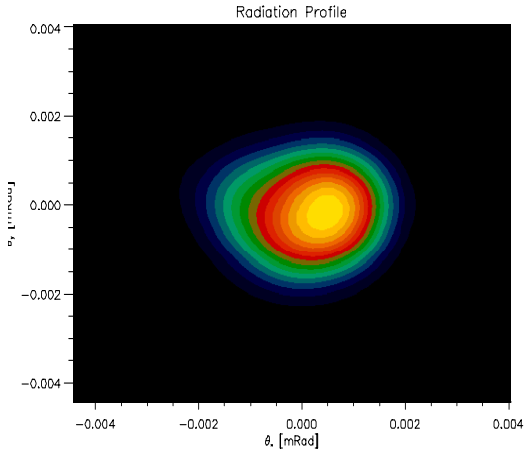

Z=75 m

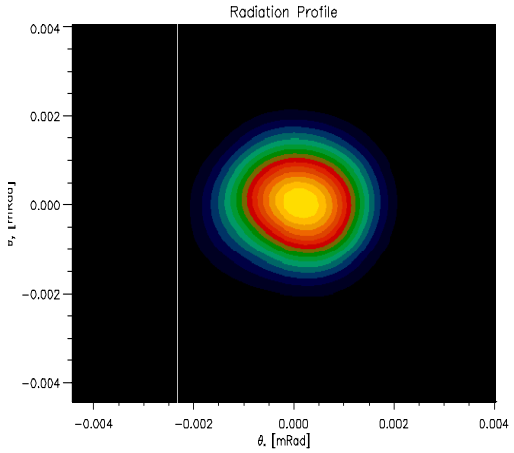

Z=87.5

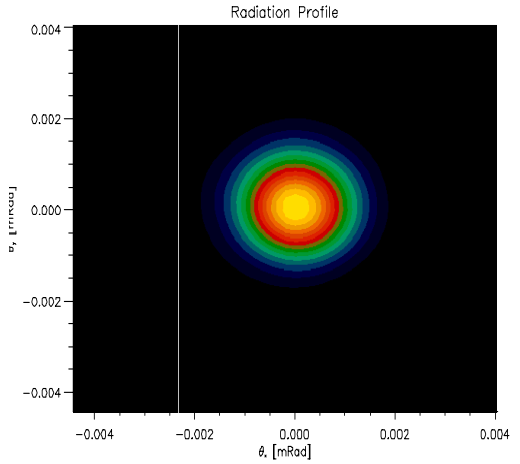

Courtesy of S. Reiche (UCLA)

Temporal Characteristics

- $E(t)=\sum_j E_0(t-t_j)$, t_j is the random arrival time of j^{th} e^-

E_0: wave packet of a single e^-

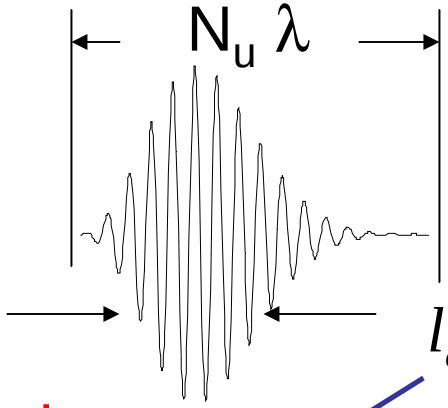

$$l_c \approx \frac{2c}{\sigma_\omega} \approx \frac{\lambda}{\pi}\sqrt{\frac{N_u}{\rho}}$$

- l_c ~ 100-1000 λ < bunch length

- Sum of all packets ➔ E(t)

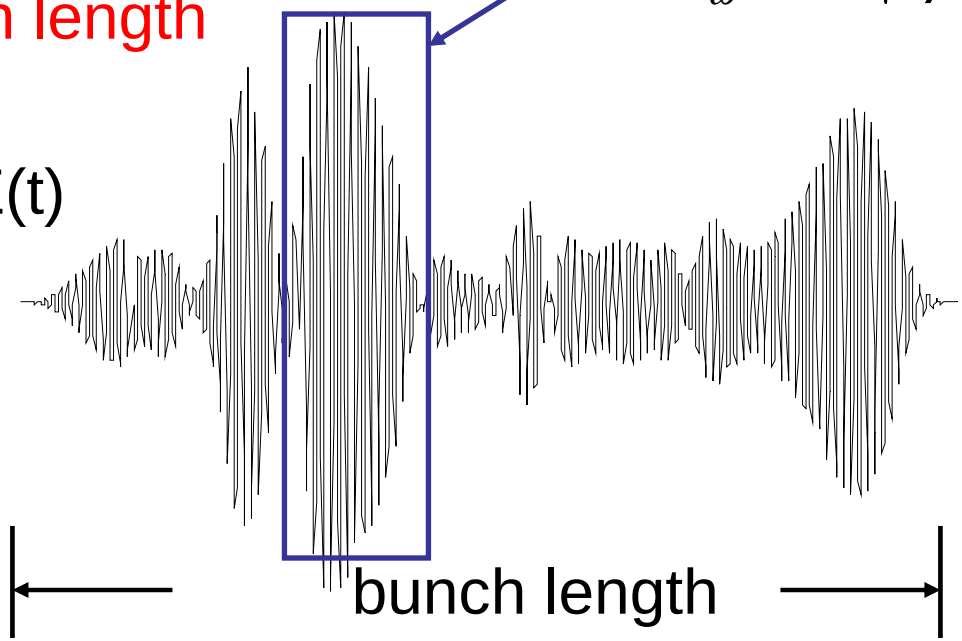

Longitudinal Modes

- Due to noise start-up, SASE is a chaotic light temporally with M_L coherent modes (M_L spikes in intensity profile)

$$M_L \approx \frac{\text{bunch length}}{\text{coherence length}}$$

- Its longitudinal phase space is M_L larger than FT limit (rooms for improve!)

- Integrated intensity fluctuation $\frac{\Delta I}{I} = \frac{1}{\sqrt{M_L}}$

- M_L is NOT a constant, decreases due to increasing coherence in the exponential growth, increases due to decreasing coherence after saturation)

- Statistical fluctuation is large for long-wavelength exps since M_L is only a few, but much smaller for X-ray FELs (most likely dominated by jitter etc…)

LCLS near saturation

$M_L \sim 200 \rightarrow \Delta I/I \sim 7\ \%$

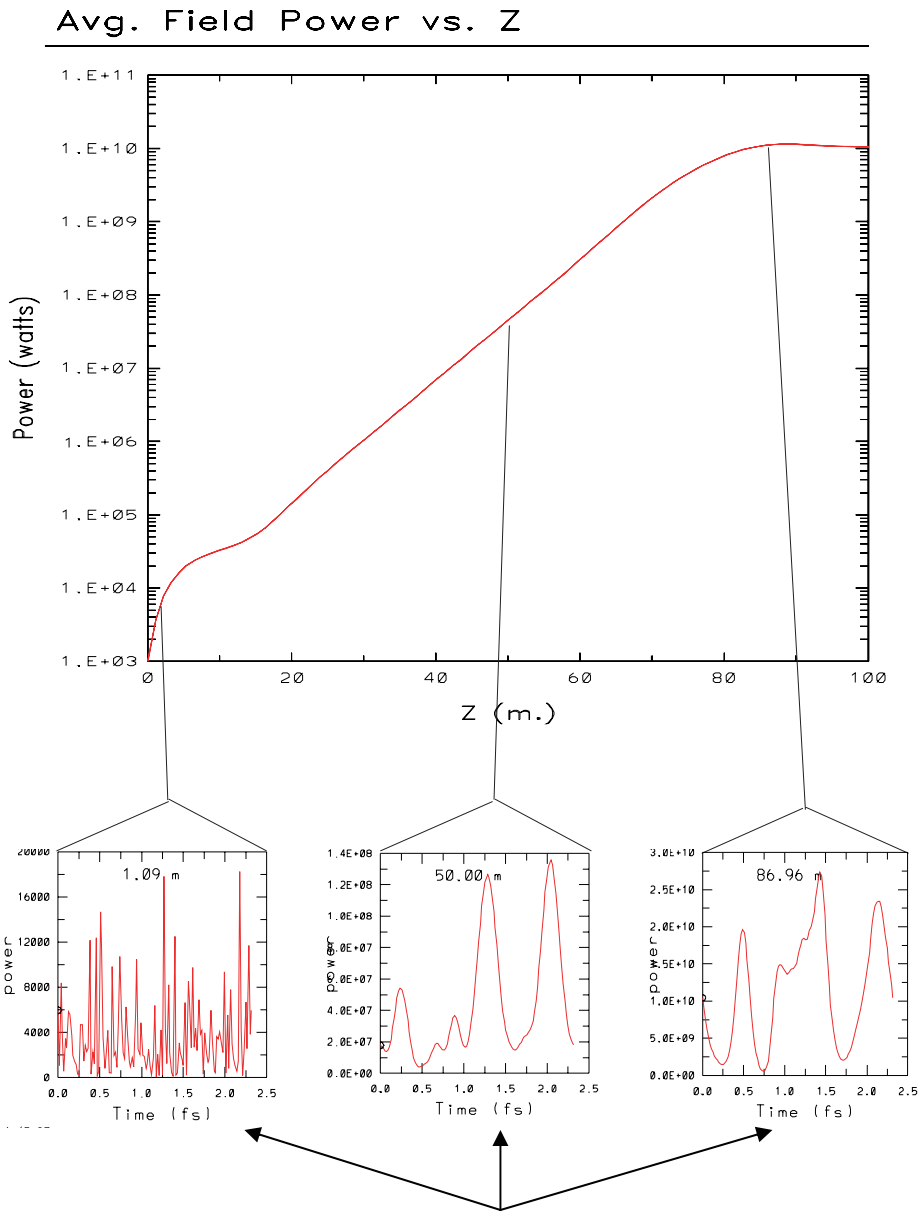

1 % of X-Ray Pulse Length

Transverse and Temporal Properties: Interplay

- Transverse coherence somewhat affected by “large” SASE bandwidth
- Different fundamental modes for different frequencies

- FEL fundamental mode and its transverse phase space

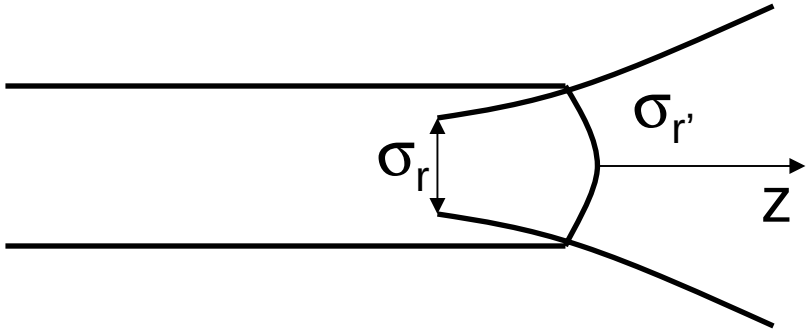

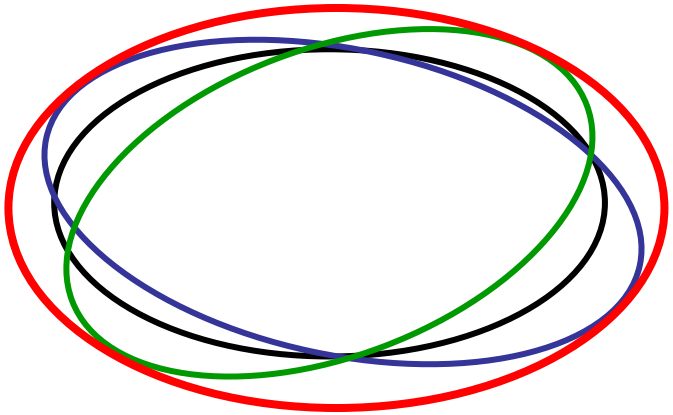

- Smearing of radiation phase space ellipses reduces transverse coherence: LEUTL~ 90%, LCLS ~ 97%

➔ M_T ¼ 1 !

Nonlinear Harmonic Generation

- FEL instability creates energy and density modulation at λ,
- Near saturation, strong bunching at fundamental λ produces rich harmonic components

small signal, linear regime

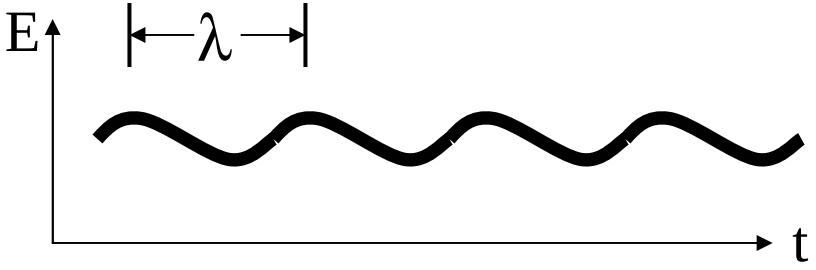

near saturation, nonlinear regime

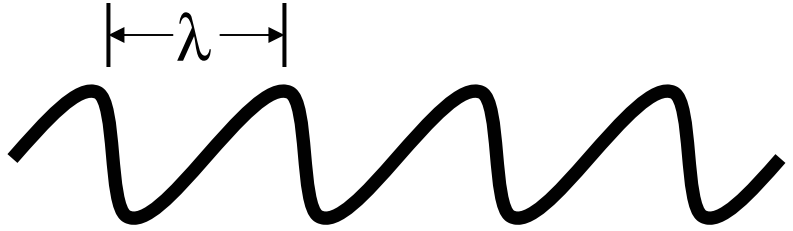

- Coherent harmonics drive by fundamental λ **(E_n / E_1^n)**
  - ➔ gain length = L_G/n (n is harmonic order)
  - ➔ transverse coherence
  - ➔ temporal structure

Plenty of Power at (3X) Shorter Wavelength

- Theory and simulations predicts third harmonic reaches 1% of fundamental

LCLS expectation

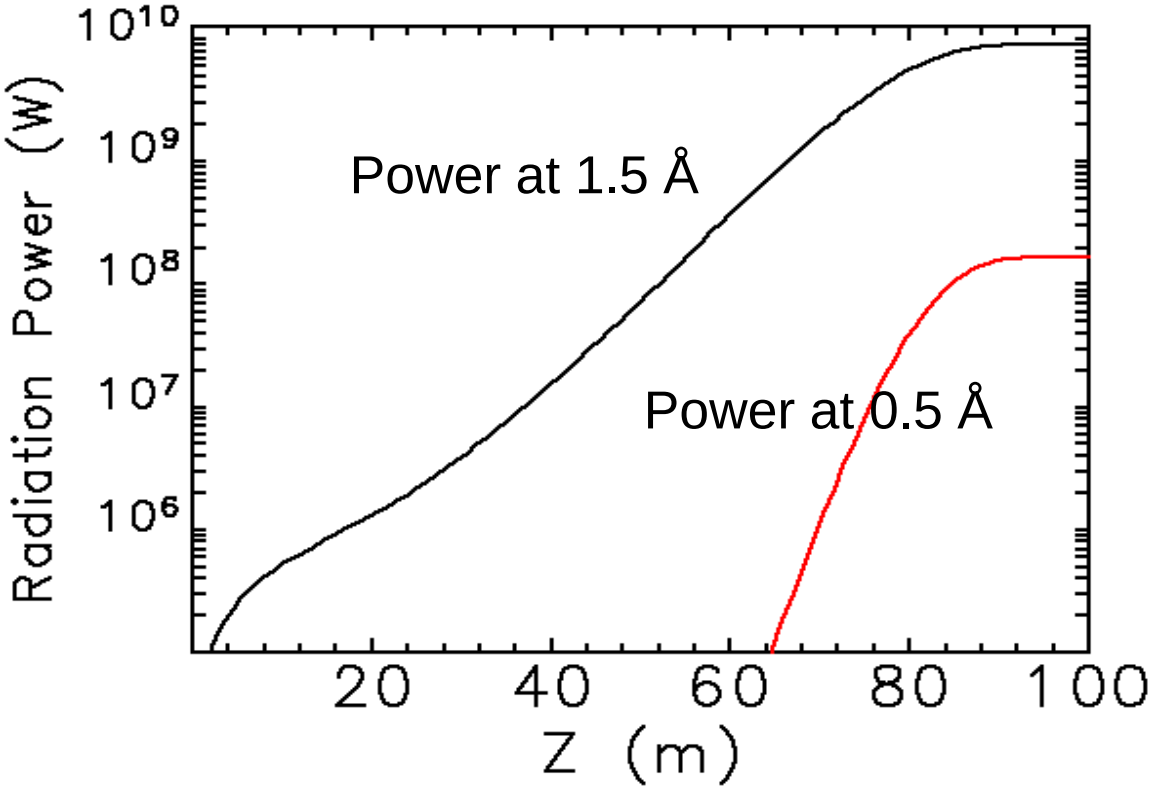

- At lower energy, significant even harmonics are present

Transverse Coherence of NHG

- Harmonic profiles created by guided mode of the fundamental

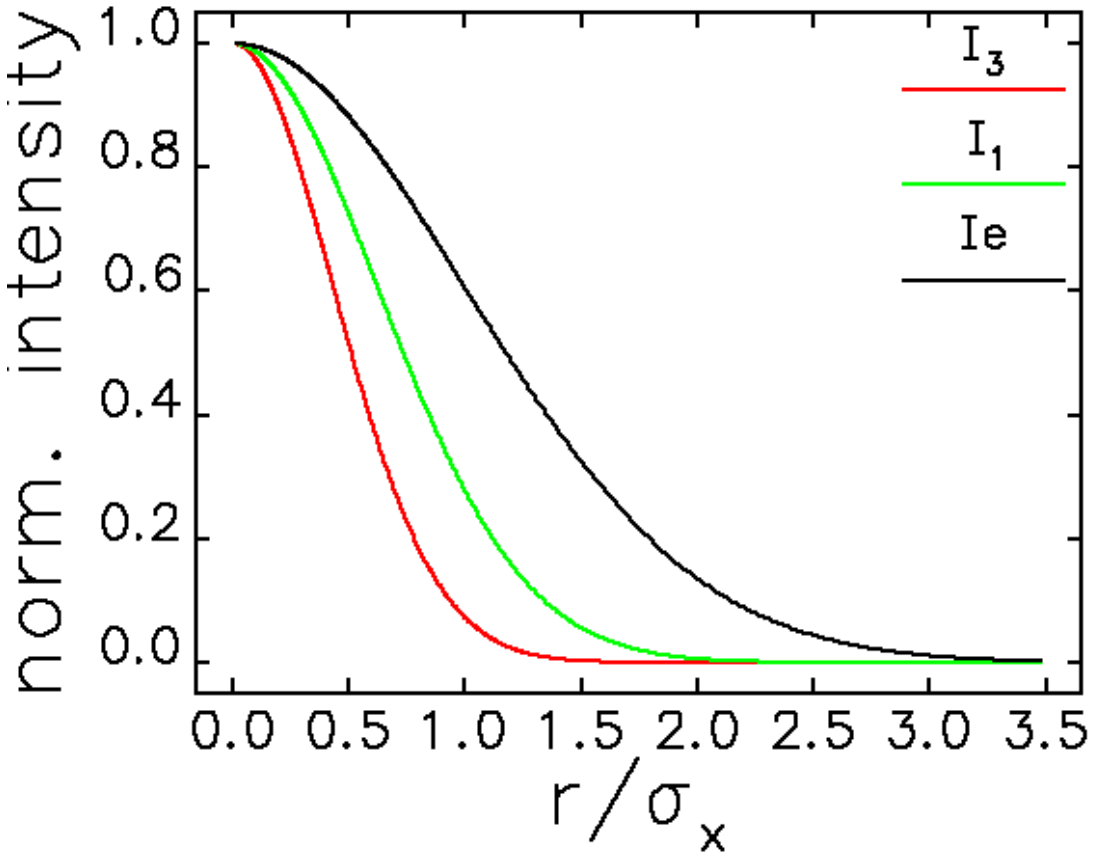

$I_3(r) \sim I_1^3(r)$

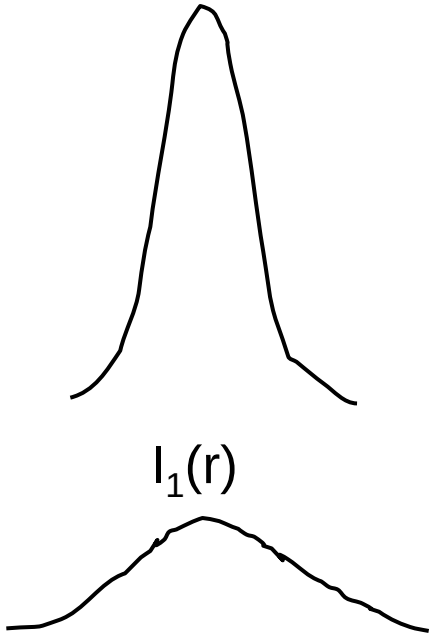

- Trasversely coherent third harmonic at 0.5 Å

(for ε_n =1.5 μ m, the diffraction limit is 7 Å)

Temporal Properties of NHG

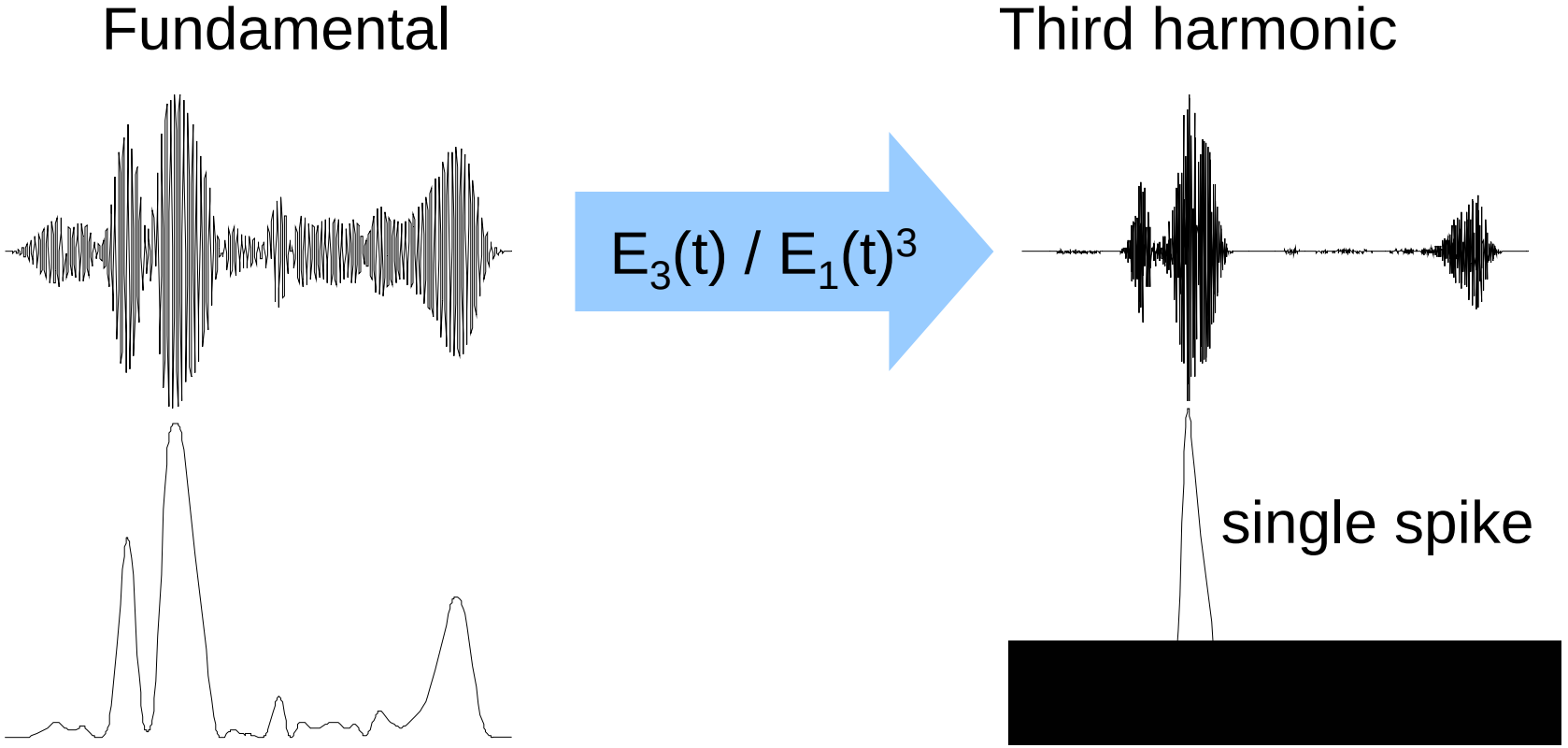

- Third nonlinear harmonic: more spiky temporally
  - → higher average power (6 £ steady state power)
  - → more shot-to-shot fluctuation
- Apply NHG statistics to select single spike (Saldin et al.)

SASE Demonstration Experiments at Longer Wavelengths

- IR wavelengths:

  UCLA/LANL ($\lambda = 12\mu$, $G = 10^5$)
  LANL ($\lambda = 16\mu$, $G = 10^3$)
  BNL ATF/APS ($\lambda = 5.3\mu$, $G = 10$, HGHG = 10^7 times S.E.)

- Visible and UV:

  LEUTL (APS): $E_e \leq 400$ MeV, $L_u = 25$ m, $120\ \text{nm} \leq \lambda \leq 530\text{nm}$
  VISA (ATF): $E_e = 70$ MeV, $L_u = 4$m, $\lambda = 800$ nm
  TTF (DESY): $E_e < 300$ MeV, $L_u = 15$ m, $\lambda = 80$–120 nm
  SDL (NSLS): $E_e < 200$ MeV, $L_u = 10$ m, $\lambda = 800$–260 nm

All Successful, TTF and LEUTL pilot user operation around 100 nm

LEUTL FEL

	A	B	C
σ_t (ps)	0.19	0.77	0.65
I (A)	630	171	184
$\gamma\varepsilon$ (mm)	8.5	8.5	7.1
σ_δ (%)	0.4	0.2	0.1
λ (nm)	530	530	385

Observations agree with theory/ computer models

(S. Milton et al., Science, 2001)

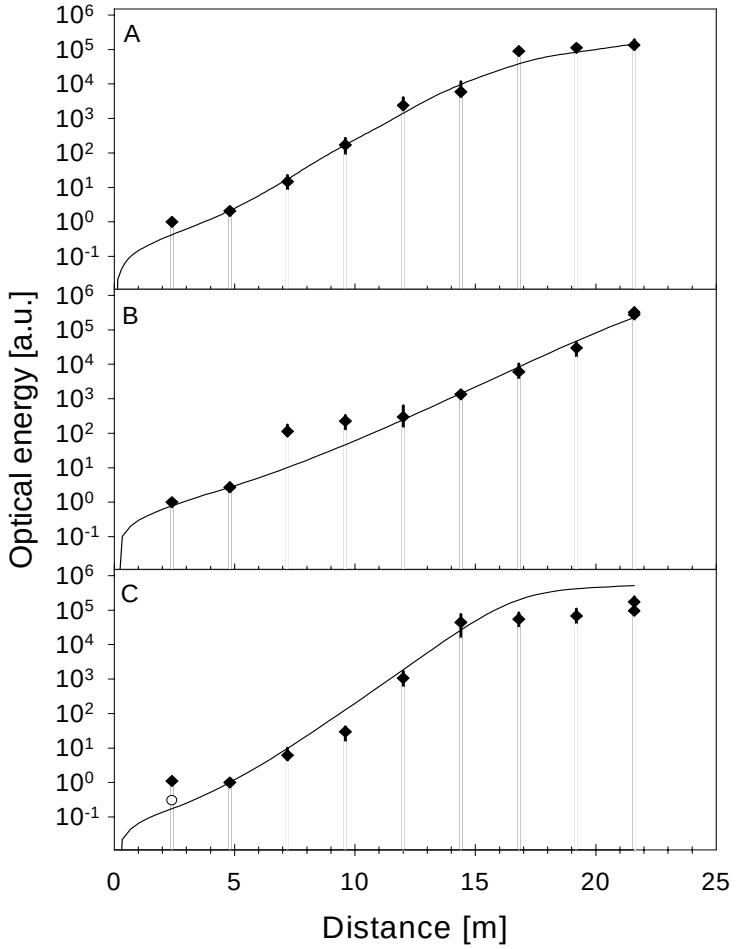

SASE bandwidth

- Before saturation, SASE spectrum undergoes gain narrowing
- After saturation, spectrum redshifts and broaden because trapped electrons create sideband instability
- At saturation, bandwidth reaches minimum ~ ρ

- LEUTL confirms this (Sajaev et al. FEL2001)

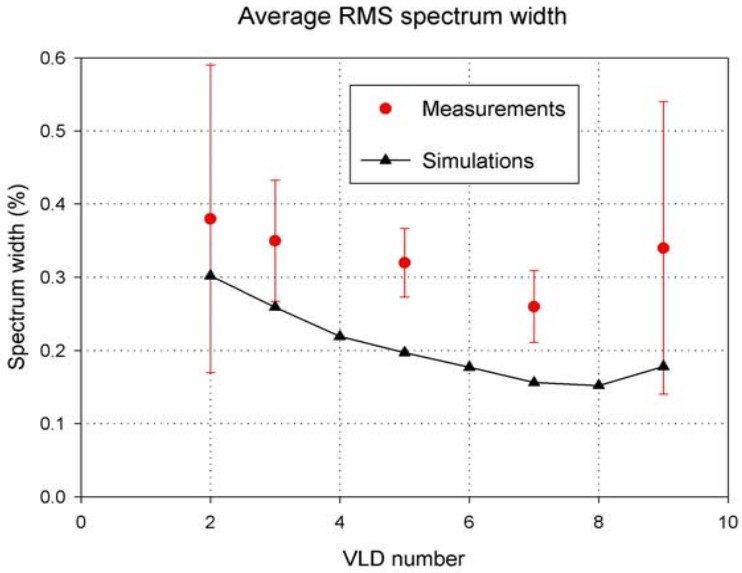

Time-Resolved Measurements (FROG)*

FROG sample 1

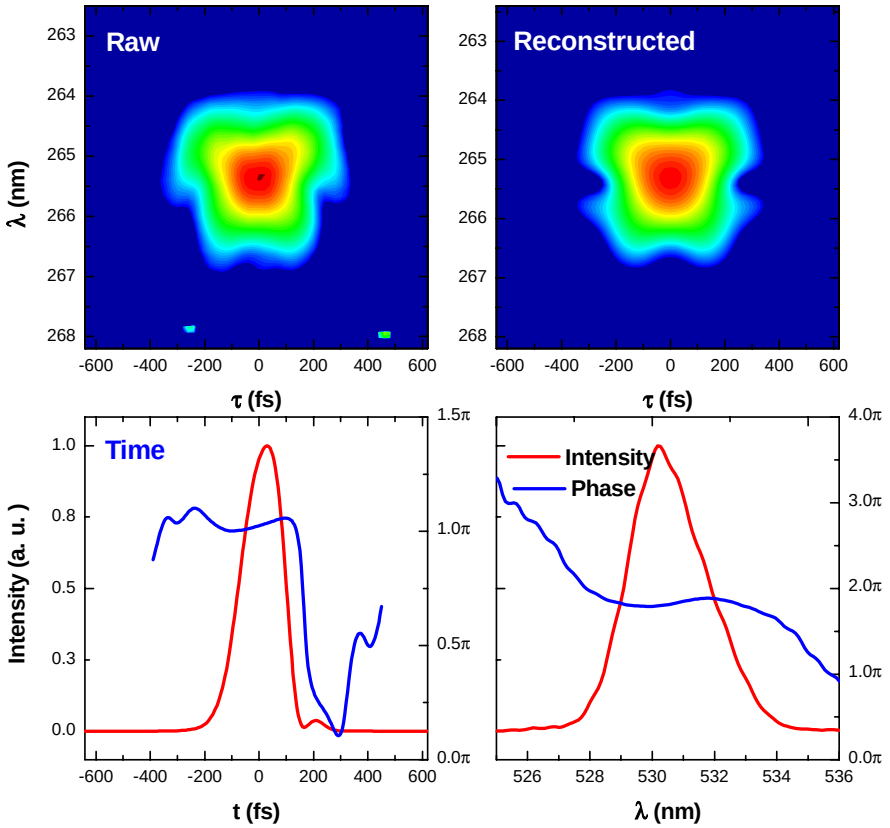

single spike

Shot A442

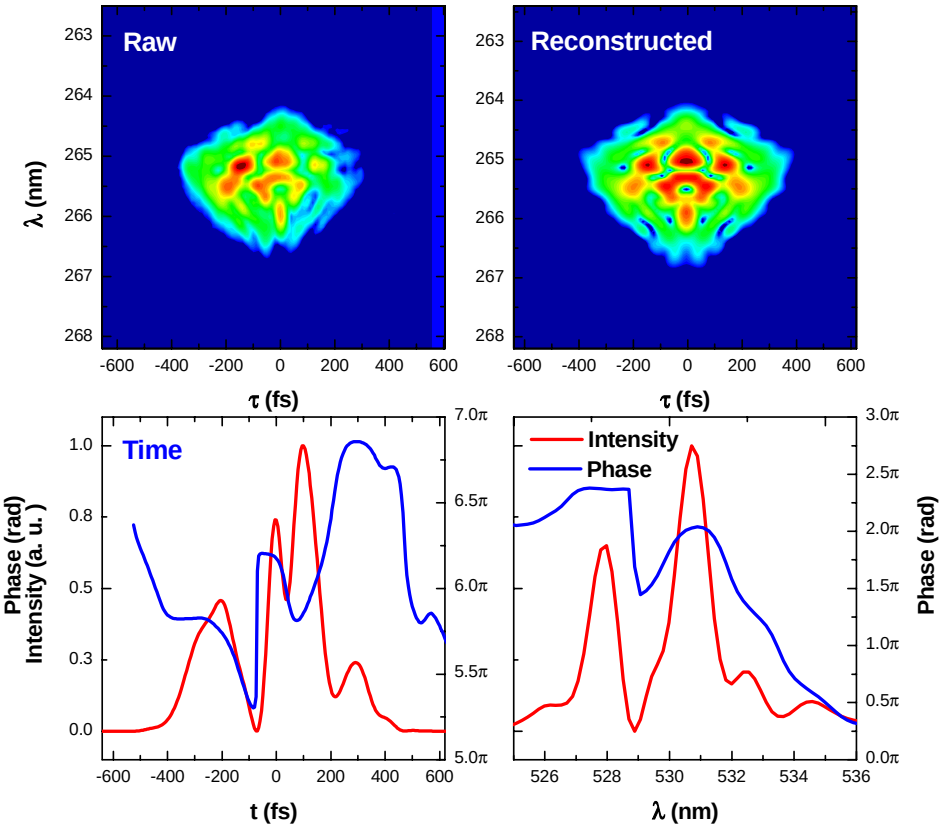

multiple spike

* Y. Li et al., PRL (2001)

Nonlinear Harmonic Radiation at VISA*

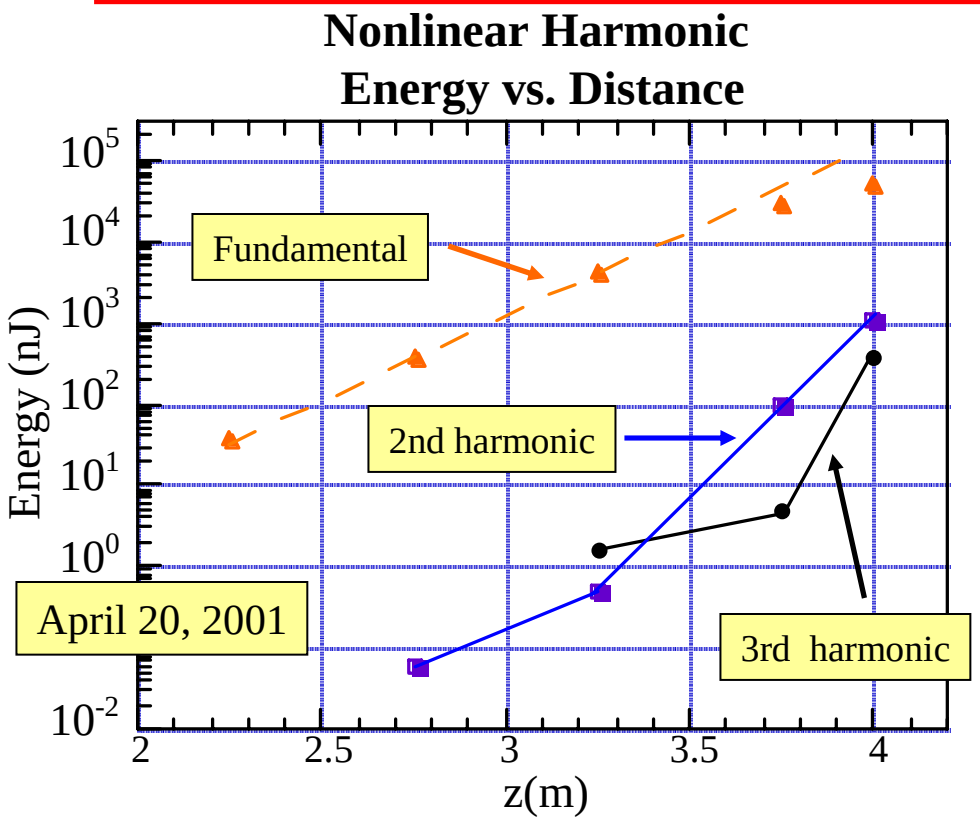

Energy Comparison

Mode (n)	Wavelength (nm)	Energy (μJ)	% of E_1
1	845	52	
2	421	.93	1.8
3	280	.40	.77

Using the relation of 2nd and 3rd harmonic energies as given by Z. Huang and K.J.Kim

$$E_2 = \left(\frac{K}{\gamma k_u \sigma_x}\right)^2 \left(\frac{K_2}{K_3}\right)^2 \left(\frac{b_2}{b_3}\right)^2 E_3$$

b -bunching parameters
K_n -Coupling coefficients

Associated gain lengths

$$L_f = 19cm$$
$$L_2 = 9.8cm \quad \Rightarrow \quad L_n = L_g / n$$
$$L_3 = 6.0cm$$

* A. Tremaine, X.J. Wang et al., PRL (2001)

Observations at TTF FEL*

Statistical fluctuation

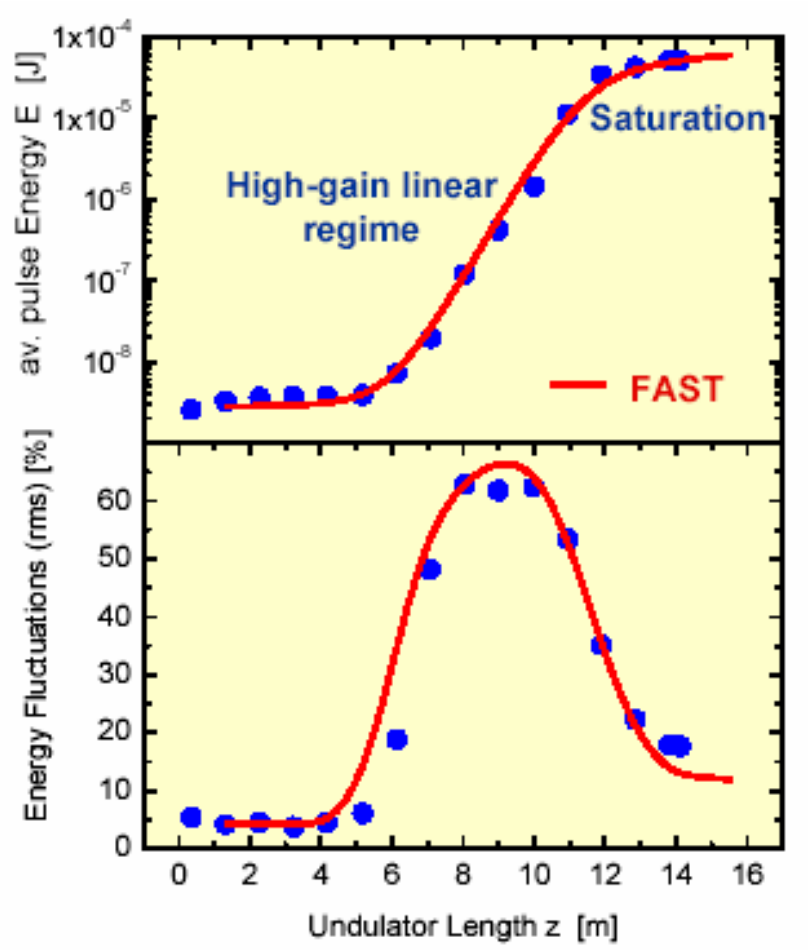

Transverse coherence

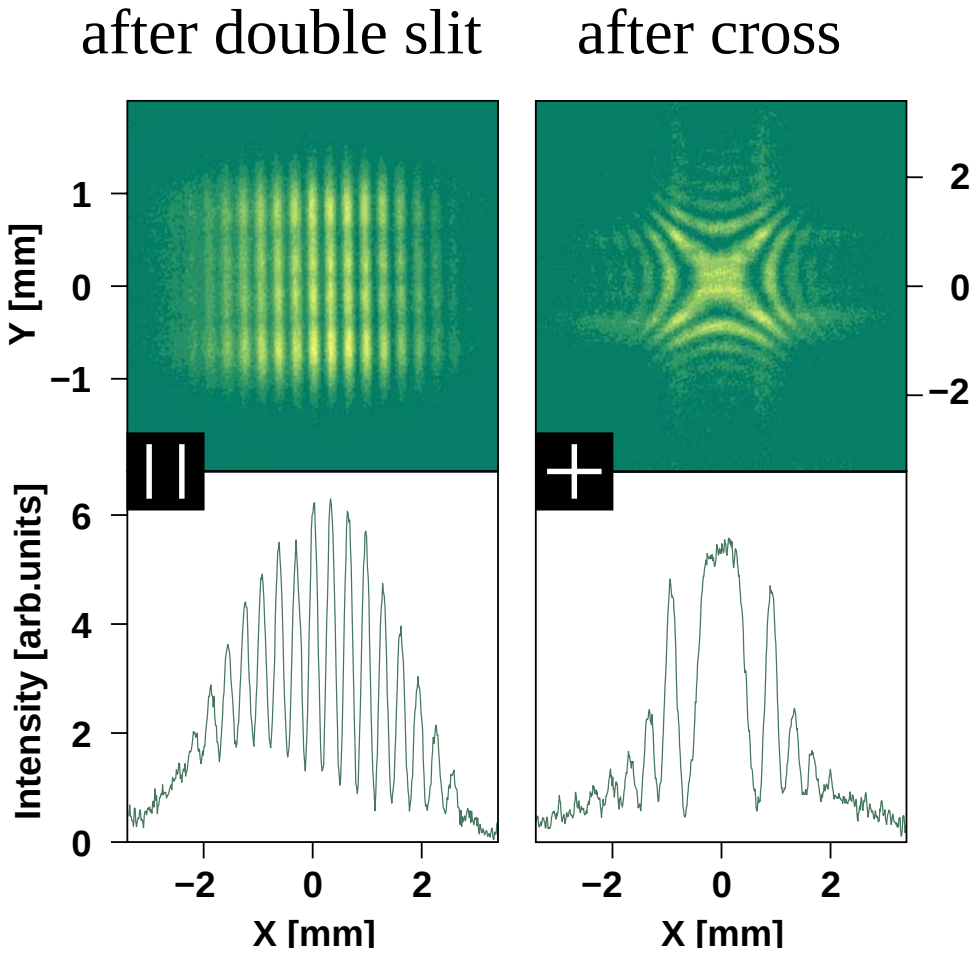

* V. Ayvazyan et al., PRL (2001); Eur. Phys. J. D (2002)

X-ray SASE (100 nm → 1 nm → 0.1 nm)

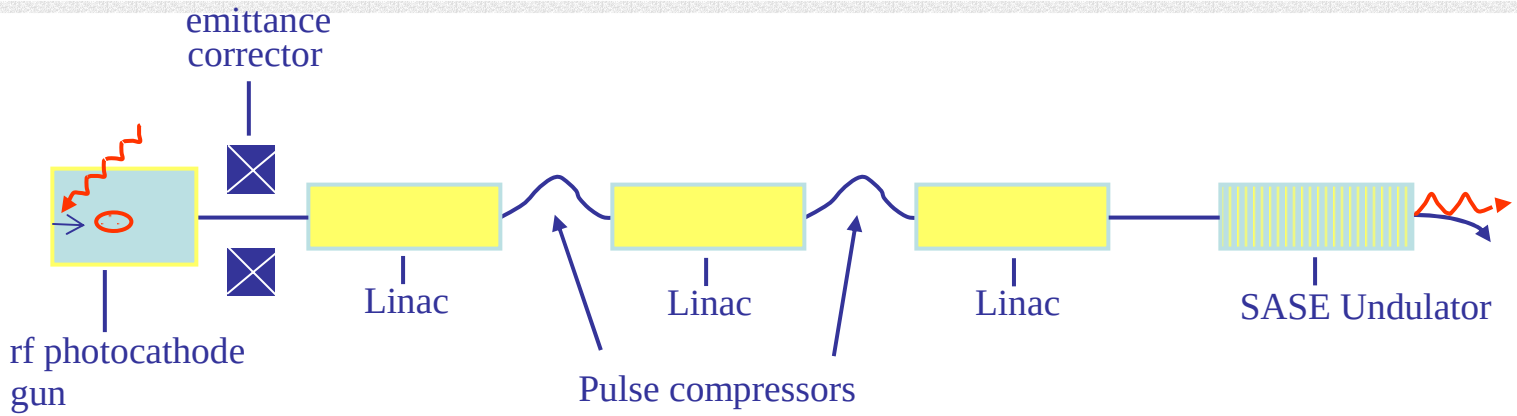

- Photocathode rf gun $\varepsilon_x^n \sim 1\ \mu$ m, $I_p \sim 100$A
- Bunch compression $I_p \sim 2$-5 kA, $\Delta\tau < 1$ ps
- Acceleration 3–20 GeV, $\lambda \sim \lambda u/(2\gamma^2)$

  adiabatic damping $\varepsilon_x \sim \varepsilon_x^n/\gamma \sim \lambda/4\pi$, $\sigma_\gamma/\gamma < \rho \sim 10^{-3}$
- Undulator 100-m long, segmented, a few μm tolerance

Projects undertaken at US, Germany, Japan, Italy etc.

Techical Challenges

- RF photocathode gun
  - close to design goals, need better stability and reliability
- Emittance preservation in linacs (SLC experiences)
  - Transverse wakefields (only important when bunch is longer)
  - Misalignment and chromaticity
- Bunch compression
  - CSR and microbunching instability
  - Interplay with linac wakefield
- Machine stability
  - Jitter tolerances
- Undulator trajectory
  - Very demanding (need beam-based alignment)

Conclusion

- SASE FEL is the most straightforward approach to achieve extremely high-brightness x-ray sources

- Longitudinal properties of SASE can be further improved

  - narrower bandwidth (HGHG, self-seeding, RAFEL)

  - Shorter pulse (laser seeding, electron chirping and manipulation)

- Excitements and Challenges ahead!

Short Pulse Program of LCLS

Sven Reiche

UCLA 12/13/02

Outline

- The standard LCLS case
- Scientific merit of short pulses
- LCLS - “Experiment 6”
  - Radiation pulse manipulation
  - Electron beam manipulation
- Conclusion

LCLS Beamline

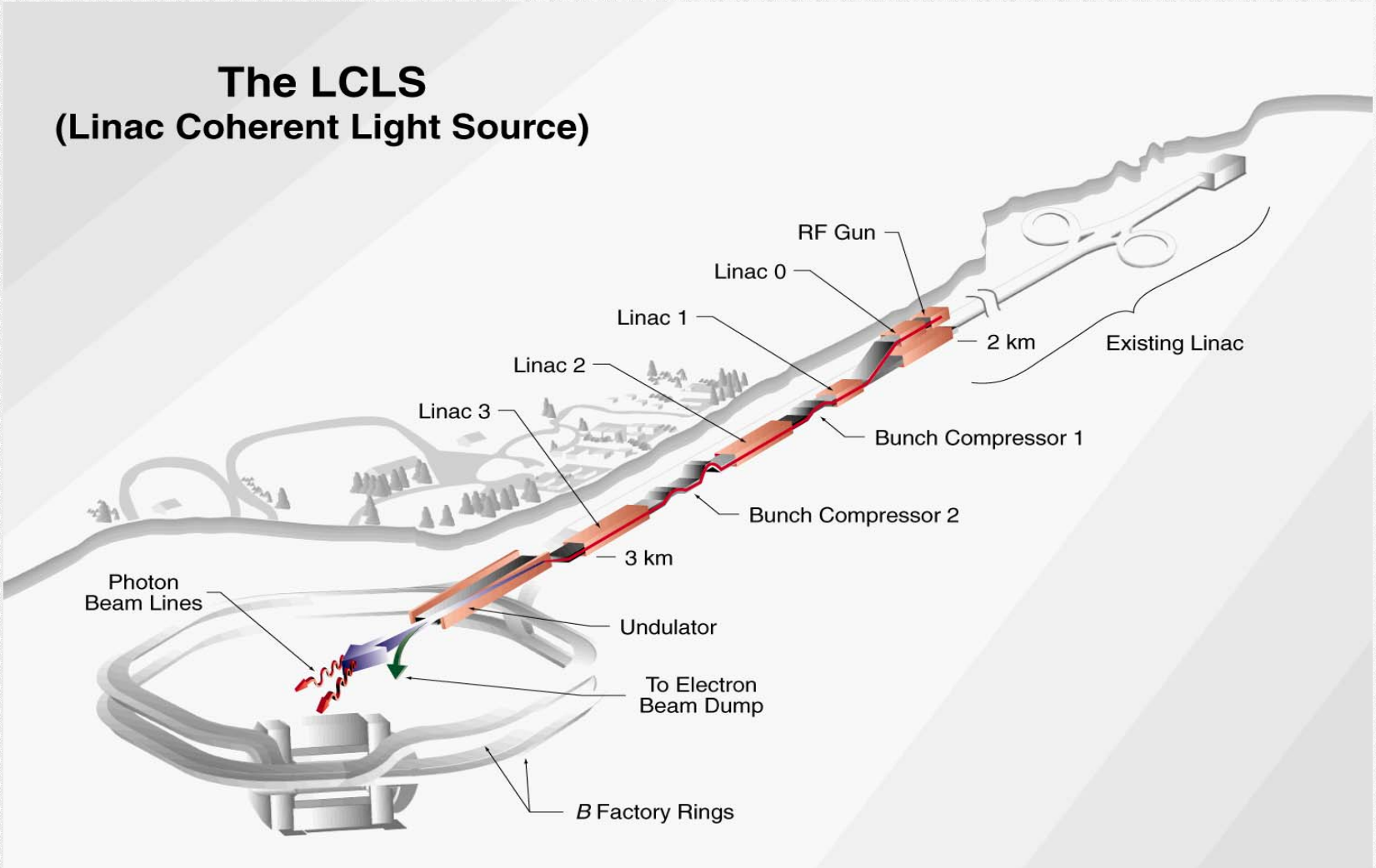

LCLS Beamline (@1.5 Å)

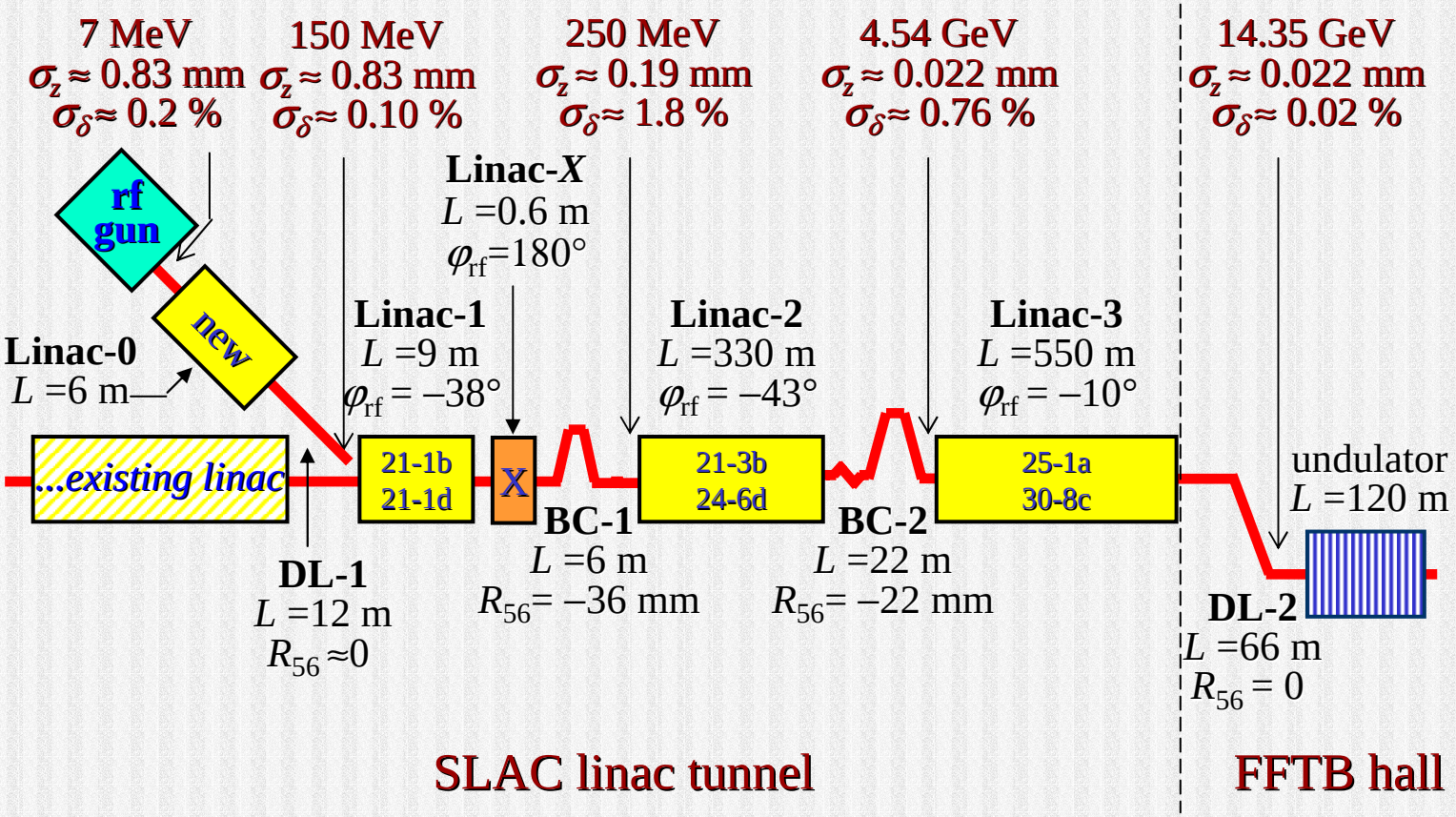

LCLS Design Parameters

- Operation between 1.5 - 15 Å

Charge [nQ]	1	0.2
Energy [GeV]	14.3 (4.5)	14.3 (4.5)
Energy Spread [%]	0.008 (0.025)	0.008 (0.025)
Norm. Emittance [mm·mrad]	1.2	0.9
Peak Current [kA]	3.4	1.6
Pulse Length, FWHM [fs]	230	100
Undulator Parameter	3.7	3.7
Udulator Period [cm]	3	3

Beam Transport

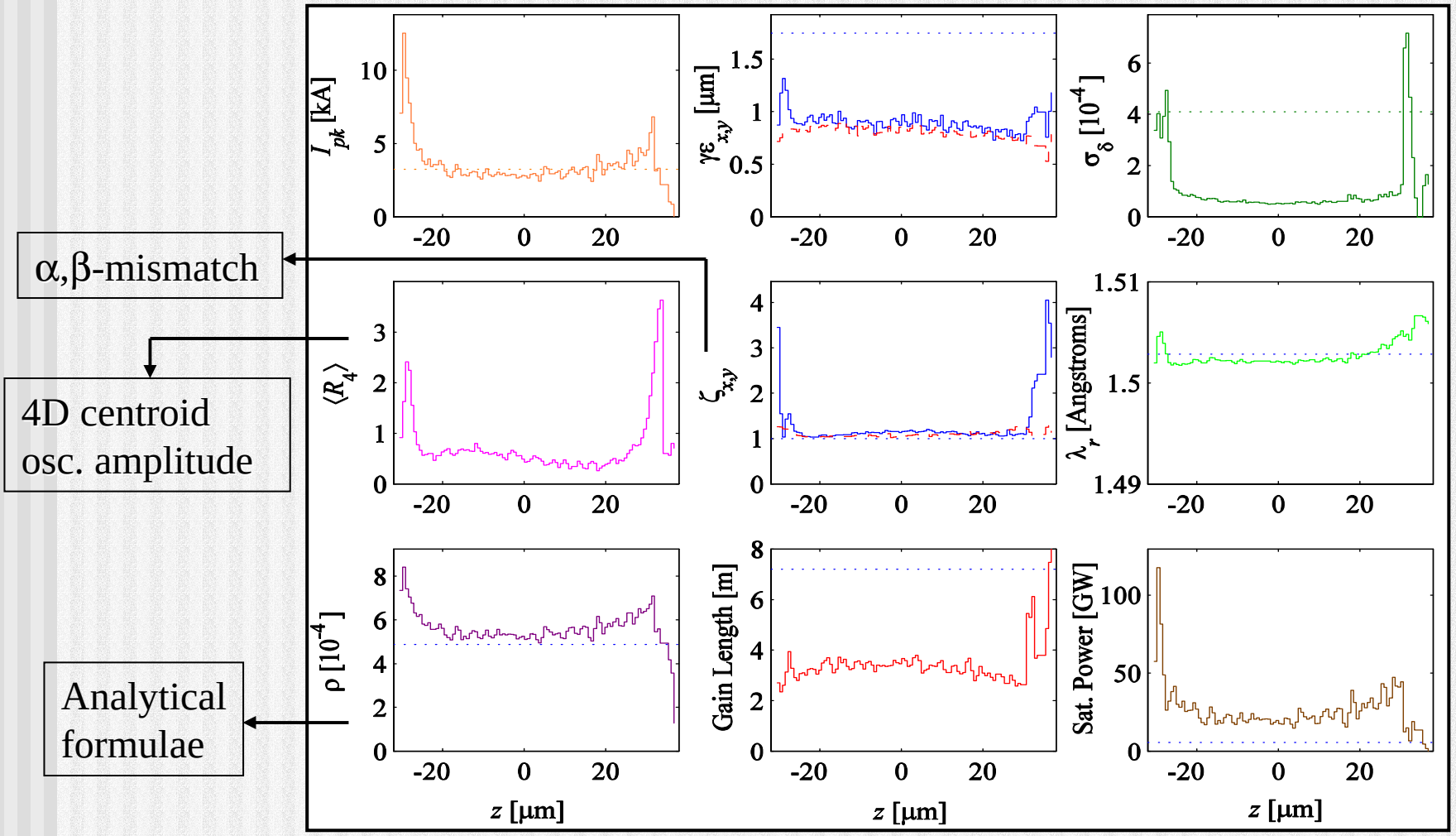

FEL Performance I

- Start-end simulations for two different initial bunch charges of 1 nC and 0.2 nC.
- Low charge case is modeled after the GTF results and then propagated through the LCLS beam line.
- Power reduction by wakefields is 35 %.
- Transverse coherence at 35 m.
- Saturation at 85 m.

Low charge case performs worse due to higher slice emittance and lower current.

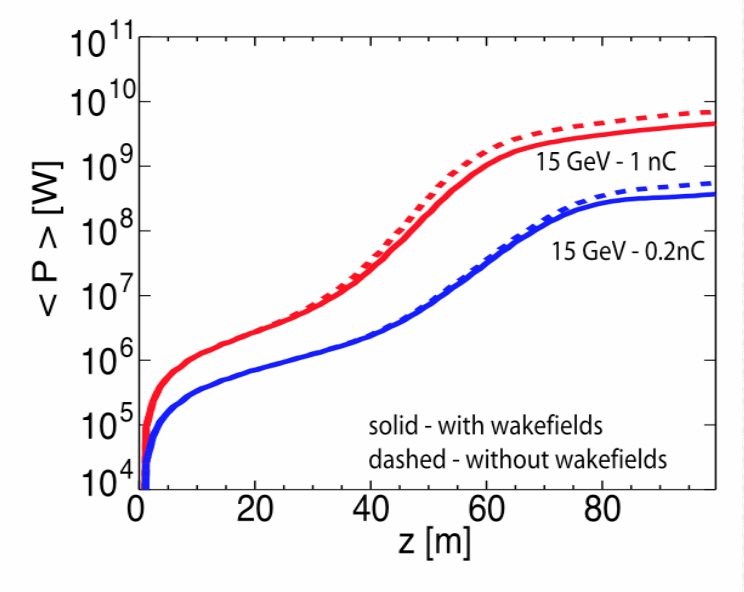

FEL Performance II

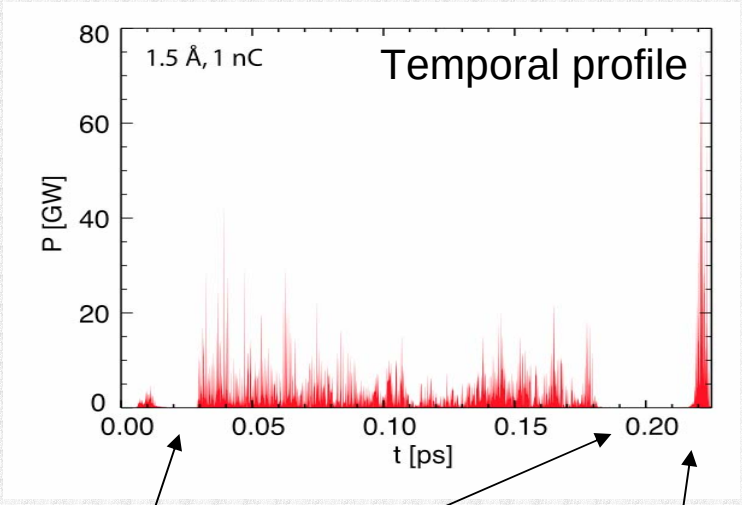

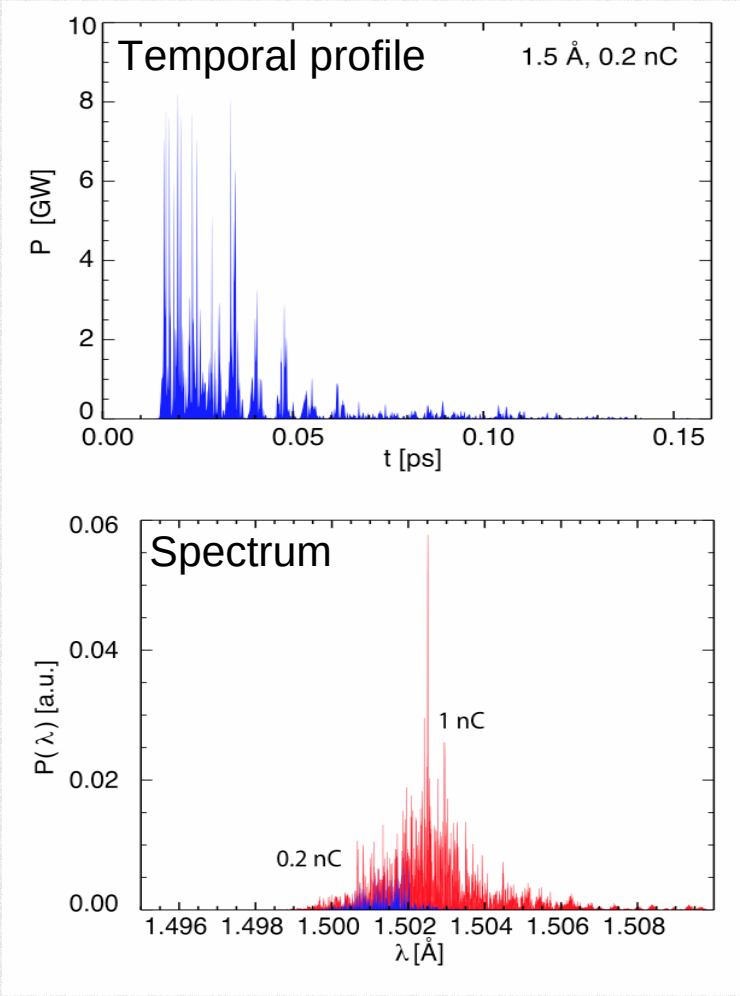

Undulator wakefields, large energy spread + emittance

Current spike (~16 kA)

Short Pulses

- Pump-Probe experiments for femto-chemistry
  - Pulse length around 10 fs
  - Low jitter between pump and probe pulse
  - Synchronization with external laser
- Single-shot imaging of molecules
  - High photon flux
  - Resolution determined by pulse length
  - Maximum pulse length determined by damage threshold of molecules
- Less need for other experiments

“Experiment 6”

- Call for proposals of experiments, succeeding the initial set of experiments at LCLS
- Study for possible pulse length reduction at LCLS
- White paper till summer ‘03
- Proposal for “Experiment 6” will follow white paper.

Short Pulse Options at LCLS

- Use of the existing facility of LCLS (injector, linac, undulator) with minor modification.
- New optic beam line (monochromators, multilayer mirrors.
- Manipulation of radiation pulse and electron beam (e.g. chirp)

Pulse Compression

- Chirp in electron beam produces a chirp in FEL pulse twice as strong
- Pair of gratings to compress bunch
- Pulse length controlled by chirp

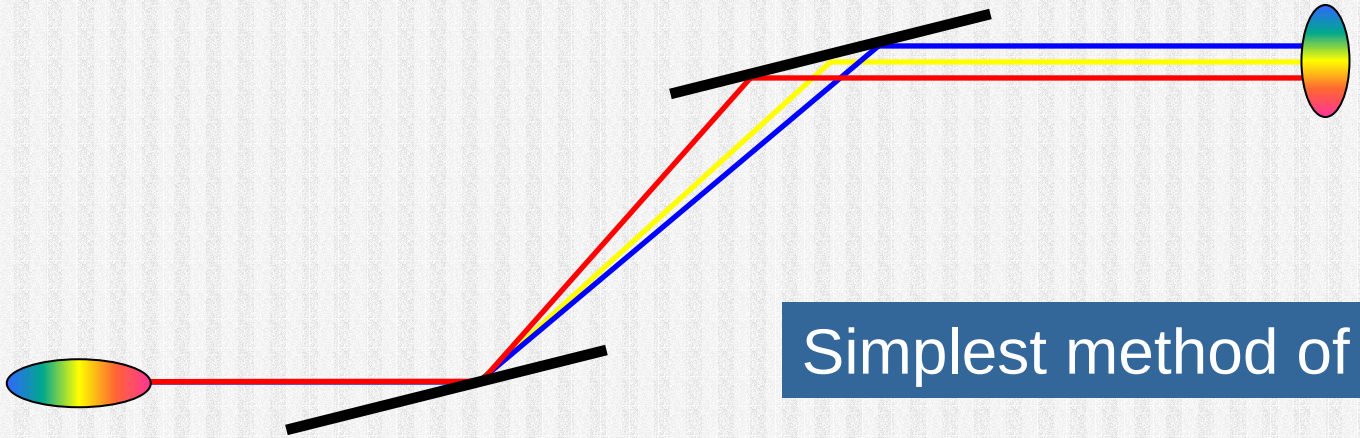

Simplest method of all

Pulse Slicing

- Monochromator selects slice of chirped radiation pulse.

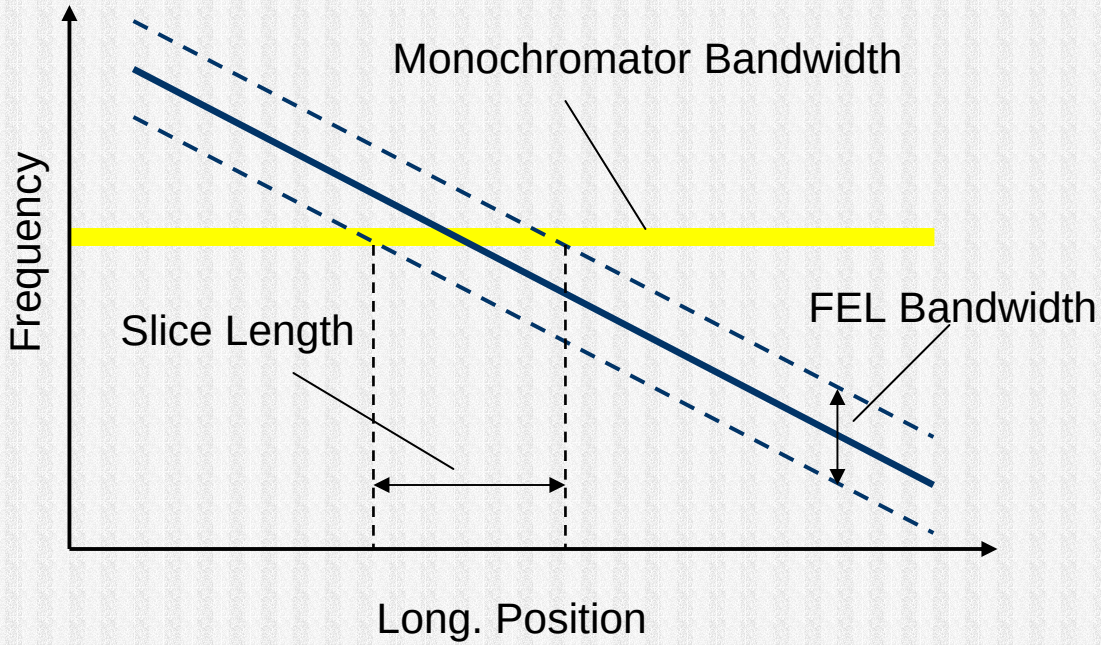

Limit

$\rho = 0.0006$
Chirp 2.5 %
$\longrightarrow$ 10 fs

Limitation of Slicing

- Power load of monochromator
- Non-linearity of energy chirp
- Strength of chirp

The chirp is applied by varying the bunch charge. The rf curvature is only compensated for a given charge. The residual effect is a (almost) linear chirp along the bunch. For LCLS the range is about 2-3% without re-optimization of the machine

Two-stage Pulse Slicing

- Slicing before saturation reduces power load on monochromator
- Second stage seeded with sliced pulse (microbunching removed by bypass)
- Allows small bandwidth for unchirped bunches

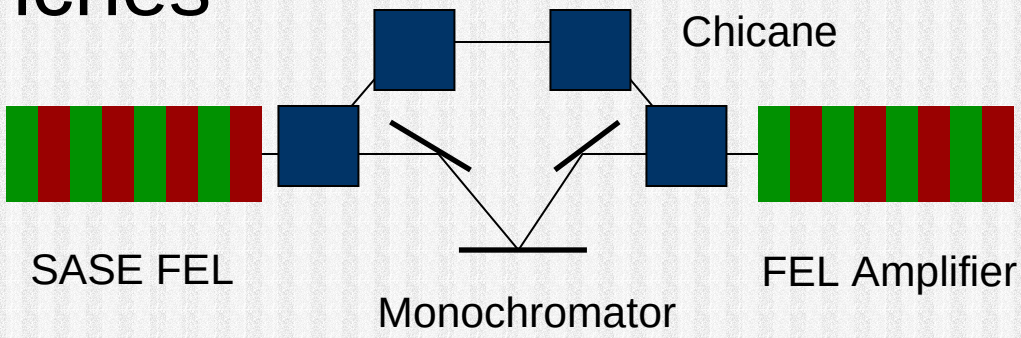

Two-stage Pulse Slicing

- No saturation in 1st stage ($\sigma_\gamma/\langle\gamma\rangle \ll \rho$)
- Seeding power level well above shotnoise

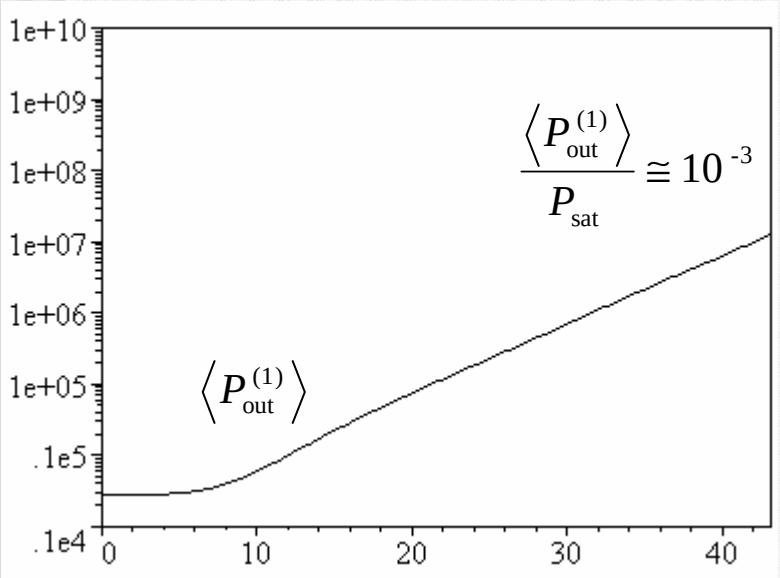

L_1 (meters)

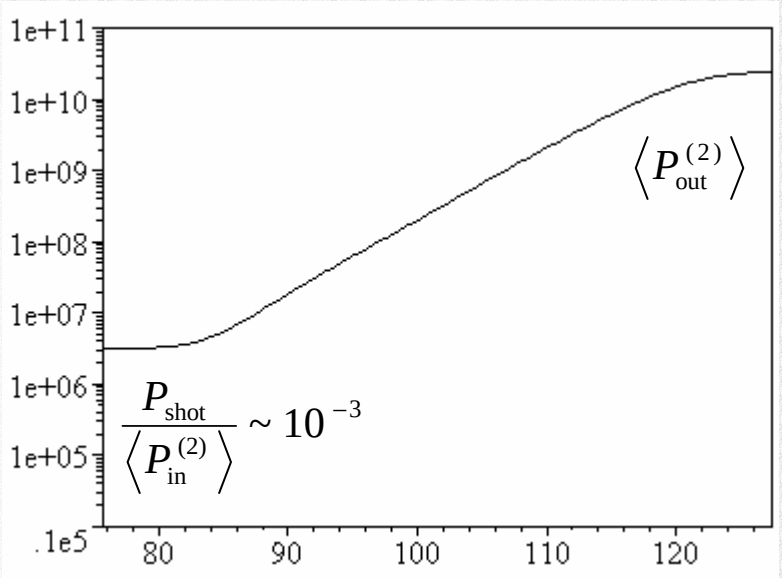

L (meters)

Two-stage Pulse Slicing

- Reduced fluctuation of pulse energy
- No deep saturation

Simulation for 10 fs slice (10 spikes)

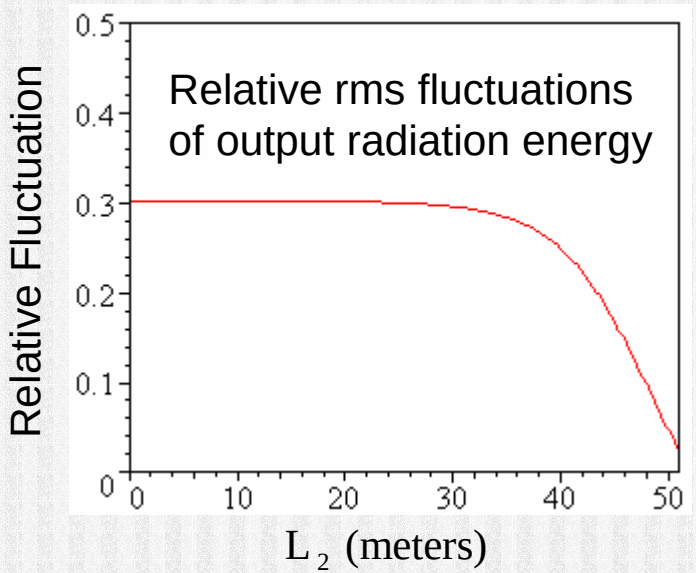

Dependence of output power on input power for FEL amplifier

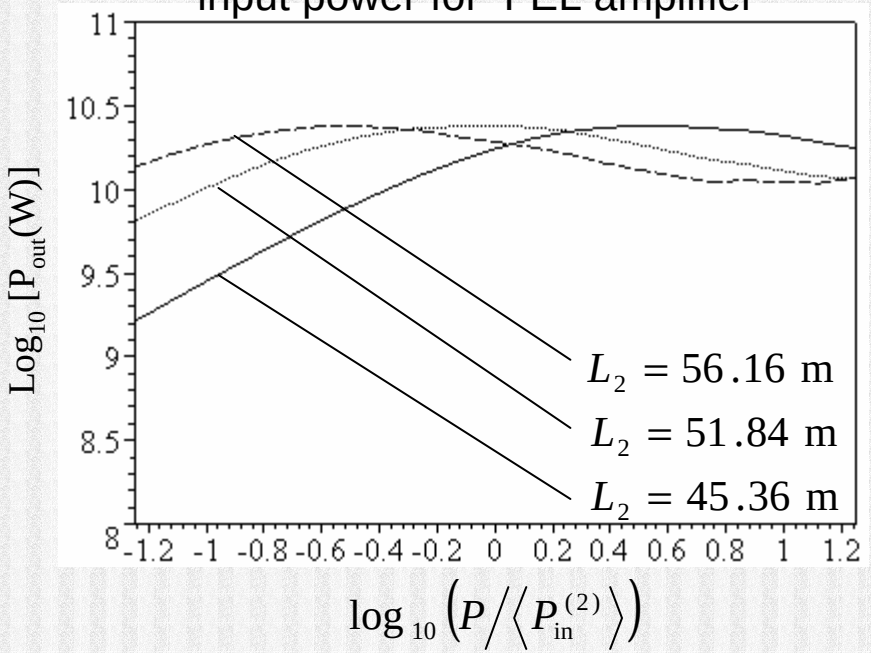

Electron Bunch Compression

- Start-end simulation modeled after GTF result for 200 pC

$I_{pk} \approx 14$ kA

$\sigma_t \approx 6$ fsec

$\sigma_E/E \approx 0.06\%$

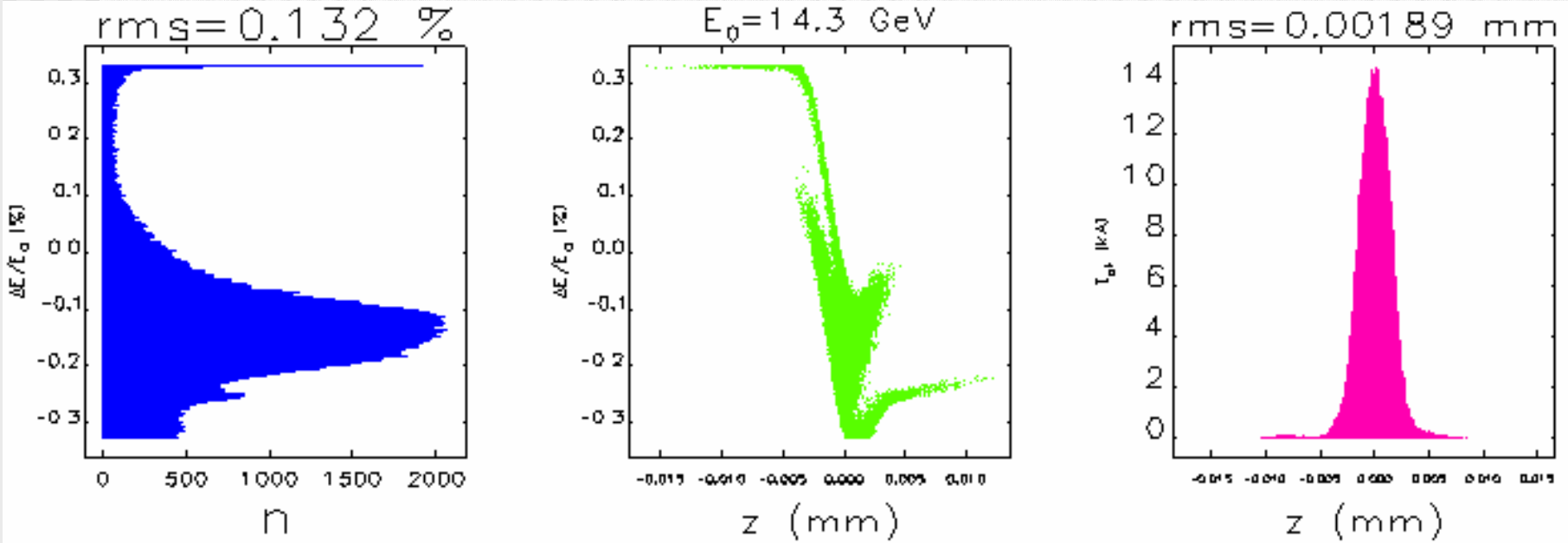

Electron Bunch Compression

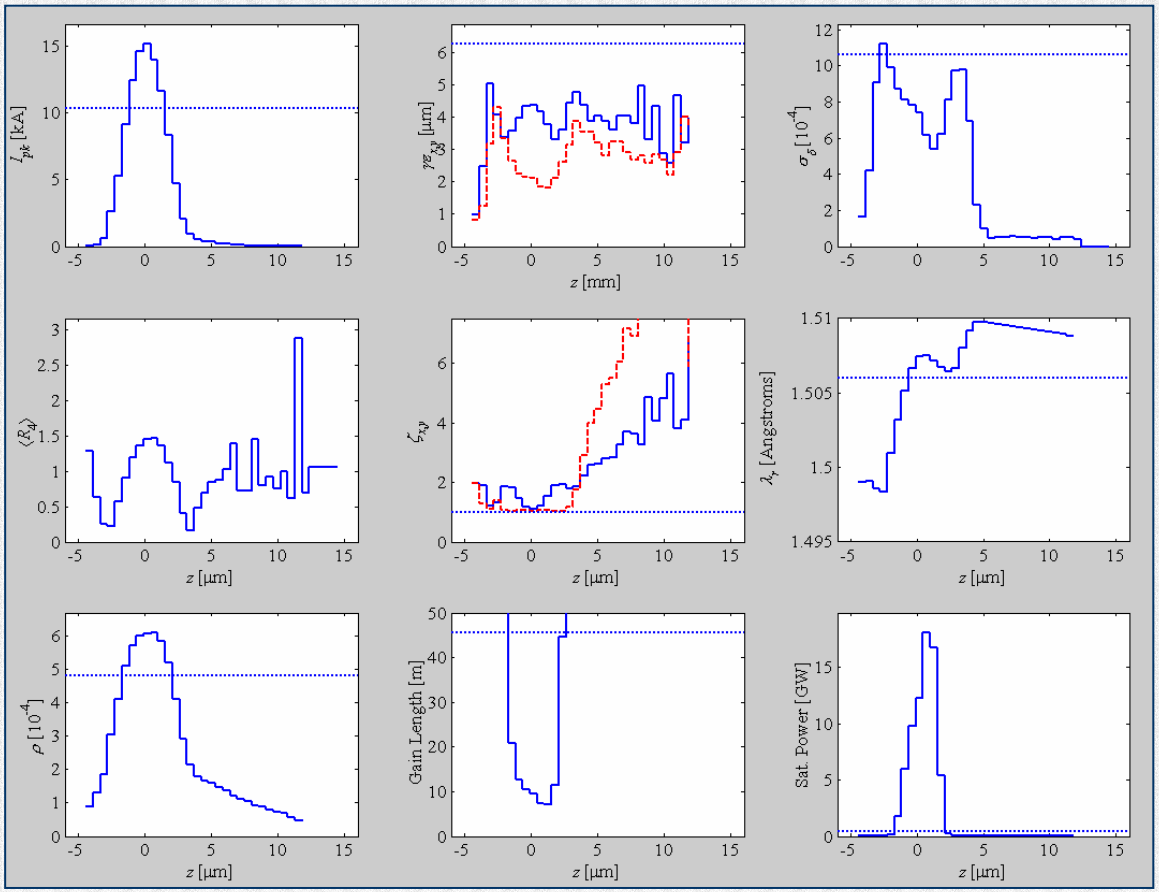

No part of the bunch provides a gain length shorter than the required 6 m to reach saturation

Undulator wakefield amplitude requires strong tapering (> 2%)

Wakefield Effects

- Undulator wakefields can push electrons out of the FEL bandwidth
- Tapering can compensate only a fixed energy loss rate, selecting those parts of the bunch where losses by wakefields and spontaneous radiation add up that value

$$\frac{da_u}{dz} = \frac{a_u^2 + 1}{\gamma a_u} \frac{d\gamma}{dz}$$

Wakefield Effects

Ideal case (step profile) with various materials for the vacuum chamber to control wakefield amplitude

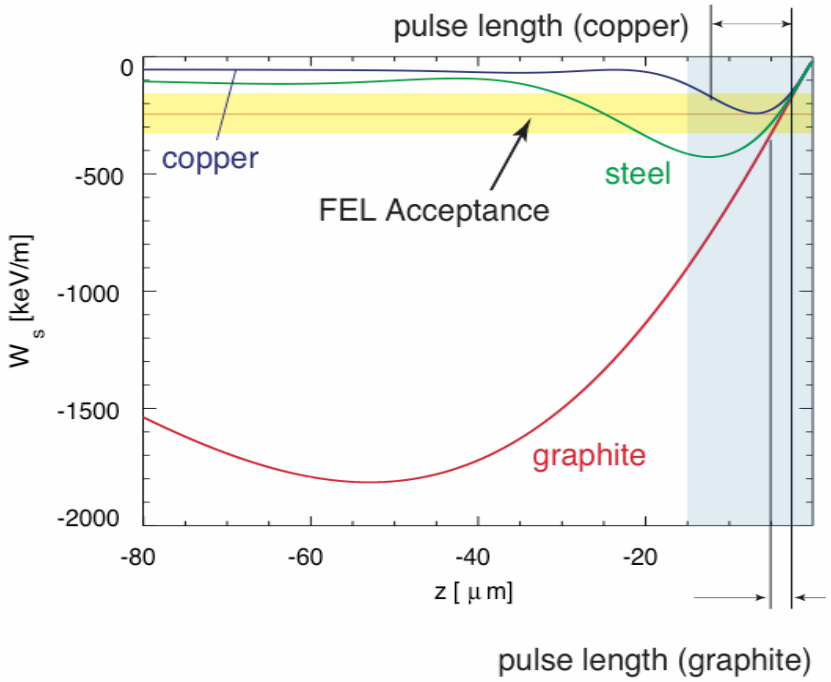

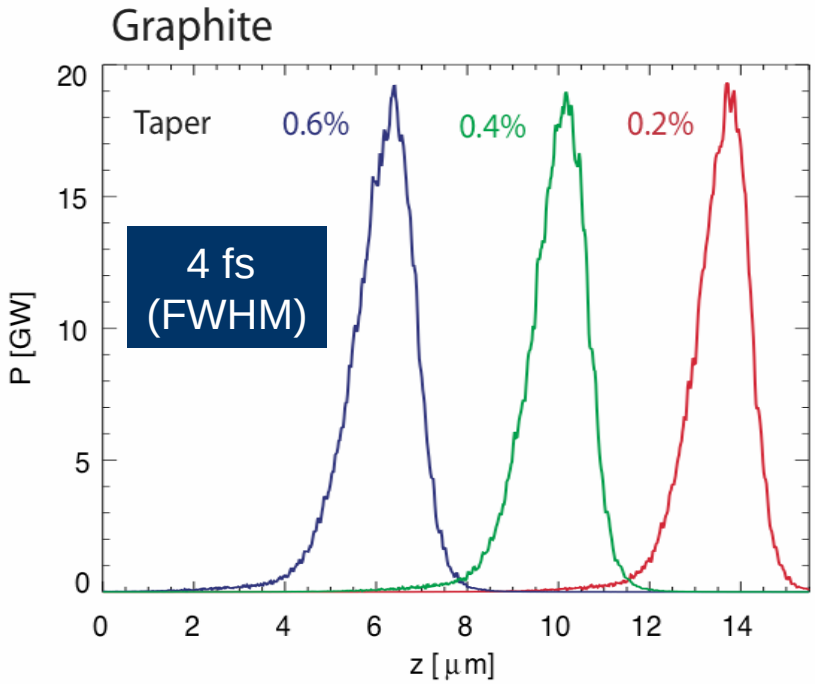

Wakefield Effects

Realistic case (start-end simulation). Local Wakefield enhancement due to current spike at bunch head

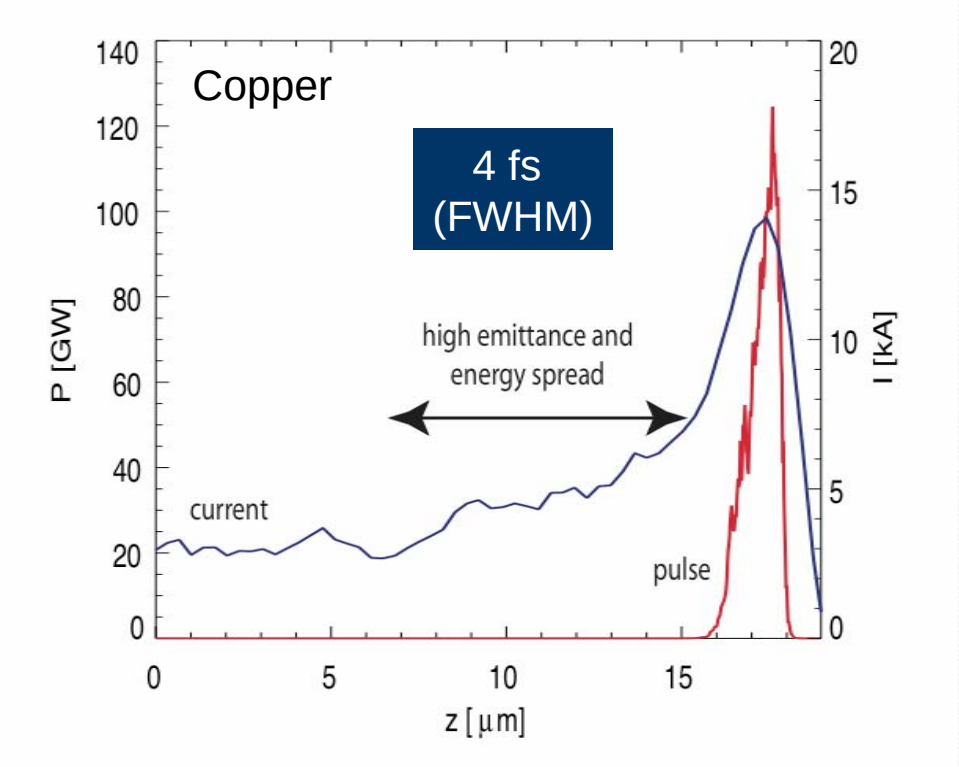

Works for all vacuum chamber materials

Additional area is prevented from lasing due to poor beam quality (uniform parameters increses pulse length to 30 fs)

Transverse Effects

- Electron Beam cannot conditioned to compensate emmitance effects
- Higher-order mode rf cavities + solenoid field produce a strong beta-mismatch along the beam

  Only a short section of the bunch is matched to undulator lattice

- Similar argument for x-z correlation by deflecting cavities

Conclusion

- FEL pulse manipulation easiest method to implement
- Pulses are limited to 10 fs
- Electron beam manipulation more complex and required changes in the beam line
- Pulse length below 5 fs possible

Outlook

- Study of different schemes by LCLS group
- Results been published in white paper
- Most promising schemes are used for proposal “Experiment 6” at LCLS
- Task force initiative at LCLS for attosecond pulses (fundamental limit at a few 100 as)

The Seeding Option for the Free Electron Laser at TTF

Bart Faatz

HASYLAB @ DESY

Project coordinator: R. Treusch

The Regenerative FEL

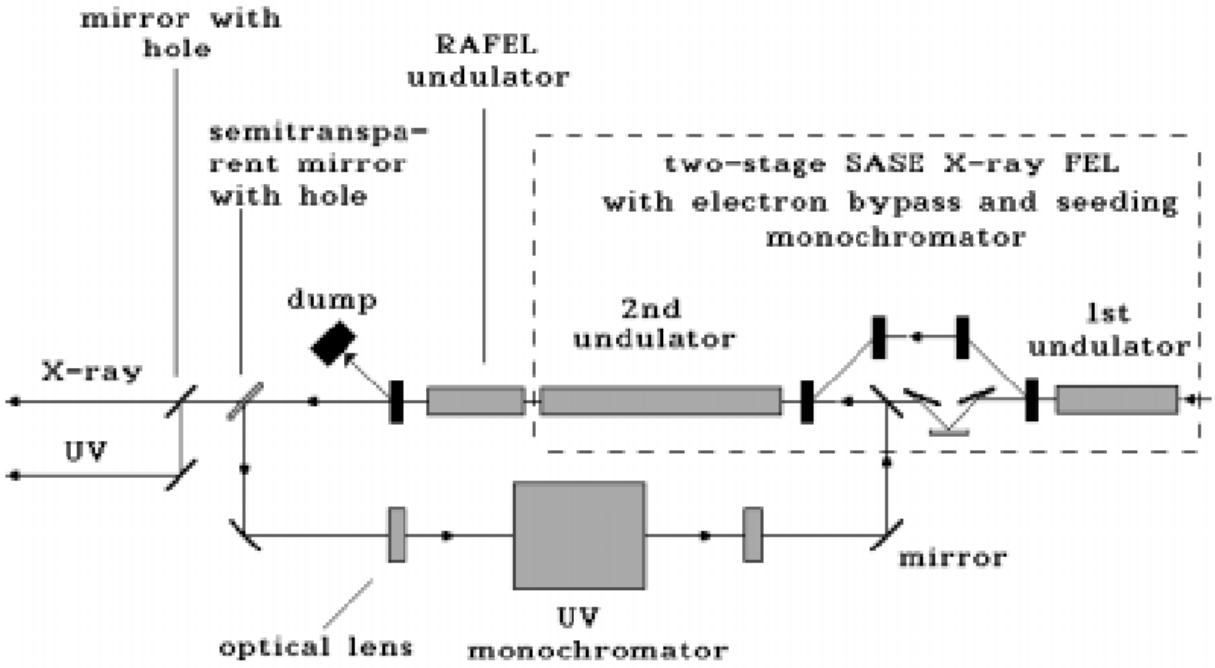

Undulator	
Type	Planar (permanent)
Period	7 cm
Peak magnetic field	1.4 T
Number of periods	60
Output radiation	
Wavelength	200-400 nm
Bandwidth	Transform limited
Micropulse duration	200 fs
Micropulse energy	1 mJ
Bunch spacing	111 ns

Far Infrared Coherent Radiation

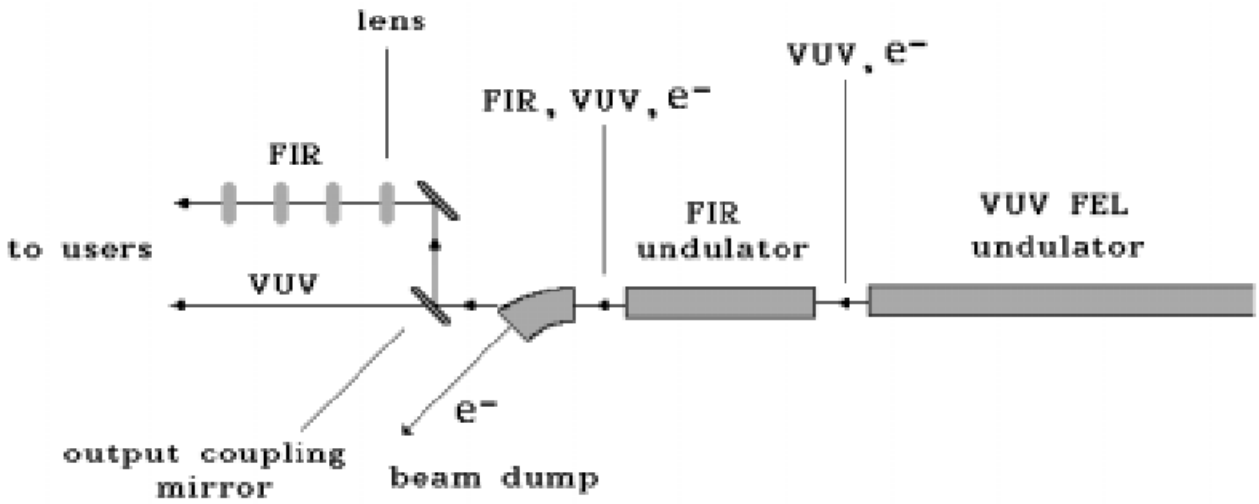

Undulator	
Type	Planar (electromagnetic)
Period	60 cm
Peak magnetic field	1-1.5 T
Number of periods	10
Output radiation (in central cone)	
Wavelength	100-300 μm
Bandwidth	Transform limited
Peak power	30-100 MW
Average power	30-100 W
Micropulse duration (rectangular profile)	3-10 ps
Micropulse energy	0.3-1 mJ
Bunch spacing	111 ns

X-ray backscattering facility: 100 fs

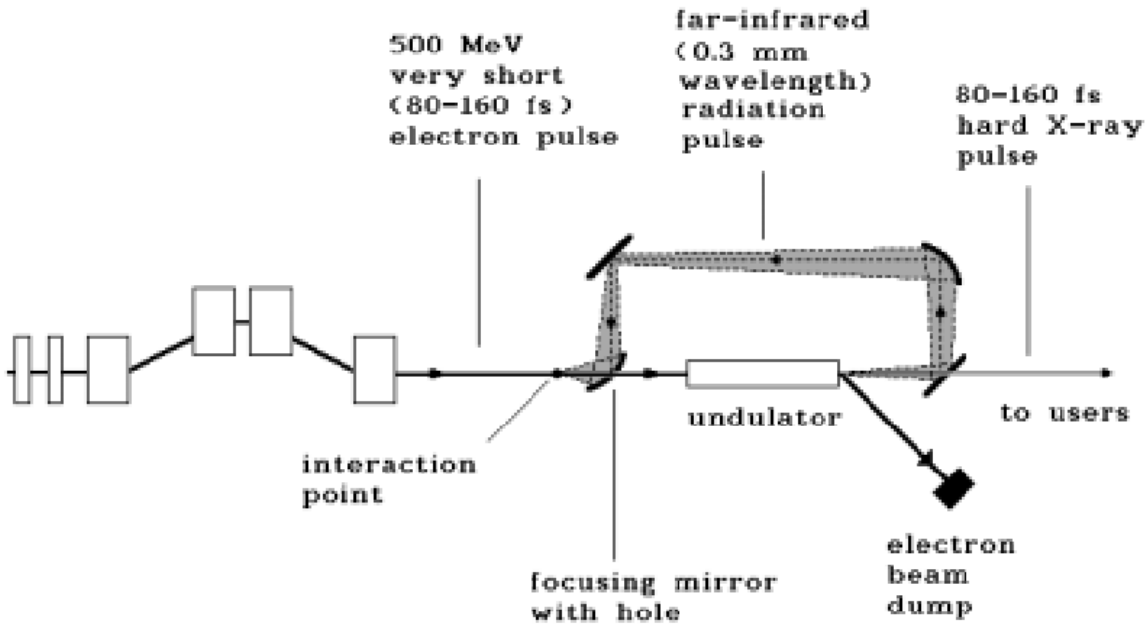

Beam energy	500 MeV
Photon energy	15 keV
Pulse length	100 fs
Number of photons per second	2×10^{13}

Generation of High Power Femto second Pulses by Sideband-Seeded X-ray FEL

W. Brefeld, B. Faatz, J. Feldhaus, M Körfer, J. Krzywinski, T. Möller, J. Pflüger, J. Rossbach, E.L. Saldin, E.A. Schneidmiller, S. Schreiber and M.V. Yurkov

Features of the proposal:

- Possibility to produce femtosecond coherent X-ray pulses
- Natural integration into present TTF-FEL design
- Possibility of precise synchronization (20-30 fs) of femtosecond optical pulses and X-ray pulses for pump-probe experiments
- Main parameters of femtosecond X-ray pulses from the sideband-seeded FEL at the TESLA Test Facility:

Wavelength, nm	10-40
Min. pulse duration, fs (FWHM)	30
Peak power	Up to 0.5-1 GW
Number of photons per pulse	10^{11}
Spectral width, % (FWHM)	0.5

Basic scheme of a sideband seeded SASE FEL

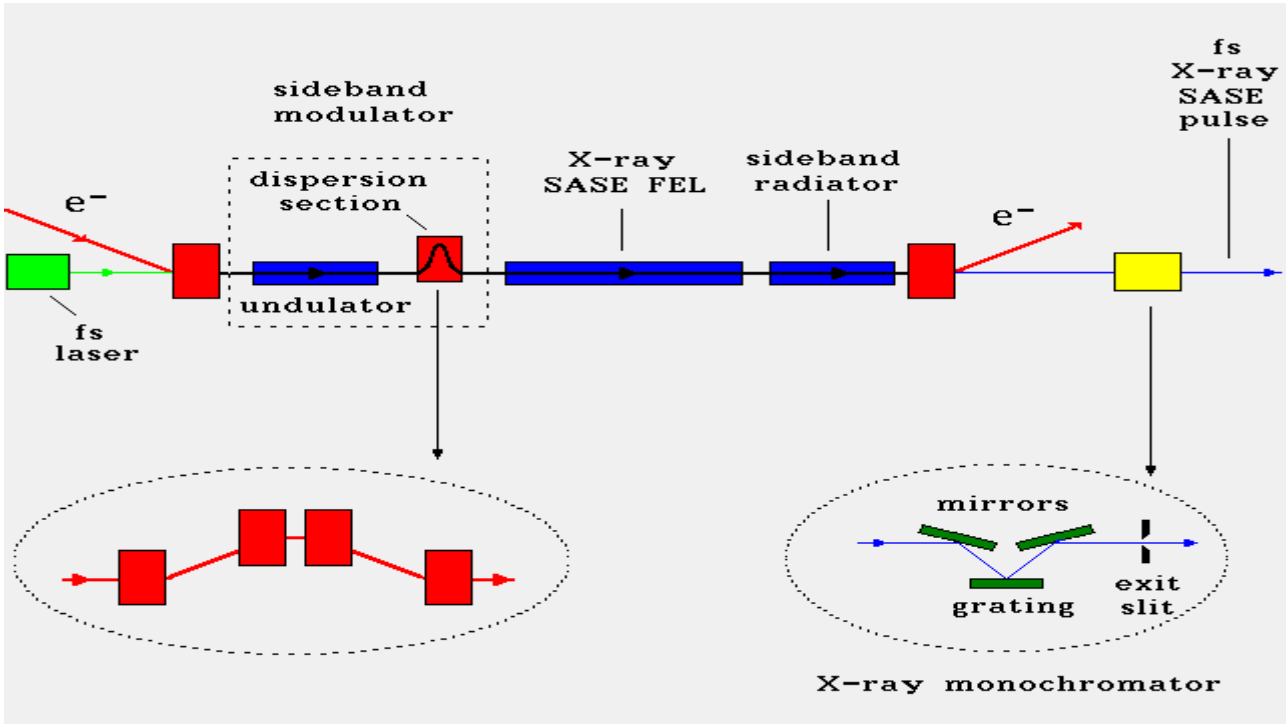

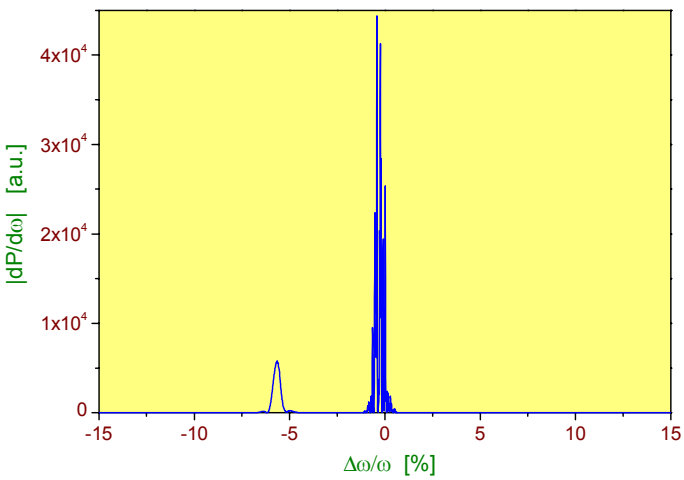

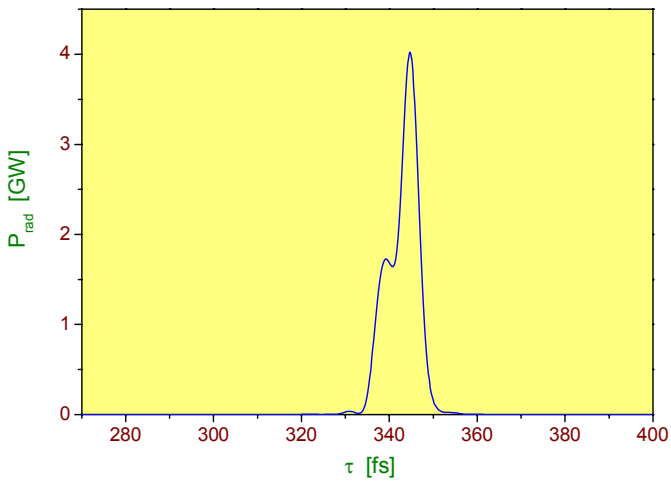

- An ultrashort laser pulse is used for modulation of the energy and density of the electrons within a slice of the electron bunch at a frequency ω_{opt}
- This leads to an amplitude modulation of the beam density at the sidebands $\omega_0 \pm \omega_{opt}$ when bunch passes main undulator.
- Coherent emission at the sideband is produced within fs slice of the electron bunch modulated by optical pulse.
- Separation of the sideband frequency from the central frequency by a monochromator is used to distinguish the fs pulses from the sub-ps intense SASE pulses.

Schematic layout of the soft X-ray SASE FEL facilities at TTF

Phase I: conventional SASE FEL

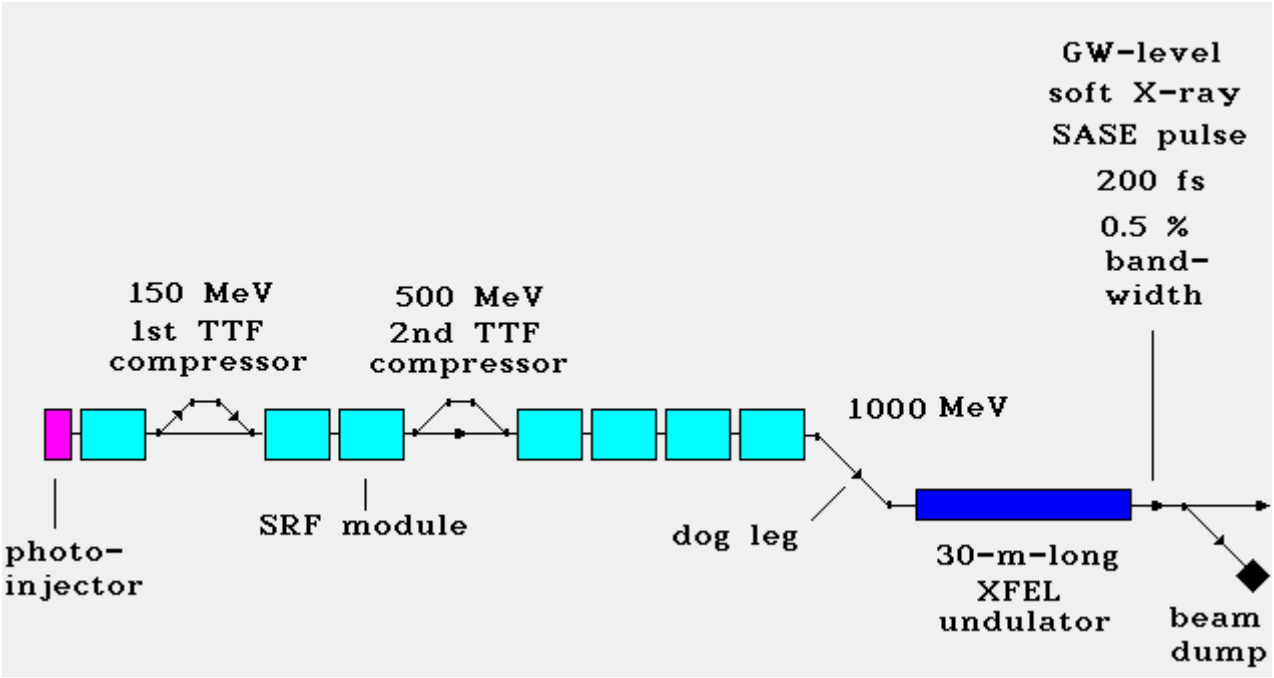

Phase II: self-seeding option

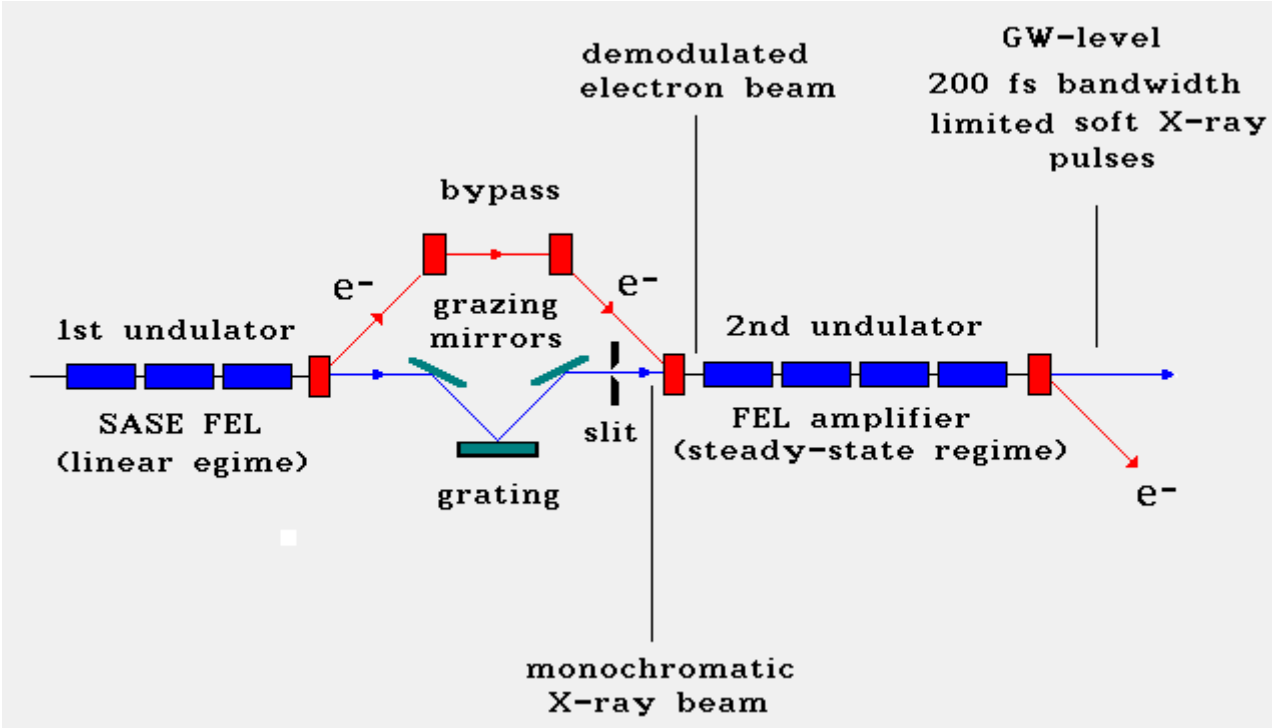

Schematic layout of the femtosecond pump-probe facilities integrated into soft X-ray SASE FELs at TTF

Phase I: conventional SASE FEL

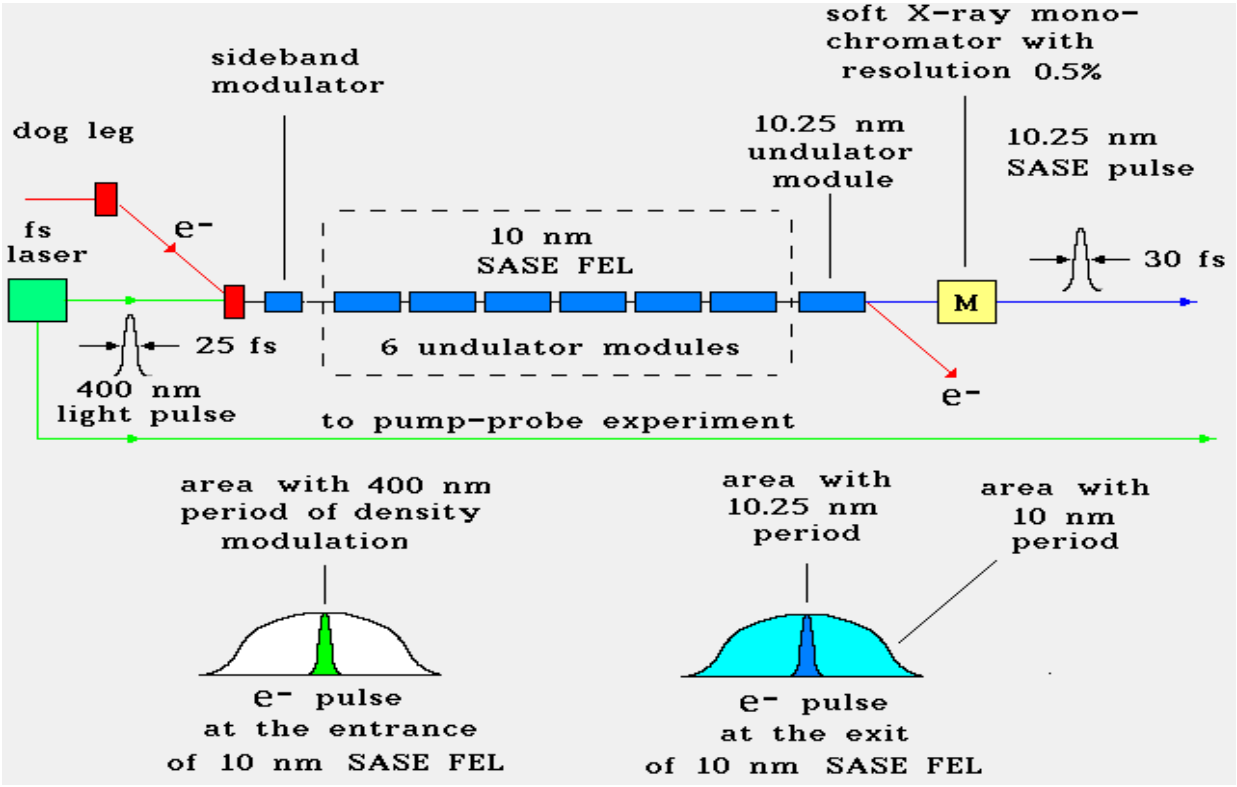

Phase II: self-seeding option

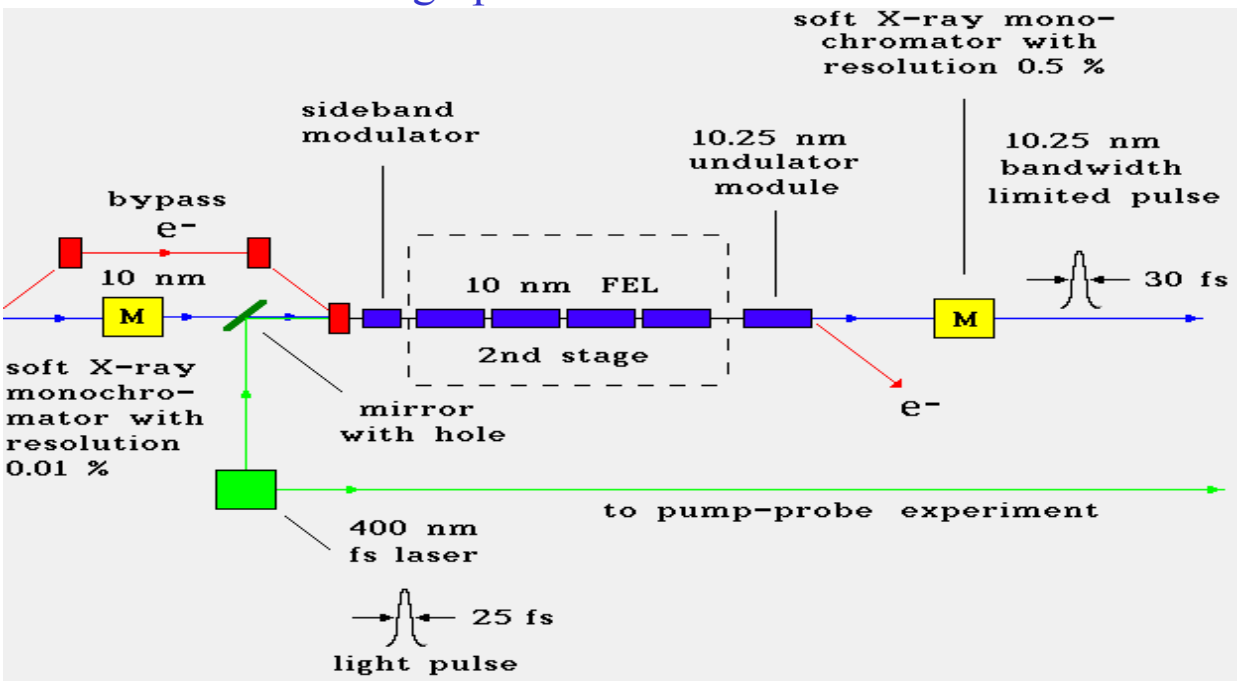

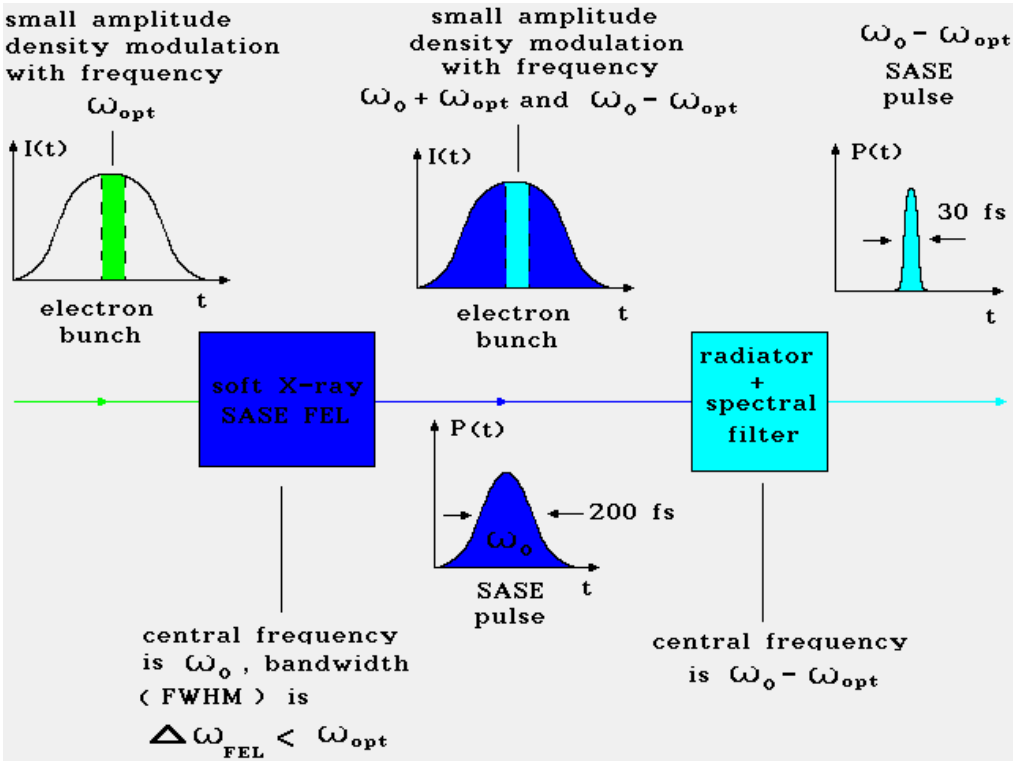

Sketch of femtosecond soft X-ray pulse synthesation through sideband generation and spectral filtering

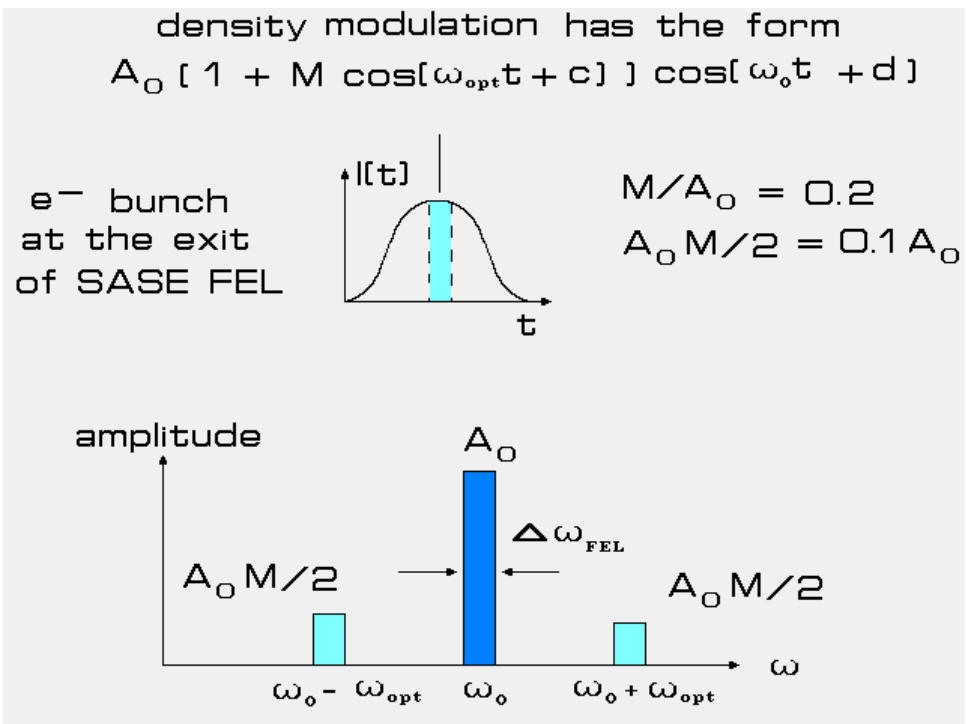

Summary of the description of the sideband generation for the case of the density modulation as initial conditions.

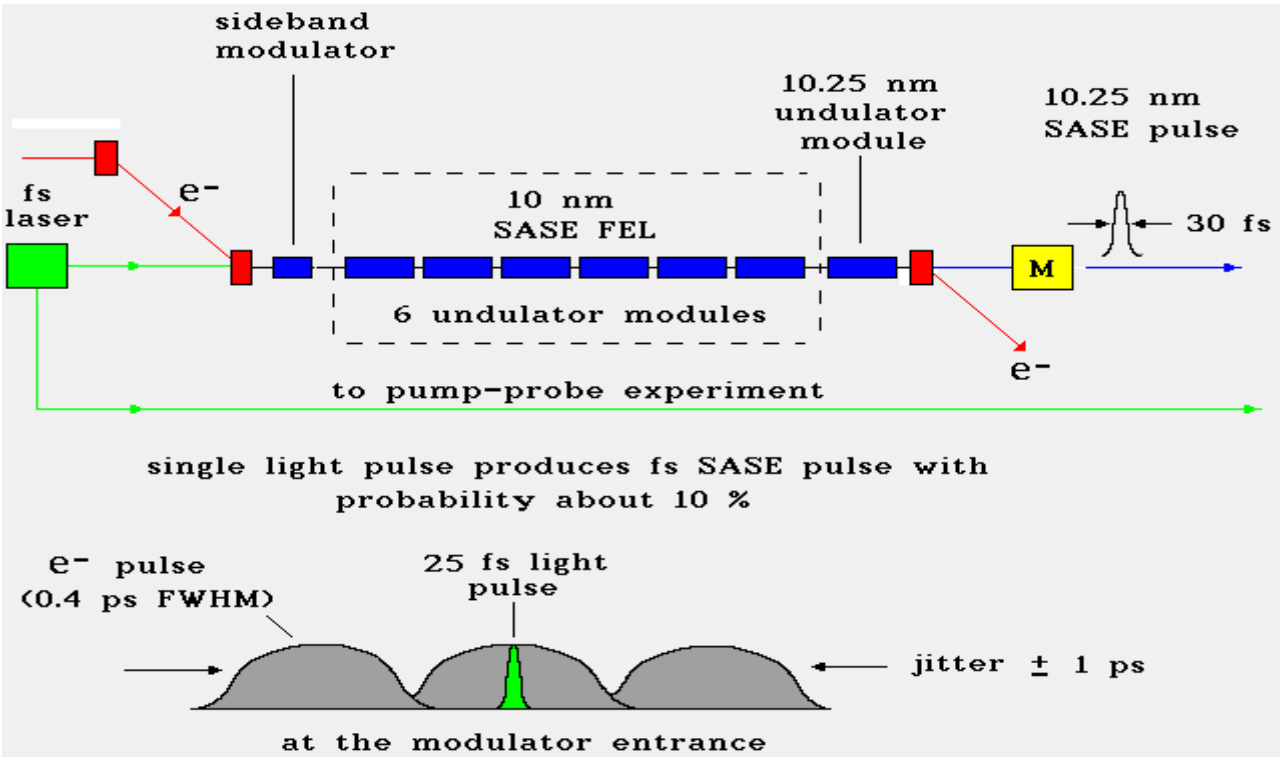

Effect of a electron pulse jitter on the femtosecond soft X-ray facility if a single optical pulse is used as a seed signal

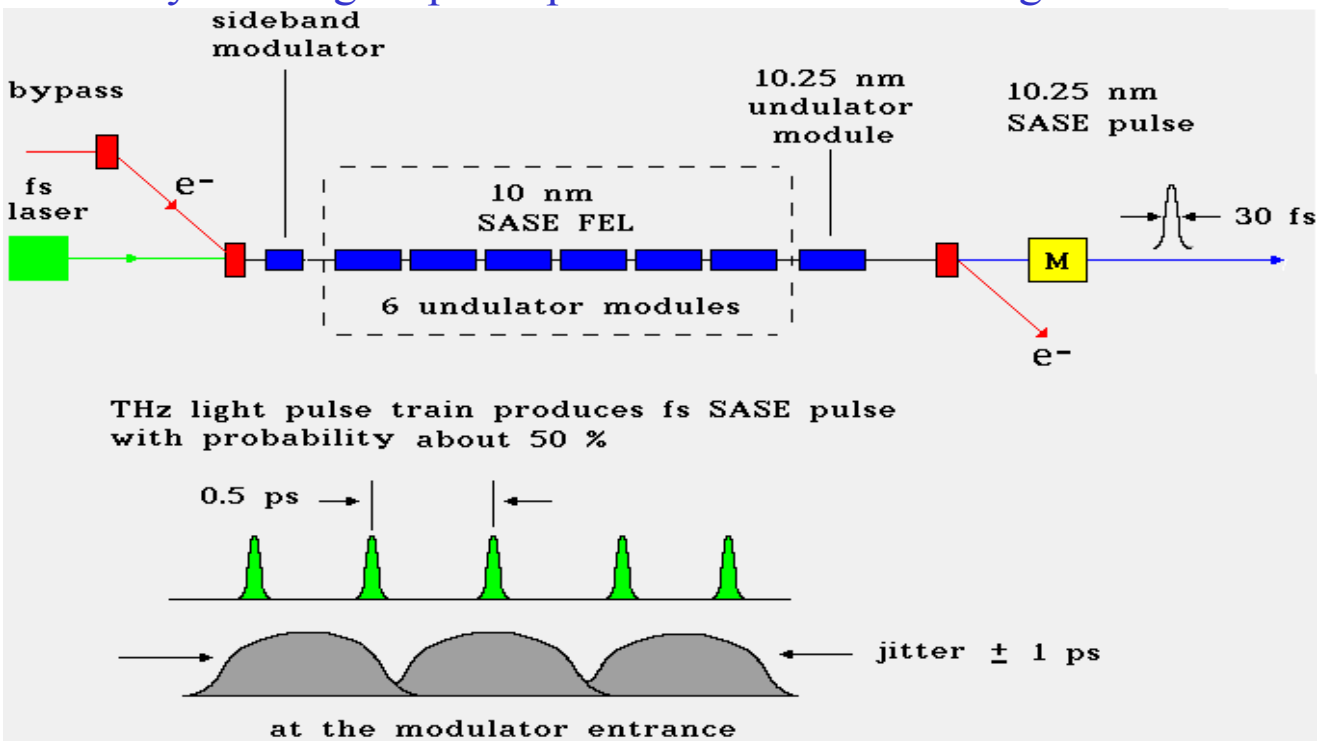

Effect of a electron pulse jitter on the femtosecond soft X-ray facility if a THz optical pulse train is used as a seed signal

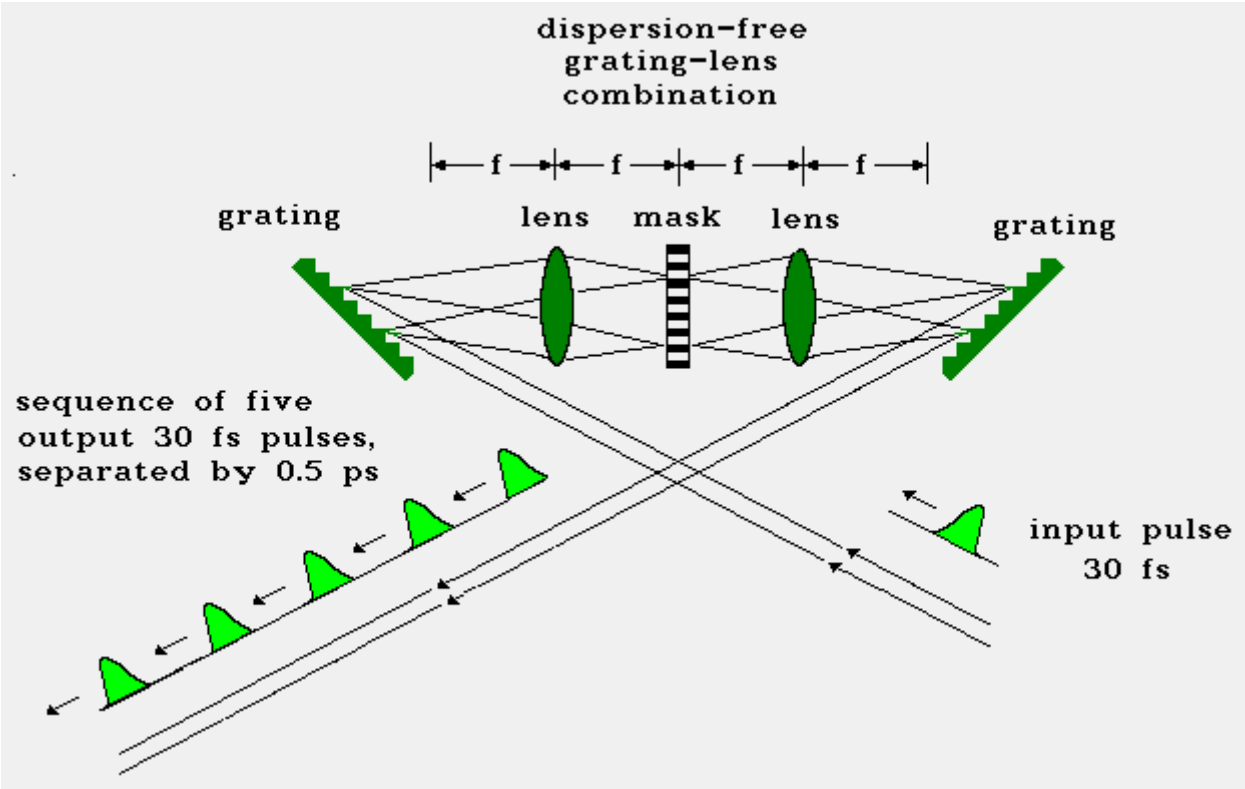

Typical experimental set-up for THz pulse train generation

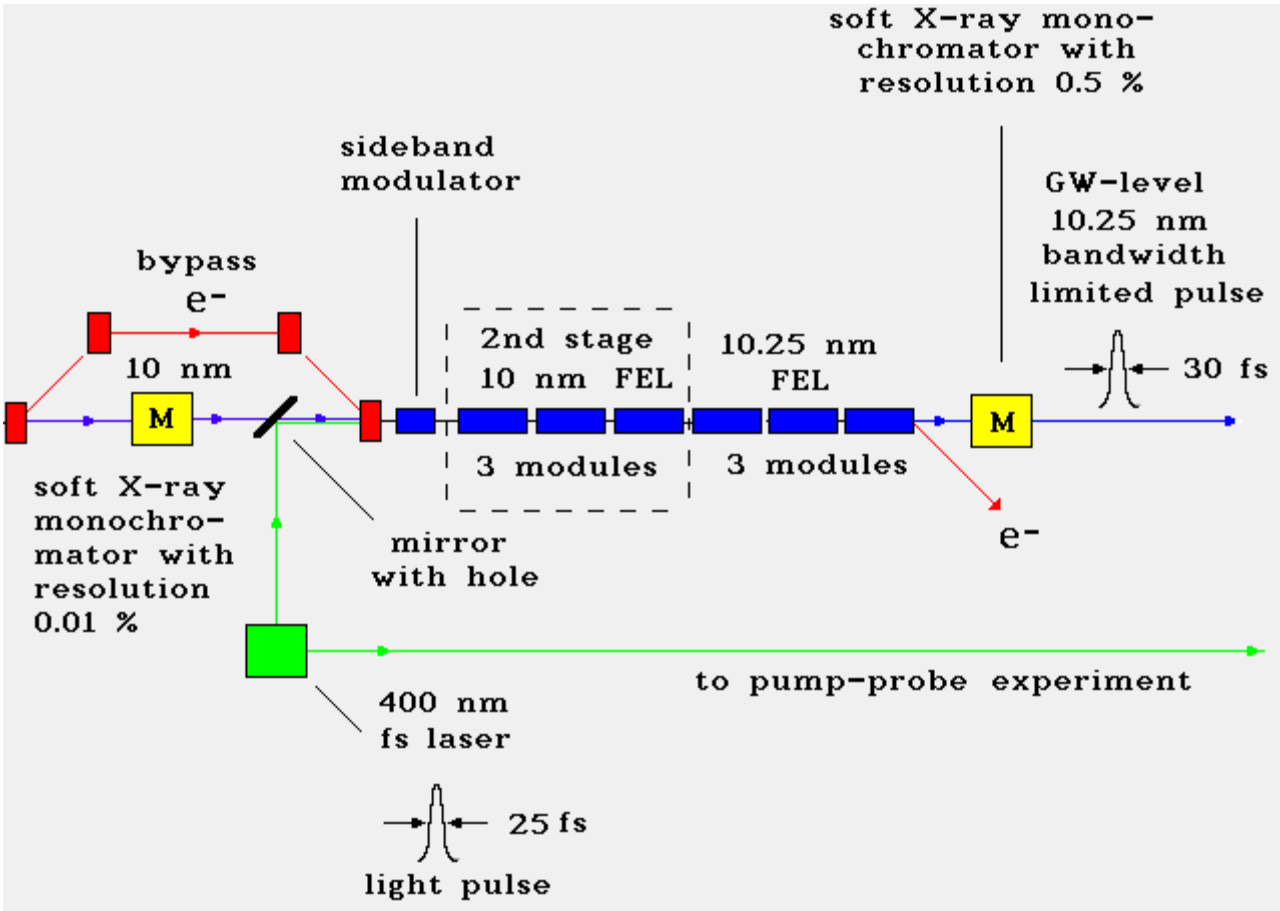

Possible scenario for the soft X-ray fs pulse power upgrade. Schematic layout of the full scale soft X-ray femtosecond facility which fits with self-seeding option

Details of sideband modulator operation

Laser pulse of the optical seeding laser

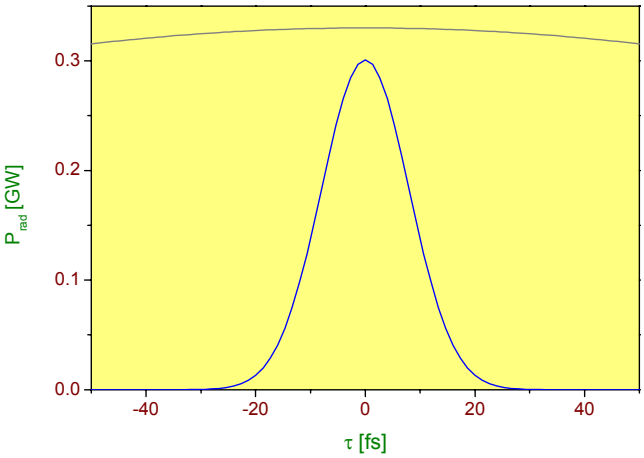

Energy modulation of the electron beam at the exit of the modulator undulator

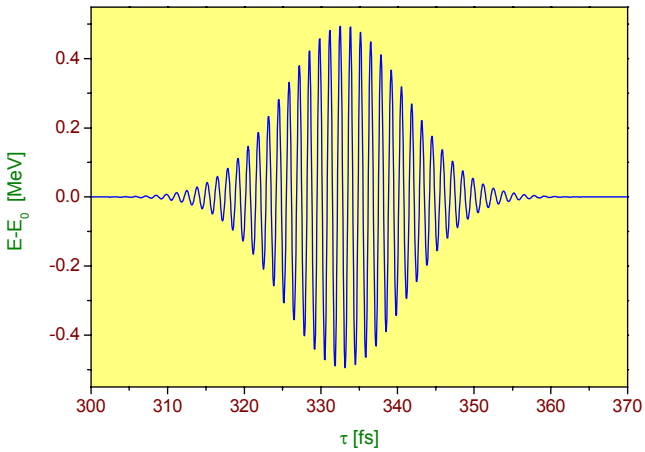

Density modulation of the electron beam at the exit of the dispersion section

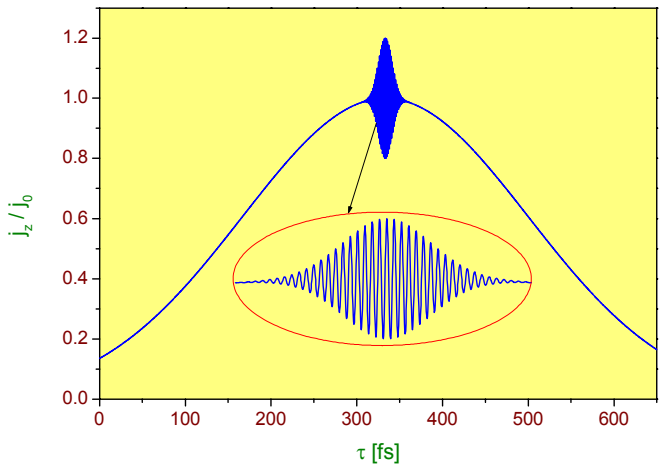

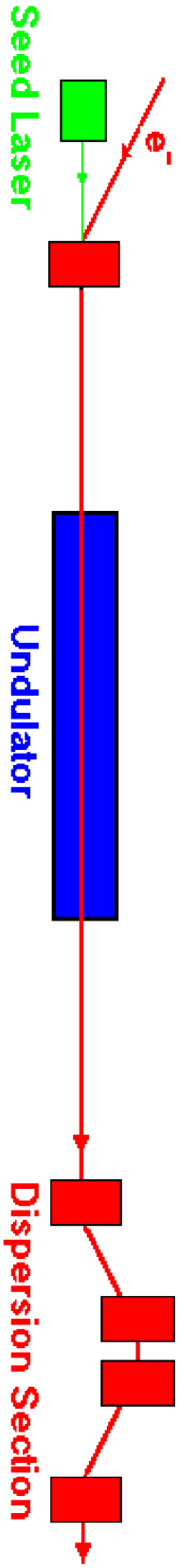

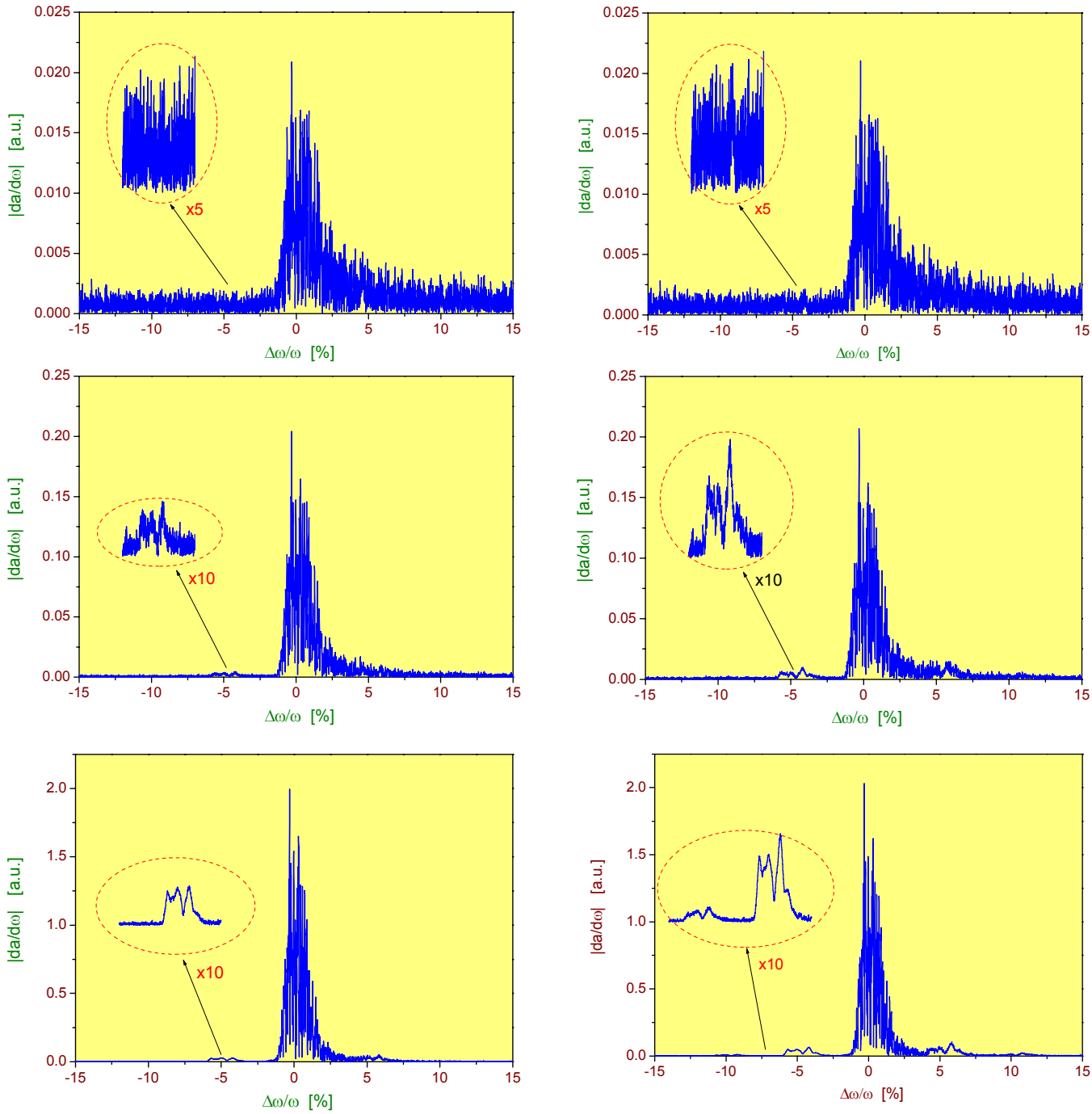

Spectral distribution of the beam density modulation at different length of main undulator: normalized z = 4.7, 7.5, and 10.3 (upper, middle and lower plots, respectively). Left column corresponds to initial conditions of the density modulation, and right column is the case of the energy modulation. Calculations have been performed within framework of one-dimensional model.

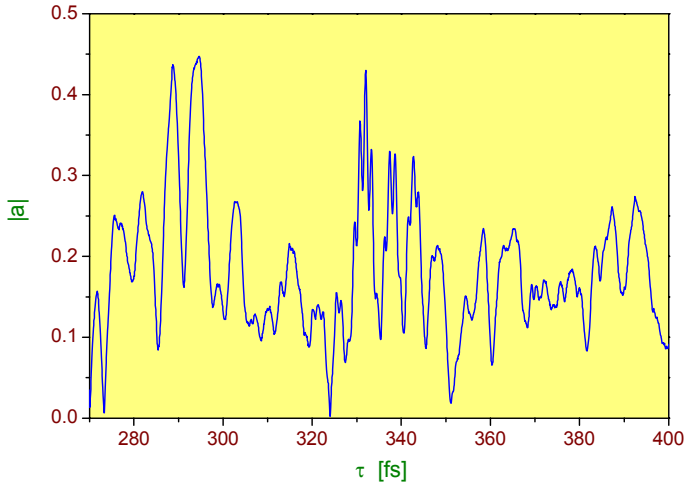

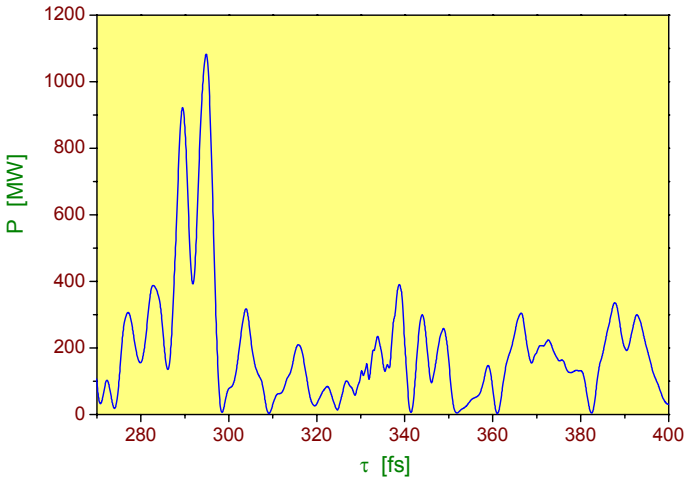

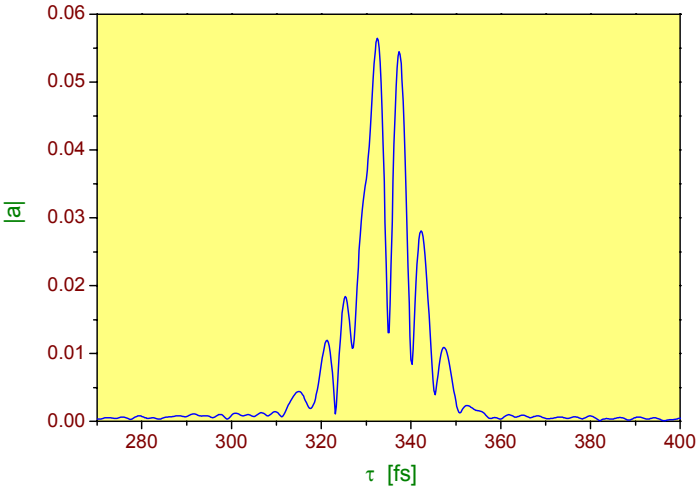

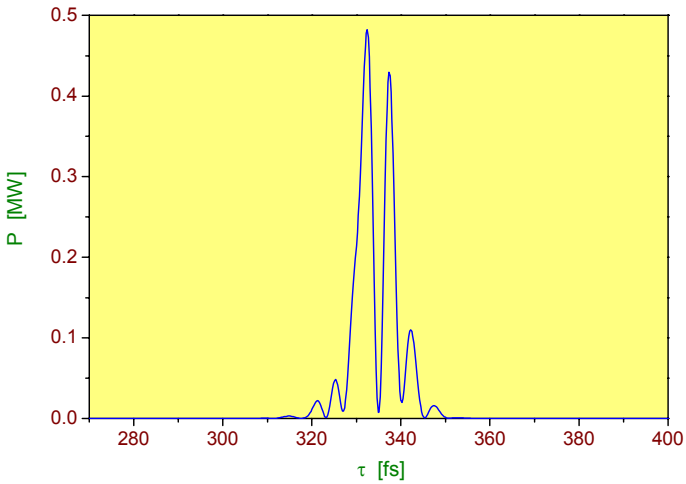

Details of the sideband generation process at a point corresponding to the maximal contrast of the sideband in the main undulator (effective z = 10.6). Left column: plots of the full density modulation and that filtered at the sideband frequency. Right column: full radiation power and that filtered at the sideband frequency. Initial conditions corresponds to general case (c). Calculations have been performed within framework of one-dimensional model.

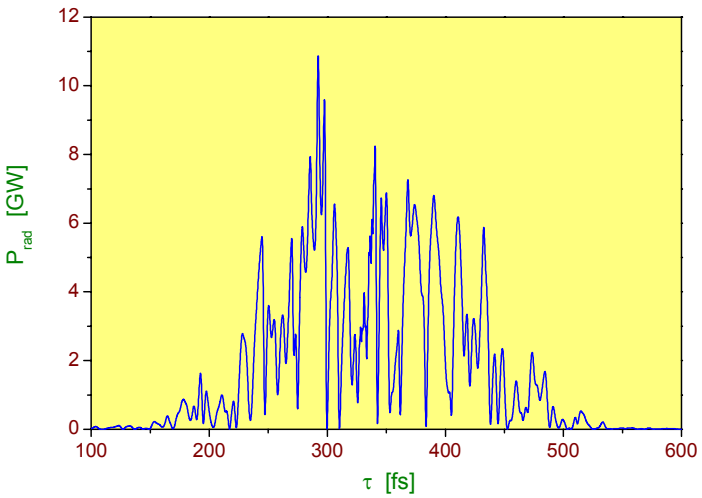

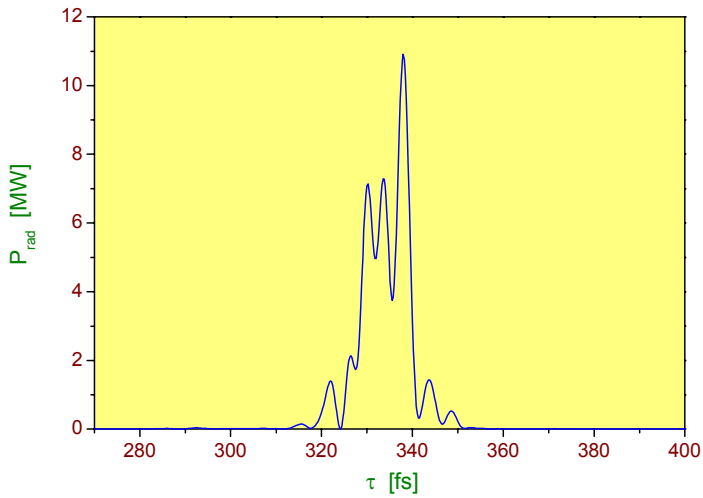

Left plot: Time structure of the radiation pulse from SASE FEL operating at saturation. Right plot: Radiation pulse after spectral filtering at the sideband frequency. Here the length of the effective main undulator is equal to z = 13, and there is no sideband radiator undulator. Initial conditions correspond to general case (c). Calculations have been performed within framework of one-dimensional model.

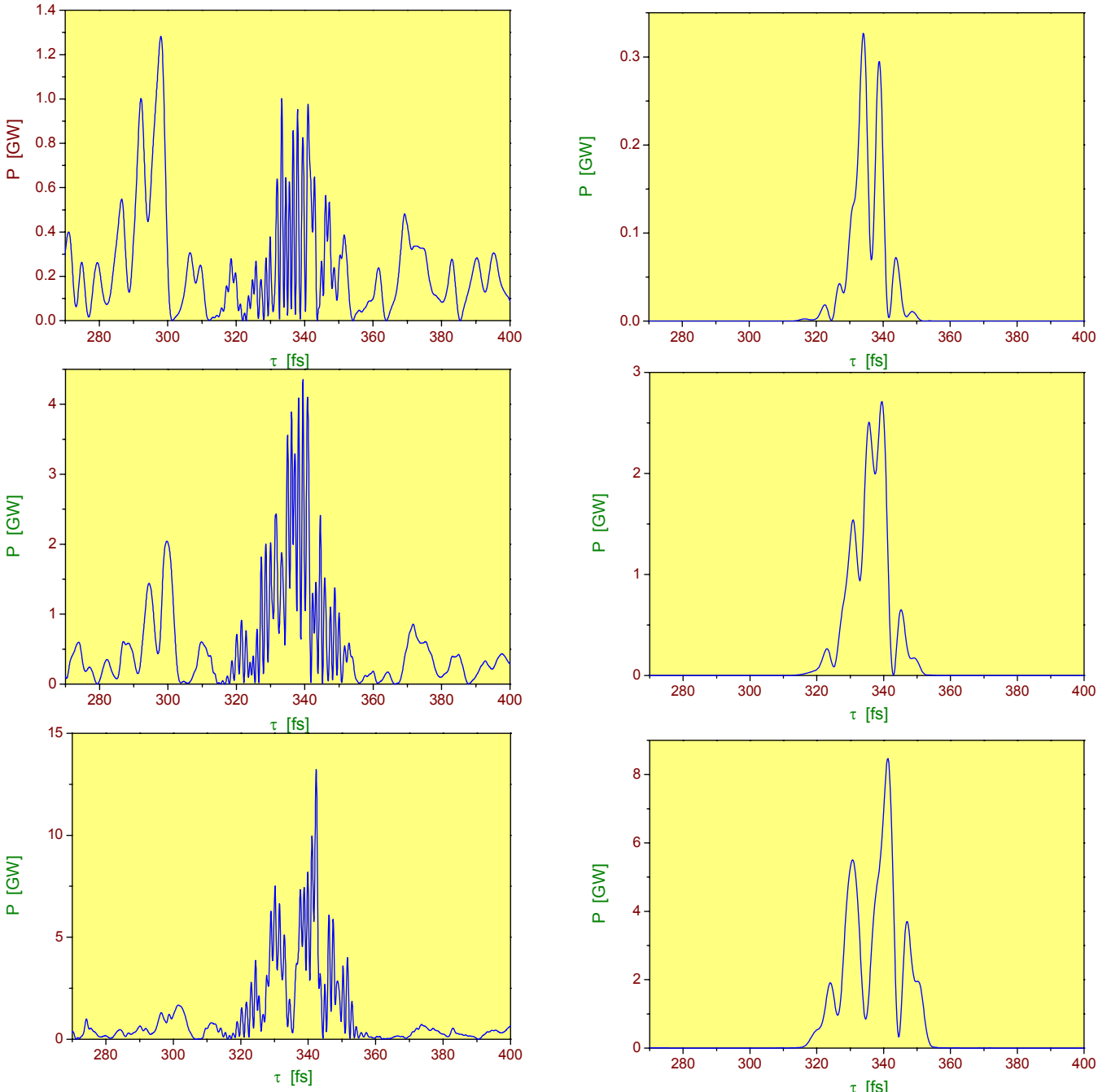

Evolution of the radiation pulse in the radiator undulator at different length of the radiator undulator: normalized z = 1.5, 3.3, and 5.2 (upper middle, and lower plots, respectively). In the left plots we present total pulse, and in the right plots - spectrally filtered at the sideband. The length of the main normalized undulator is equal to z = 10.6 and provides maximum contrast of the sideband. Calculations have been performed within framework of one-dimensional model.

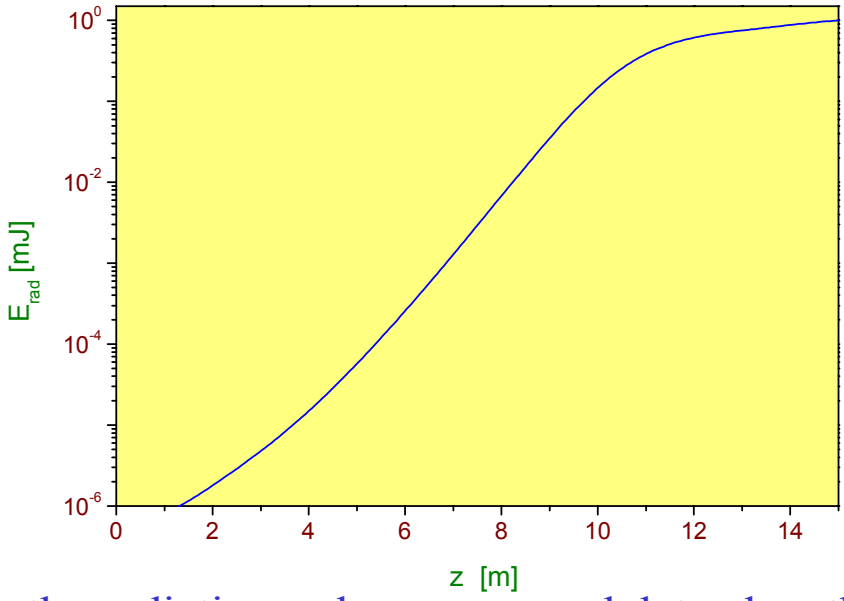

Energy in the radiation pulse versus undulator length for 20 nm SASE FEL at the TESLA Test Facility. Calculations have been performed with three-dimensional, time-dependent simulation code FAST

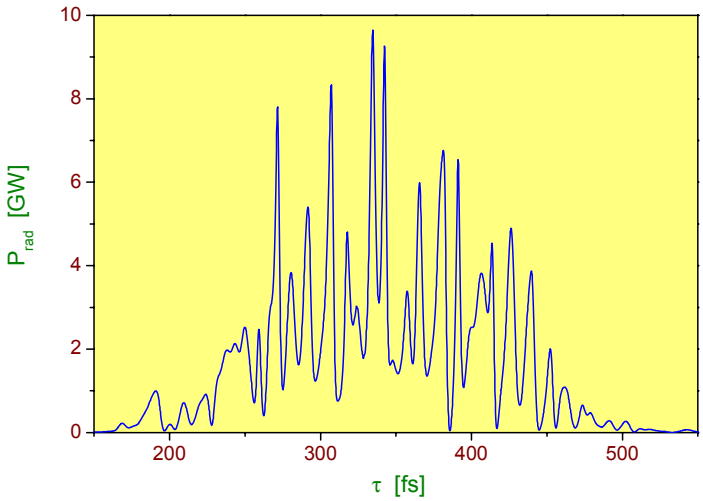

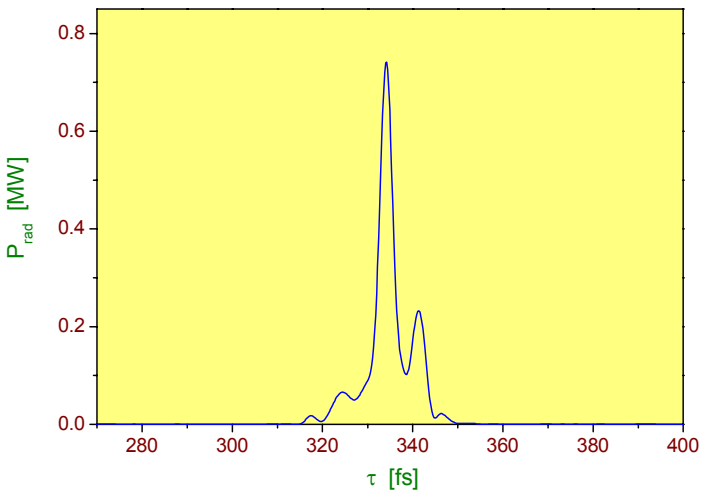

Left plot: Time structure of the radiation pulse for 20 nm SASE FEL at the TESLA Test Facility operating at saturation. Right plot: Radiation pulse after spectral filtering at the sideband frequency. Calculations have been performed with three-dimensional, time-dependent simulation code FAST.

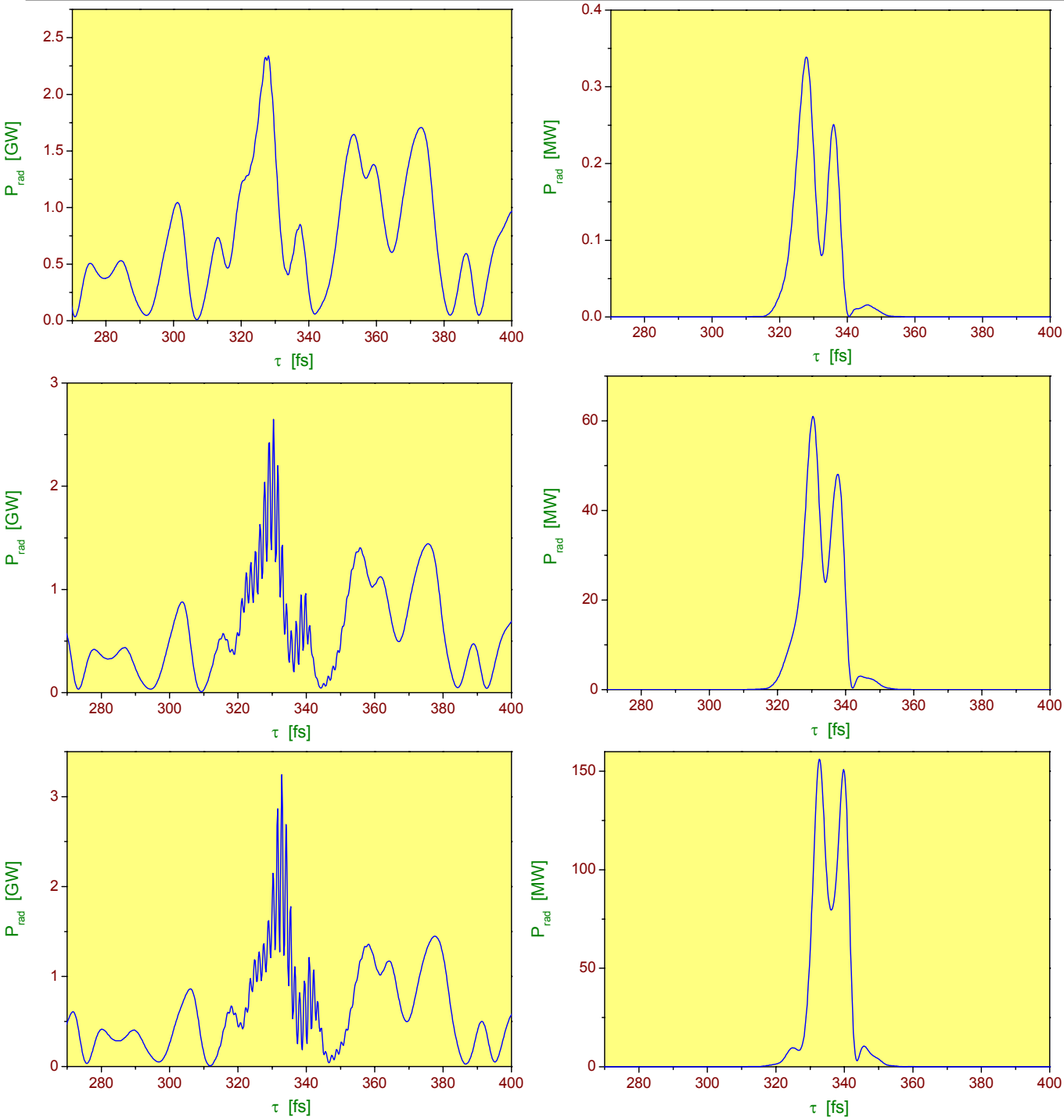

Evolution of the radiation pulse in the radiator undulator. In the left plots we present total pulse, and in the right plots - spectrally filtered at the sideband. The length of the radiator undulator is equal to 0, 1 and 2 m for upper, middle and lower plots, respectively. Calculations have been performed with three-dimensional, time-dependent simulation code FAST.

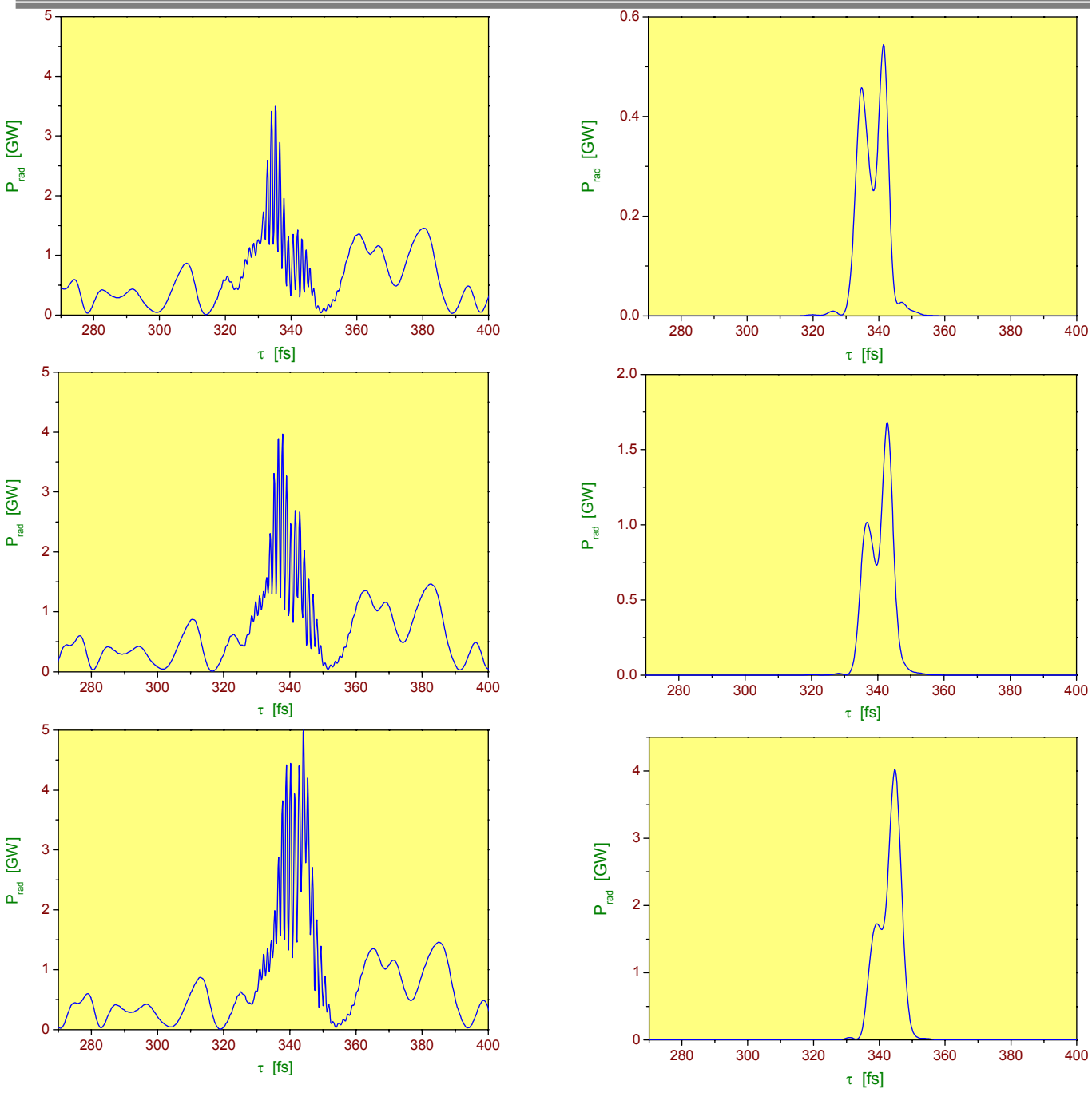

Evolution of the radiation pulse in the radiator undulator. In the left plots we present total pulse, and in the right plots - spectrally filtered at the sideband. The length of the radiator undulator is equal to 3, 4 and 5 m for upper, middle and lower plots, respectively. Calculations have been performed with three-dimensional, time-dependent simulation code FAST.

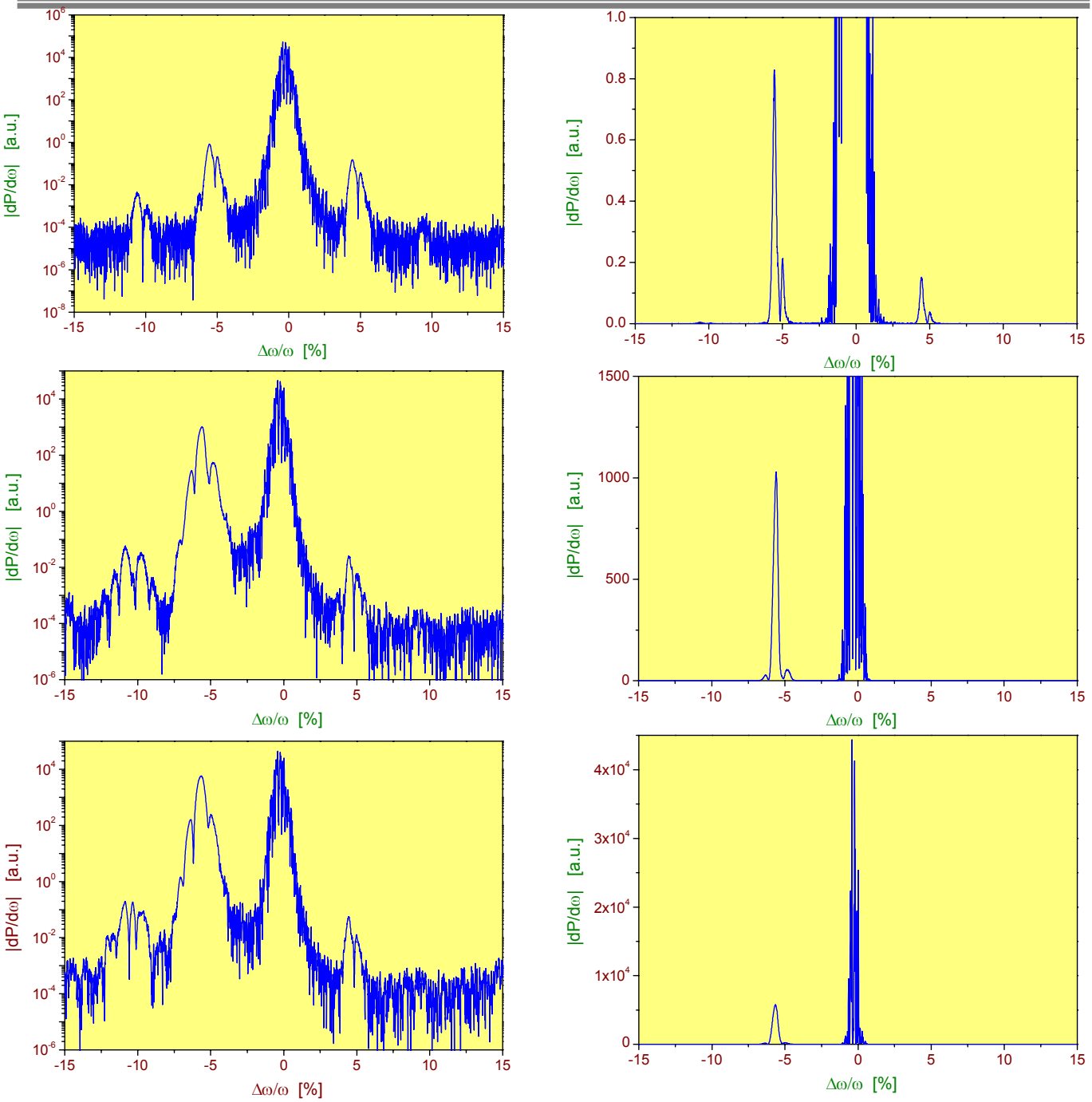

Evolution of the spectral distribution of the output radiation power in the radiator undulator. In the left plots we present spectrum in logarithmic scale, and in the right plots -- in the linear scale. The length of the radiator undulator is equal to 0, 3 and 5~m for upper, middle and lower plots, respectively. Calculations have been performed with three-dimensional, time-dependent simulation code FAST.

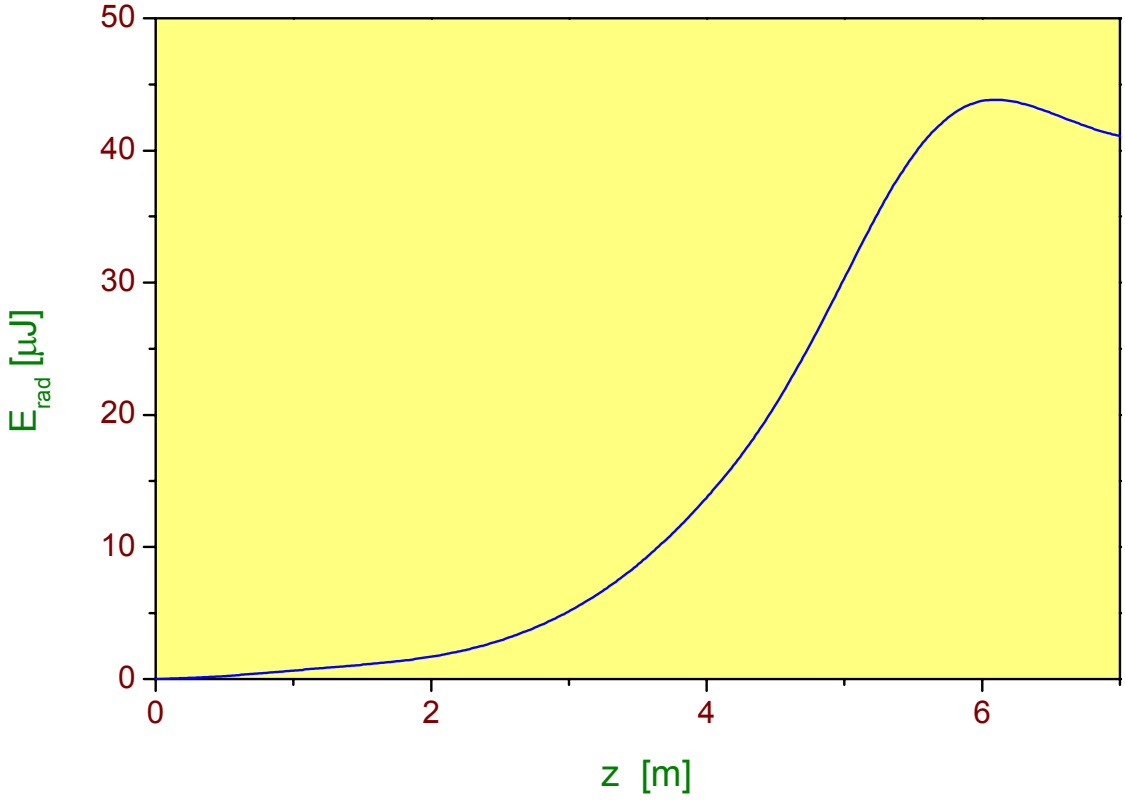

Energy in a fs pulse versus length of the radiator undulator. Calculations have been performed with three-dimensional, time-dependent simulation code FAST.

Outline

- The Seeding Project
- Seeding Principle
- Requirements
- Present status

The Seeding Project

- “ Seeding Option" is funded within the “Strategiefonds" program of the Hermann von Helmholtz-Gemeinschaft Deutscher Forschungszentren.

- The soft X-ray FEL at TTF2 will be modified to provide narrow bandwidth radiation that is coherent in space and time.

- Presently realized under the leadership of HASYLAB in collaboration with the Institute for Storage Ring Facilities of the University of Århus, Denmark (ISA) and the company Scientific Answers Solutions (SAS, R.Reininger) in Madison, Wisconsin.

Conventional SASE FEL

- The bandwidth of the FEL amplifier is an intrinsic featureof the device and is inversely proportional to the power gain length.
- The gain length should be minimized in order to reduce the scale (and the cost) of the device and to decrease the sensitivity of the FEL operation to different imperfections such as undulator errors, etc.
- To perform experiments which require a narrow bandwidth of the output radiation, a mono-chromator has to be installed at the FEL amplifier exit. The shot-to-shot fluctuation of the radiation power after this monochromator will increase with increasing energy resolution.
- Conventional X-ray optical elements will suffer from heat load due to the high output radiation power and probably filter s have to be installed before the monochromator. As a result, the brilliance of the FEL radiation available at the experimental station might be reduced signifi-cantly.

Parameters of the conventional SASE FEL at DESY (CDR 1995)

Electron Beam	
Energy	1000 MeV
Peak current	2500 A
Rms bunch length	50 μm
Rms normalized emittance	2π mm mrad
Rms energy spread	0.1%
External β-function	300 cm
Rms transverse beam size	57 μm
Number of bunches per train	7200
Repetition rate	10 Hz
Undulator	
Type	Planar
Period	2.73 cm
Peak magnetic field	4.97 kGs
Length of undulator	20 m
Output radiation	
Wavelength	6.4 nm
Bandwidth	5×10^{-3}
Rms angular divergence	15 μrad
Rms spot size	90 μm
Coherence time	2 fs
Power average of pulse	5 GW
Flash energy	1.5 mJ
Average power	100 W

Seeding principle

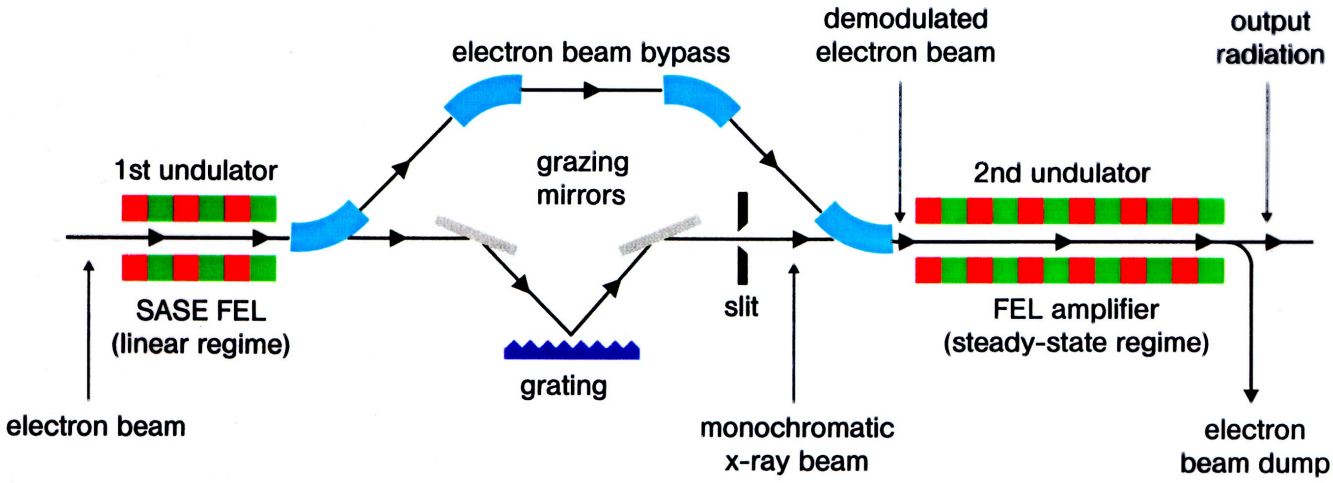

Spectral power distribution

Behind 1st undulator

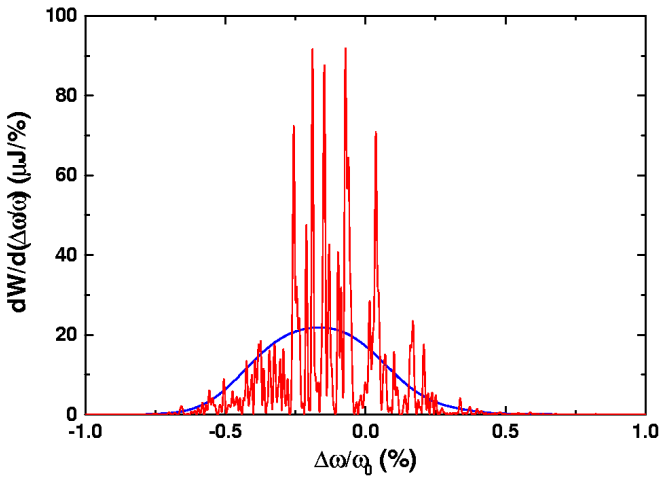

Behind 2nd undulator

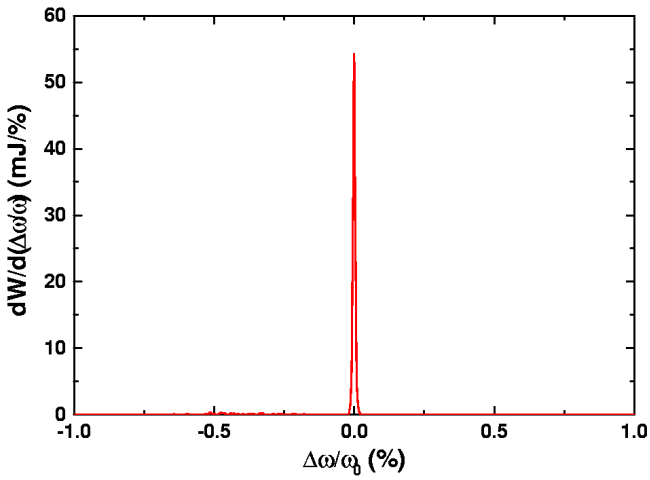

Parameters of the two-stage X-ray FEL at DESY

Electron Beam	
Energy	1000 MeV
Peak current	2500 A
Rms bunch length	50 μm
Rms normalized emittance	2π mm mrad
Rms energy spread	0.1%
External β-function	300 cm
Rms transverse beam size	57 μm
Number of bunches per train	7200
Repetition rate	10 Hz
Undulator	
Type	Planar
Period	2.73 cm
Peak magnetic field	4.97 kGs
Length of 1st undulator	13 m
Length of 2nd undulator	17 m
Output radiation	
Wavelength	6.4 nm
Bandwidth	7×10^{-5}
Rms angular divergence	15 μrad
Rms spot size	90 μm
Coherence time	100 fs
Power average of pulse	2 GW
Flash energy	0.6 mJ
Fluctuations of flash energy	5%
Average power	40 W

Two-stage SASE FEL

- In a two-stage SASE FEL the monochromator is placed between the undulators.
- This allows one to reduce the bandwidth of the output radiation by two orders of magnitude with respect to a single-pass scheme, while the peak and average output power are the same.
- Shot-to-shot fluctuations of the output radiation power of the two-stage SASE FEL can be reduced to below 10%.
- In a two-stage scheme the heat load on the monochromator is 10^3 times less than that on a monochromator installed at the exit of a conventional single-pass SASE FEL.
- The output radiation of a two-stage SASE-FEL possesses all the features which usually refer to laser radiation: full transverse and longitudinal coherence of the radiation within the radiation pulse and stability of the output power

Requirements

Electron Bypass:

- some dispersion needed to remove the micro-bunching, but avoid too large increase of total bunch length
- minimize deterioration of beam quality caused by coherent synchrotron radiation (CSR) in the dipoles tolerable limit of about 10% growth of the slice emittance
- small central "tuning bypass" to vary the electron beam pathlength by about 1 mm which necessary to cope with the changes in photon beam pathlength introduced by changing the monochromator energy

Photon Beamline:

- 1:1 imaging of complex conjugated wavefront onto entrance of 2nd undulator
- monochromator resolution 20000
- overall efficiency 10%

=> optimum longitudinal and transverse overlap with electron bunch
monochromatized beam dominates shot noise in 2nd undulator and is amplified to saturation

Present status

Electron Bypass:

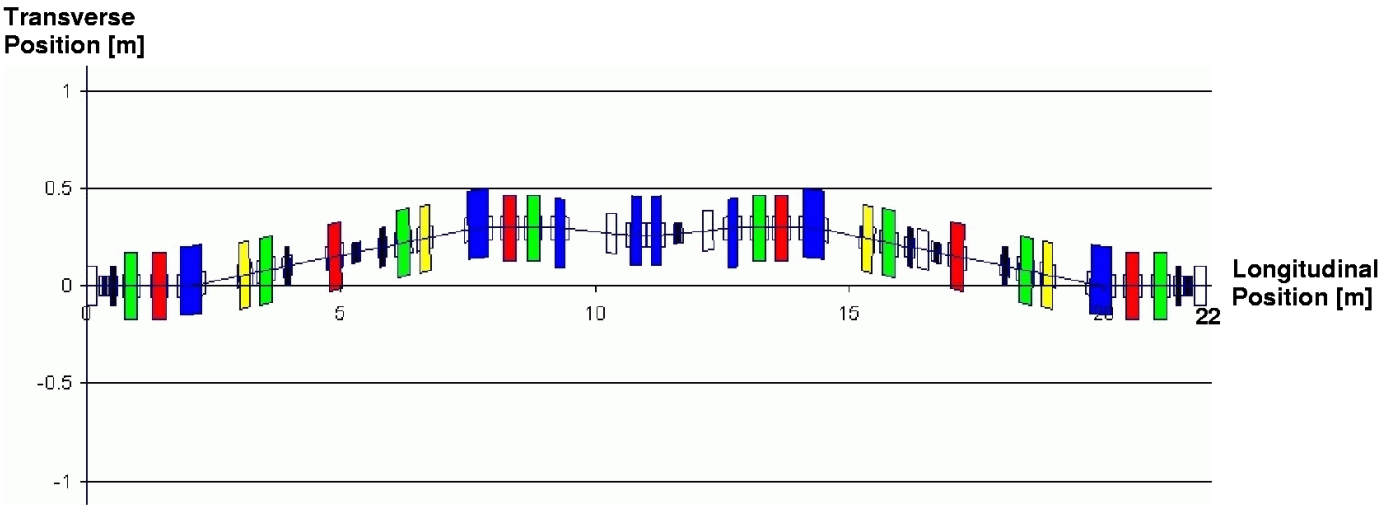

11 steerers, 8 dipoles, 8 quadrupole, vert. foc., 6 quadrupole, hor. foc., 4 sextupoles

=> 37 magnets within 22 m!

Photon Beamline:

- Electron-Bypass-Design finalized
- Photon optics finalized (ray-tracing + wavefront propagation [special development by R. Reininger] + SASE simulation, i.e. "coupling" with e-beam at 2nd undulator entrance)
- All magnets arrived at DESY
- Mechanical and vacuum design almost finished
- Mirror manipulators and monochromator in workshop (Århus, Denmark)
- Mirrors and grating to be ordered soon
- All components for seeding probably available at the end of 2003, first tests of monochromator at synchrotron late 2003/early 2004
- Installation in TTF2 most probably after first phase of operation, i.e. around early 2006

The TESLA Collaboration:

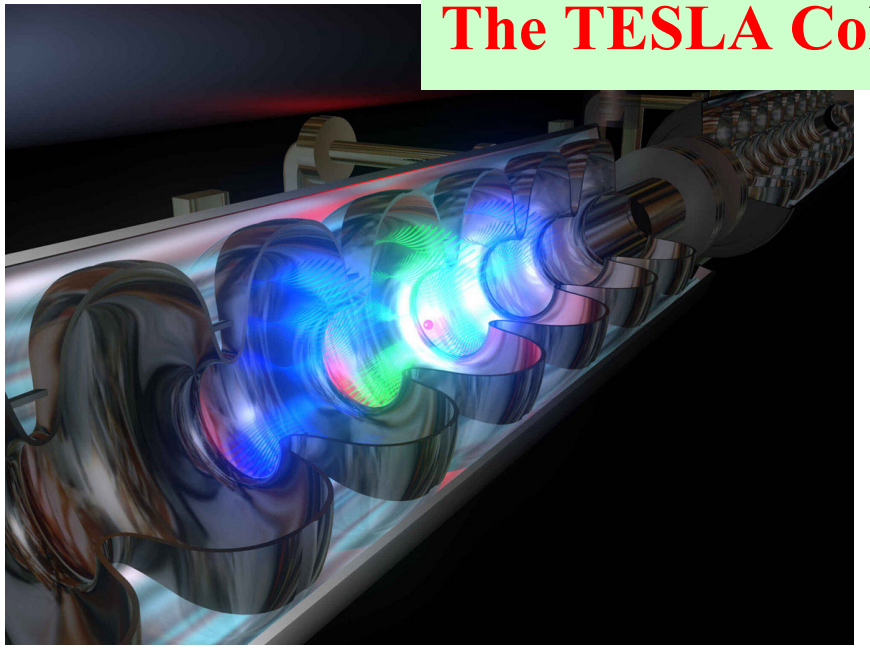

- More than 42 institutes in 10 countries are involved in the TESLA Project

- Major hardware contributions came from the France, Italy, USA, and DESY

The TESLA Test Facility at DESY: Phase I

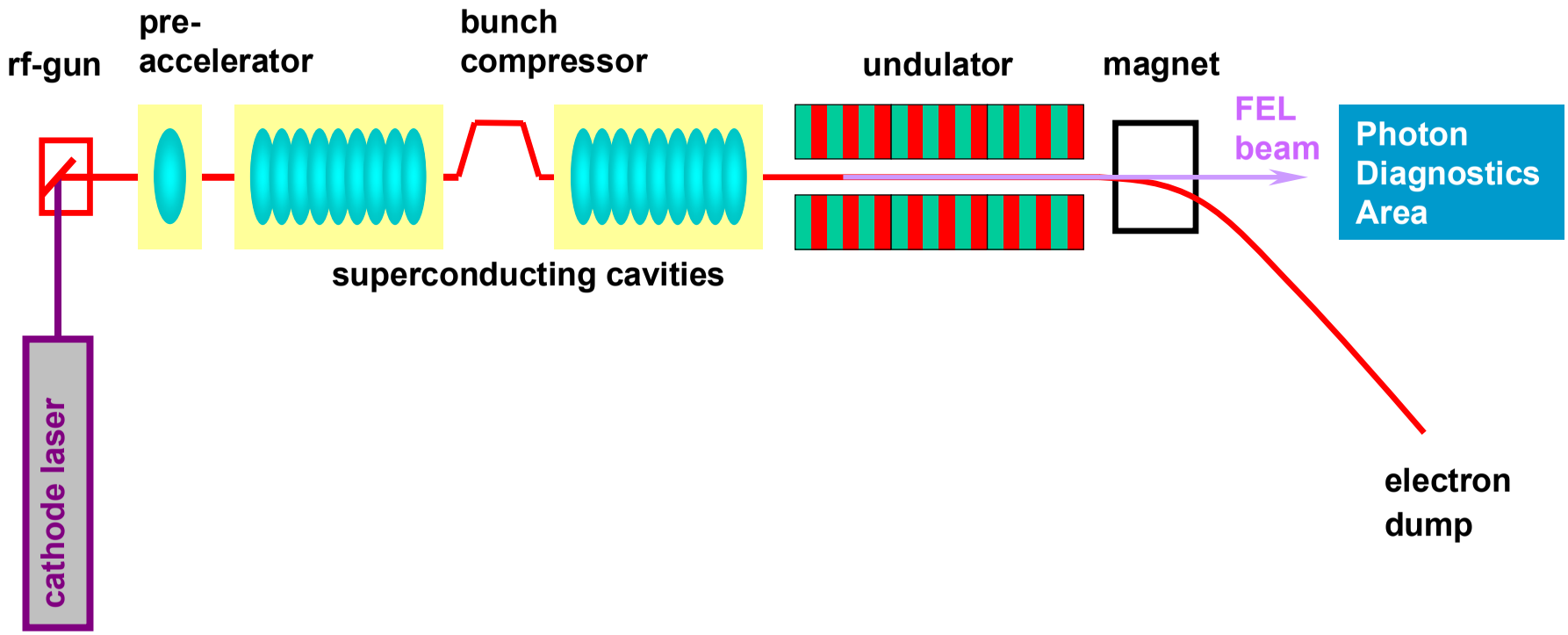

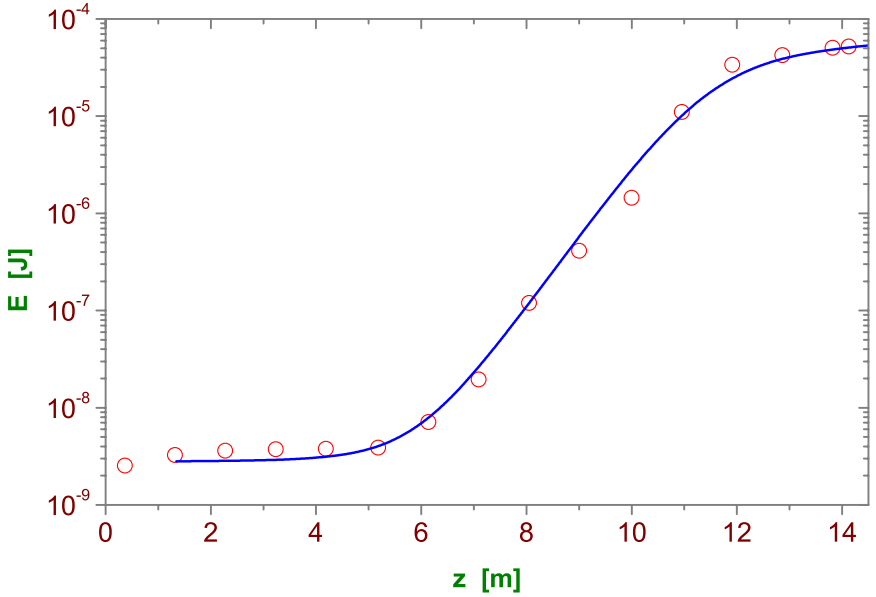

Average energy in the radiation pulse versus undulator length

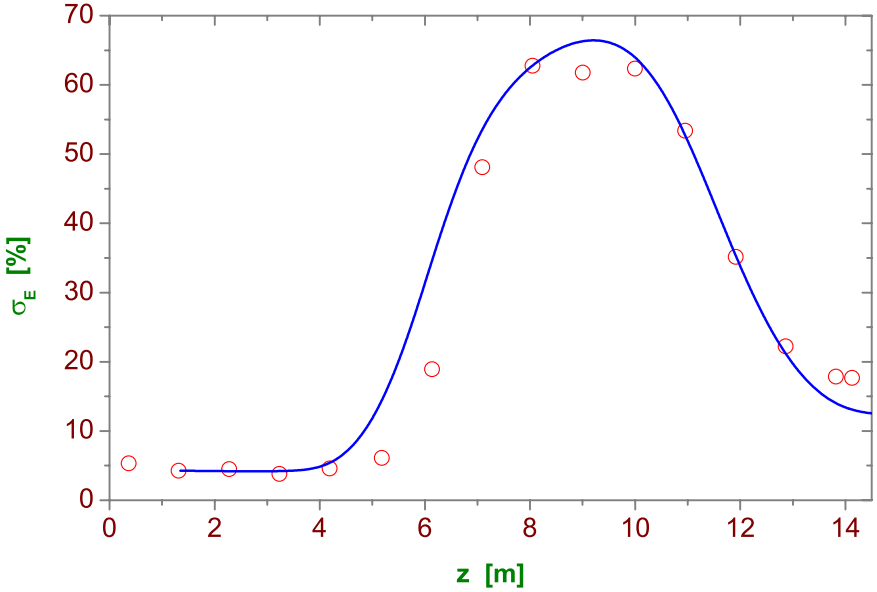

Fluctuations of energy in the radiation pulse versus undulator length

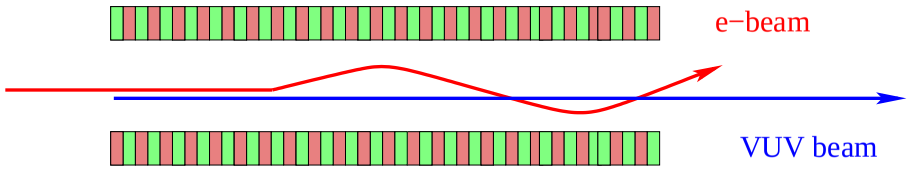

Correctors in the undulator were used to control the length of the interaction between electron beam and radiation

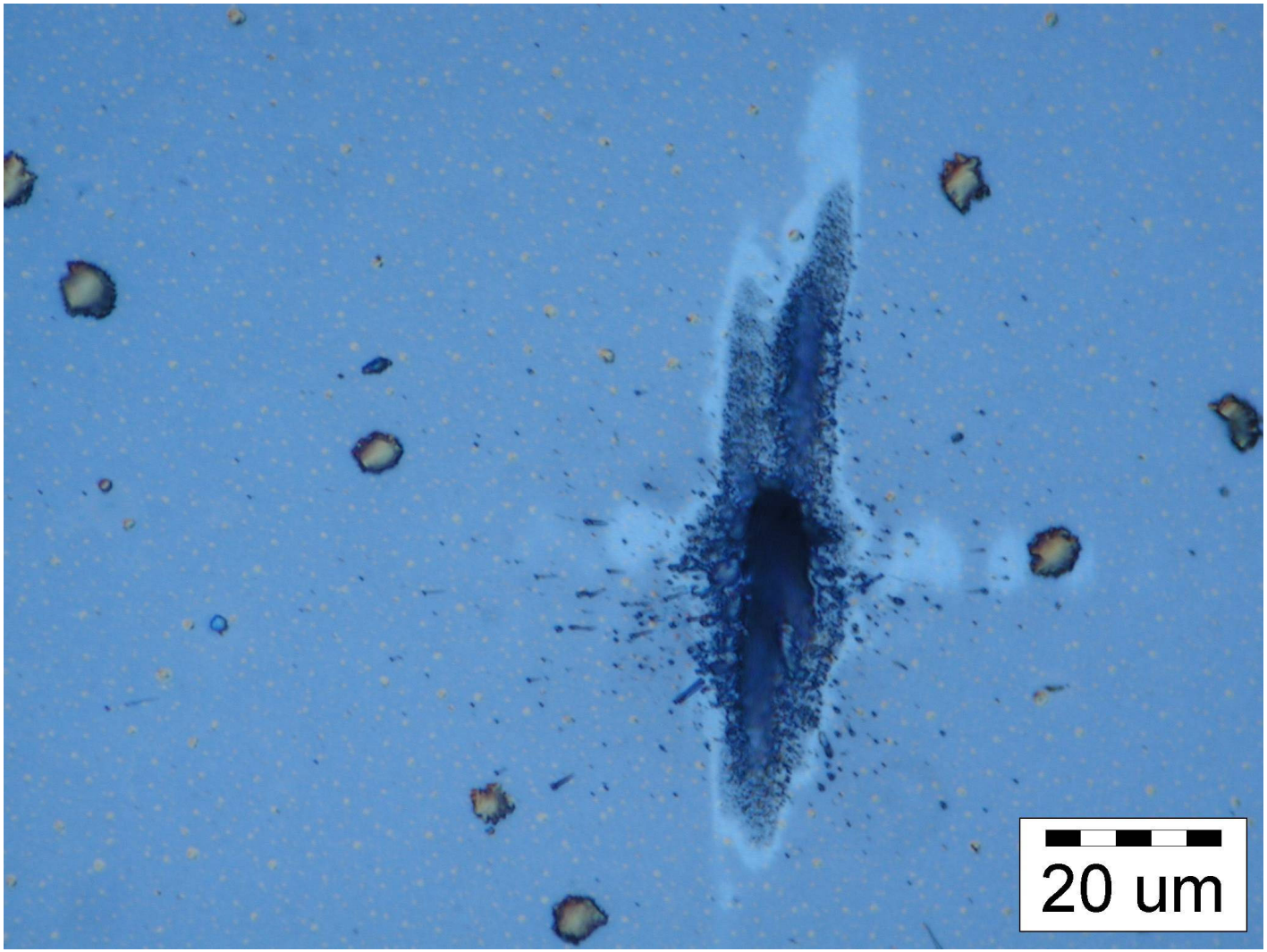
20 um

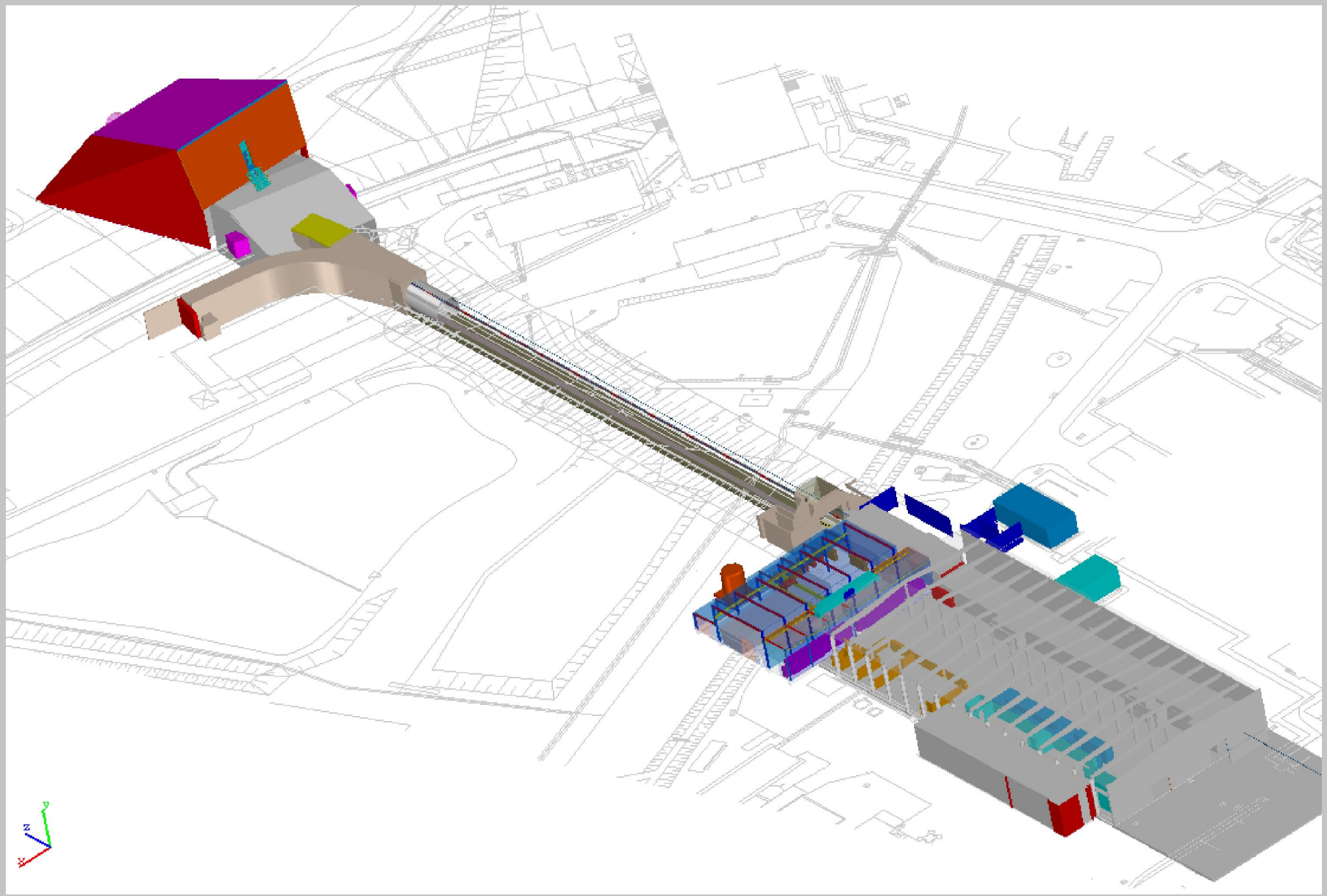

TTF1

SASE FEL

Experimental Hall

TTF Linac Extension as TESLA 500 Test Area

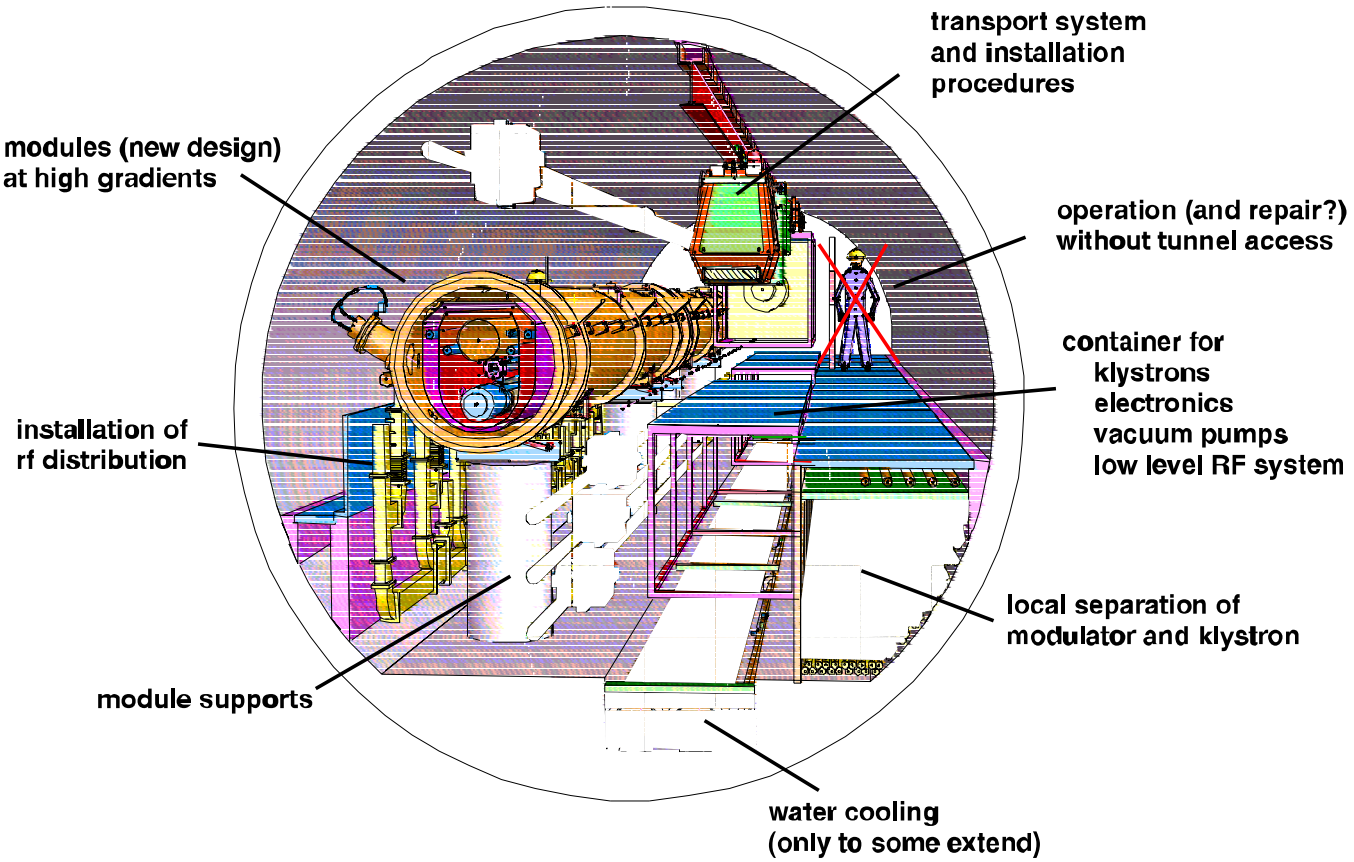

not shown: the construction cost of a tunnel like building covered with sand is less than the setup of a long shielded area; a rectangular cross section is also more expensive

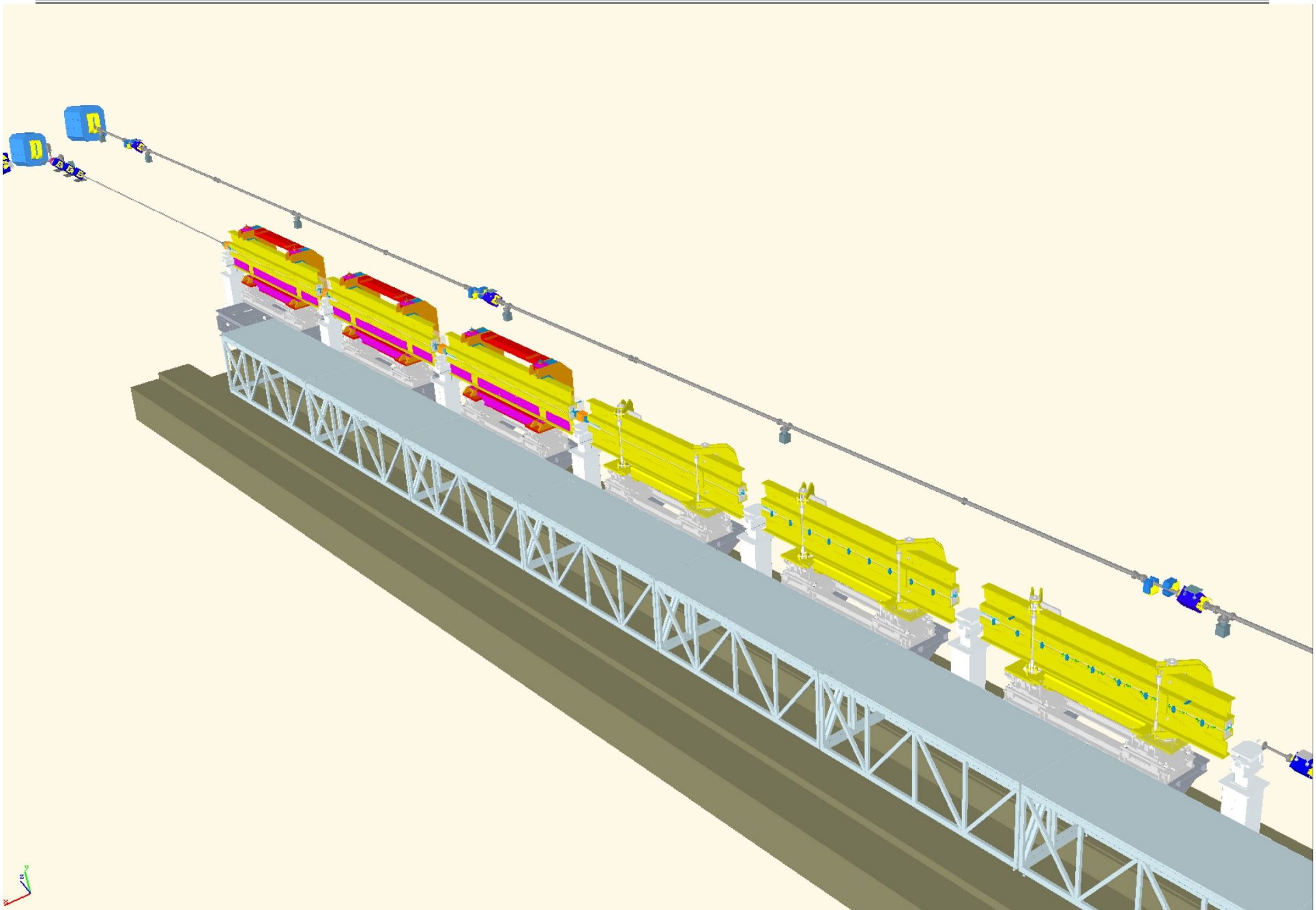

Components in Undulator Intersections TTF Phase II

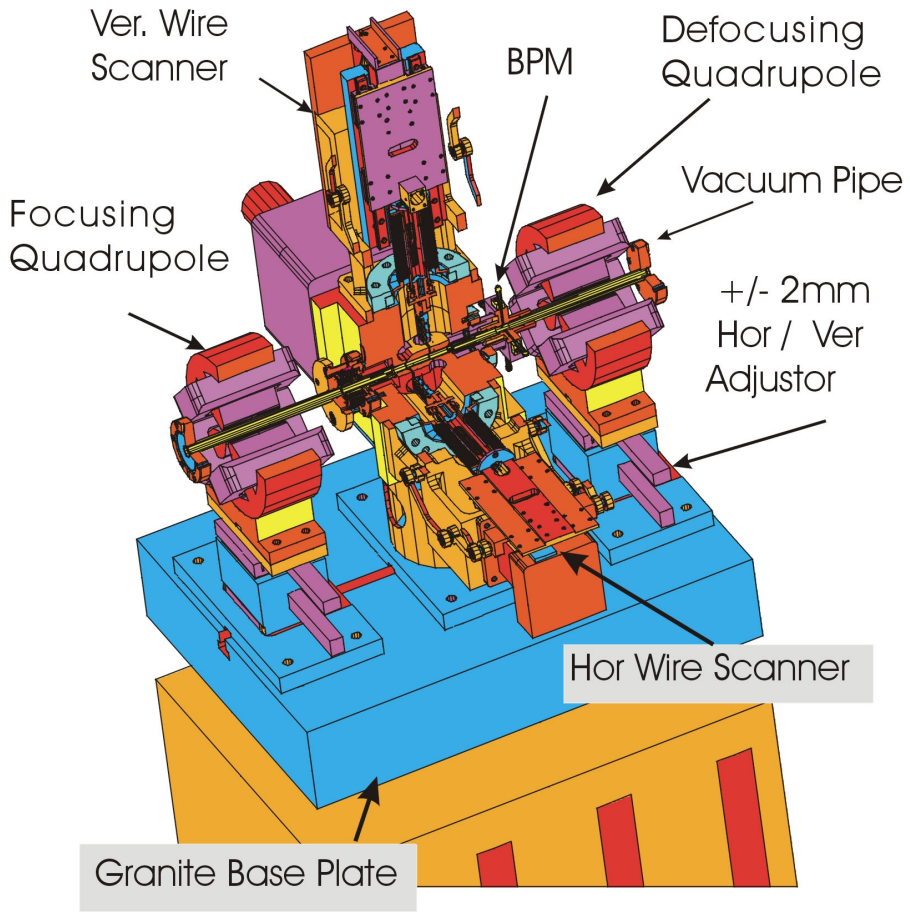

Each quadrupole on slider or hor./vert. Movement

Integrated correctors (not connected)

BPM for beam position (pickups)

Wirescanner for profile

Wire along the entire undulator for relative and absolute positioning of components

Fibers for on-line beam loss detection

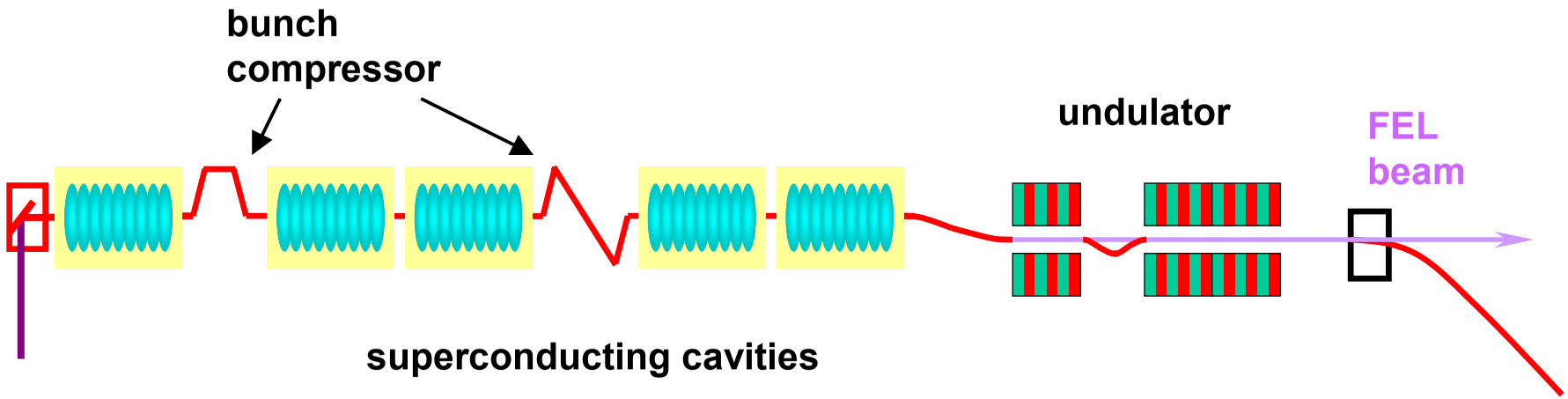

Electron beam energy to 1 GeV
⇨ 3 additional accelerating modules

Tunable in the soft X-Ray region (120-6nm)
⇨ 30 m undulator required

Short pulse length of 300 fs (FWHM)
⇨ two-color time-resolved Pump & Probe experiments with synchronized optical laser

TTF Schedule

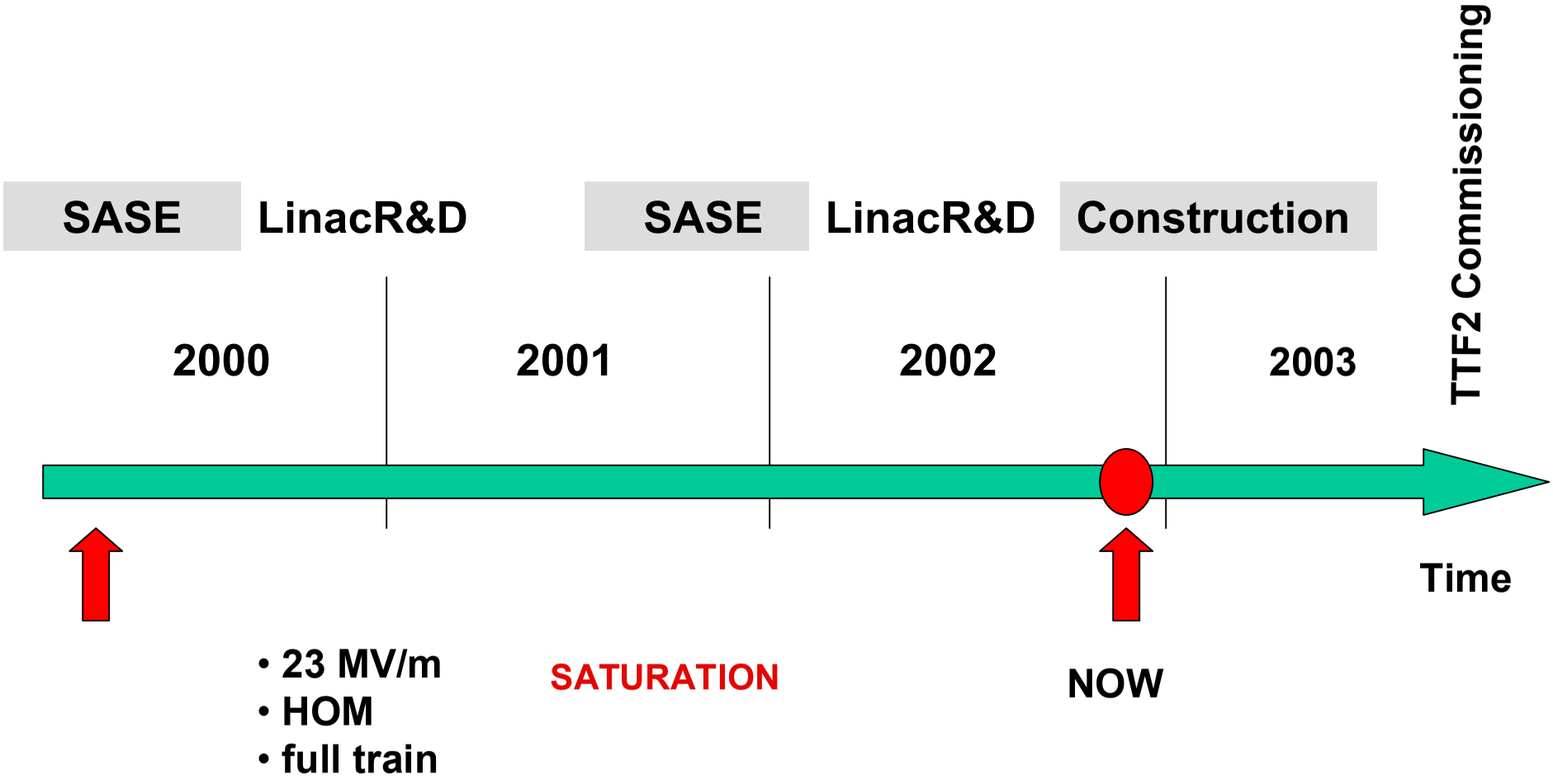

Time schedule:

- First RF test of Module 3, 4, 5: spring 2003
- Start of operation with beam: summer 2003
- First beam for users: 2004
- Full wavelength range (20-120 nm): spring 2004
- Full pulse length and 10 Hz during 2004

Full performance test of modules at intermediate and maximum gradient during 2004

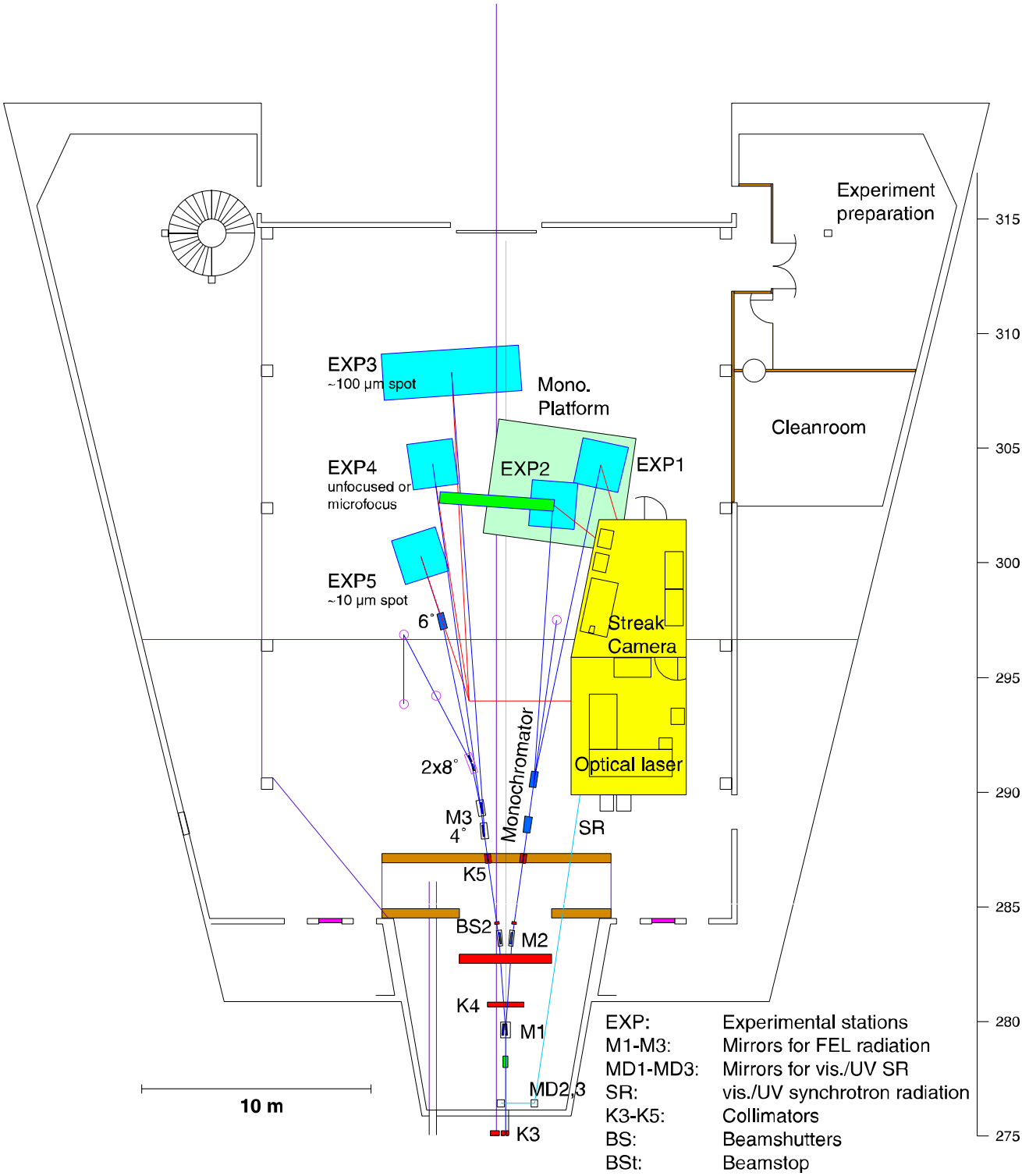
Experiment
preparation
Cleanroom
EXP3
~100 µm spot
Mono.
Platform
EXP4
unfocused or
microfocus
EXP2
EXP1
EXP5
~10 µm spot
6°
Streak
Camera
Optical laser
2x8°
Monochromator
M3
4°
SR
K5
BS2
M2
K4
M1
MD2,3
K3
10 m
315
310
305
300
295
290
285
280
275
EXP: Experimental stations
M1-M3: Mirrors for FEL radiation
MD1-MD3: Mirrors for vis./UV SR
SR: vis./UV synchrotron radiation
K3-K5: Collimators
BS: Beamshutters
BSt: Beamstop

Project Title	Photon Energy	Intensity		Pulse Timing & Pump-Probe		Category
	Preferred energy range (eV)	Acceptable spot size	Intensity variation	FEL pulse timing requirements	Requirements for Optical laser	
Pump-Probe Experiments in the Gas Phase	15-200					Developments for pump-probe
Single-Shot FEL Cross Correlator	>12	30 µm		up to 9 MHz	10 µJ	
Quantitative Investigation of Photoionisation Processes on Free Atoms in a Focused VUV FEL Beam	>12		up to 1E16 W/cm^2			Atoms, ions, molecules, non-linear effects
High-Frequency Stabilisation of Li	>10,<70	several µm	>1E16 W/cm^2	<50 fs	own diode and YAG laser	
Multiphoton Ionisation and Excitation	10-150	up to 1 mm	<1.5 mJ, 1E13-1E17 W/cm^2	100-200 fs, 200ns distance		
Resonant Single- and Multiphoton Excitation and Photoionisation of Highly charged Ions by FEL Radiation	20-140	100 µm	>0.05 mJ, >1E15 W/cm^2 desirable	<100 fs preferable		
Multi-Photon Multiple Ionisation	30-70	<20 µm	0.05-1 mJ, 1E13-1E17 W/cm^2	< 250fs		
Molecular Ion Photodissociation	7-40	~3 mm	0.1-1.6 mJ	1-10 kHz at 5 Hz		
Cluster FEL Interaction: Interaction of Intense Soft X-Rays with Atomic and Molecular Clusters	>12	~10 µm	>1E14 W/cm^2	<100 fs, 10 µs distance		Clusters
Structure of Mass-Selected Clusters	10-100	0.1-1mm, down to 10µm	>10-100	single pulse or 10µs separation	0.1-1 mJ	

Project Title	Photon Energy	Intensity		Pulse Timing & Pump-Probe		Category
	Preferred energy range (eV)	Acceptable spot size	Intensity variation	FEL pulse timing requirements	Requirements for Optical laser	
XUV Laser Desorption	8-20	1-5 mm	>100μJ, >factor 100	<300 fs, <1 μs distance in pulse trains	own ns-laser	Surfaces and solids
VUV FEL Nanospectroscopy	10-200	several 100 μm, info on beam profile and coherence	some orders of magnitude	none initially	not needed	
IHED-DESY Beam Investigation	10-400	1-20μm	1-100% of full intensity	50fs	<1mJ	
Warm Dense Matter Creation: Isochoric Heating of a Thin Foil	60-400	uniform spot up to 100 μm	none	timing of FEL to optical laser with the accuracy of l.e. pulse length	0.1J	
Equation of State Measurements	60-400	uniform spot up to 100 μm	none	timing of FEL to optical laser with the accuracy of l.e. pulse length	0.1J	
Coulomb Explosions of Biological Samples	20-600	1-20 μm	1%-100% of full intensity	no special requirements	N/A	
Diffraction Imaging of Biological Samples	100-600	1-10 μm	1%-100% of full intensity	no special requirements	N/A	
Studies of Interactions of XUV-FEL Pulses with Solids: Optics Damage and High-Field Effects	85-600	1-20 μm	1%-100% of full intensity	50 fs	< 1 mJ	

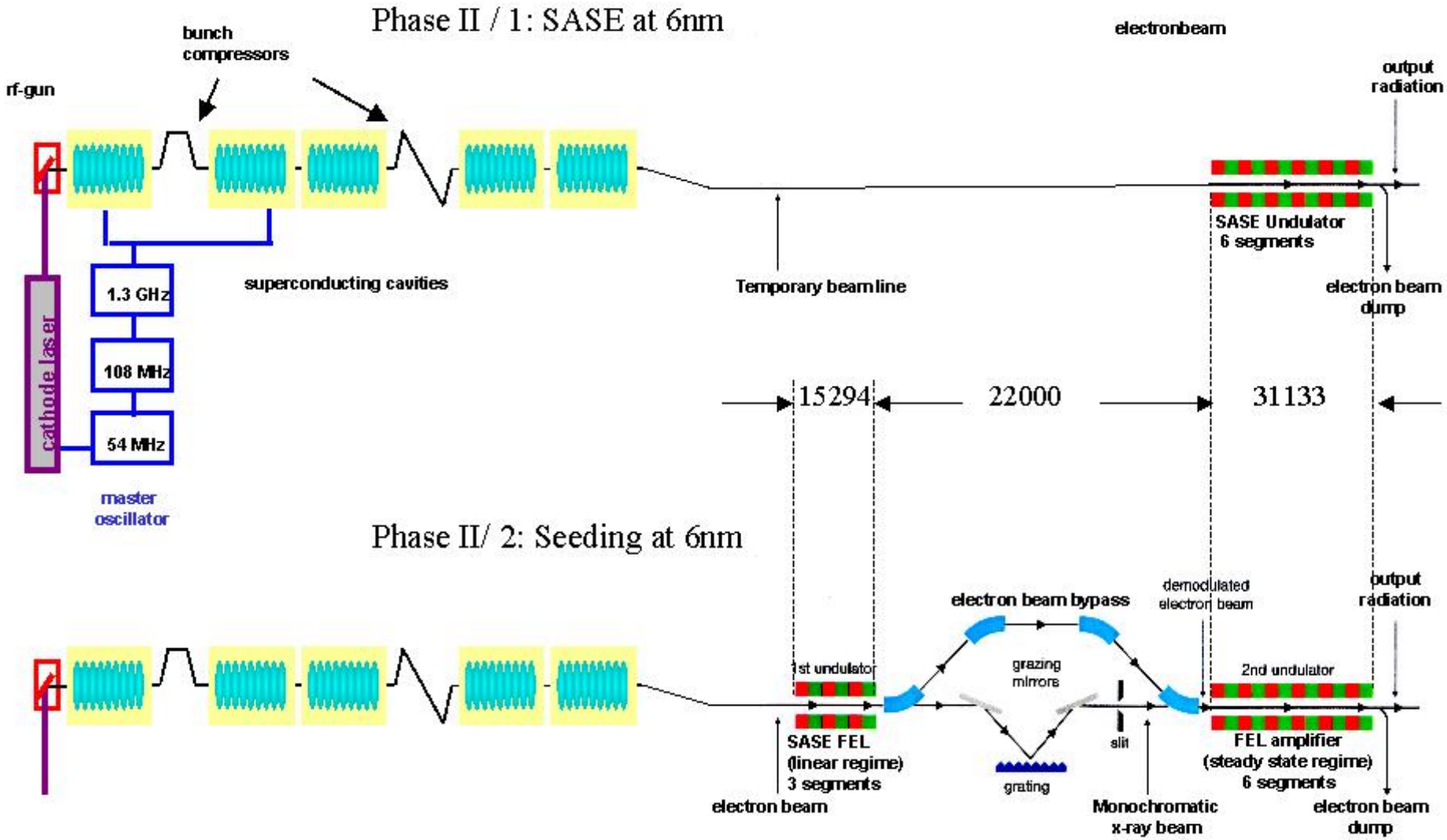
Phase II / 1: SASE at 6nm
bunch compressors
electronbeam
rf-gun
output radiation
SASE Undulator 6 segments
superconducting cavities
Temporary beamline
electron beam dump
1.3 GHz
108 MHz
54 MHz
cathode laser
master oscillator
15294
22000
31133
Phase II/ 2: Seeding at 6nm
electron beam bypass
demodulated electron beam
output radiation
1st undulator
grazing mirrors
2nd undulator
SASE FEL (linear regime) 3 segments
slit
FEL amplifier (steady state regime) 6 segments
grating
electron beam
Monochromatic x-ray beam
electron beam dump

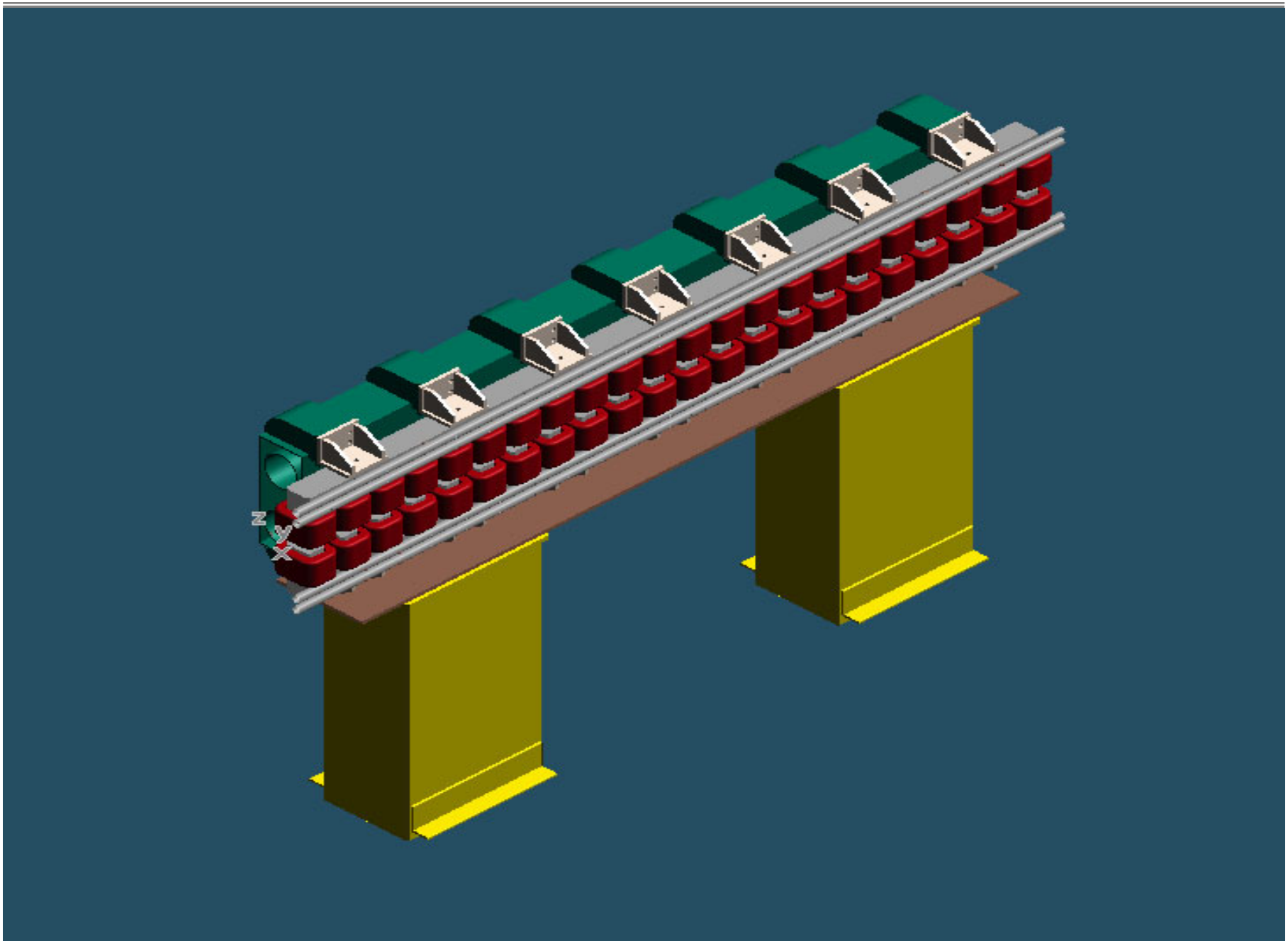
z
y
x